Sensitivity Analysis of the Unscented Kalman Filter Method for Synchronous Generator Parameter Estimation

A Thesis

Presented in Partial Fulfillment of the Requirements for the

Degree of Master of Science

with a

Major in Electrical Engineering

in the

College of Graduate Studies

University of Idaho

by

Abdulwahab A. Aljabrine

Major Professor: Brian K. Johnson, Ph.D.

Committee Members: Joseph Law, Ph.D.; Yacine Chakhchoukh, Ph.D.;

Department Administrator: Joseph D. Law, Ph.D.

August 2021

Authorization to Submit Thesis

This Thesis of Abdulwahab Aljabrine, submitted for the degree of Master of Science with a major in Electrical Engineering and titled "Sensitivity Analysis of the Unscented Kalman Filter Method for Synchronous Generator Parameter Estimation," has been reviewed in final form. Permission, as indicated by the signatures and dates given below, is now granted to submit final copies to the College of Graduate Studies for approval.

Major Professor: _____ Date: _____
Brian K. Johnson, Ph.D.

Committee Members: _____ Date: _____
Joseph D. Law, Ph.D.

_____ Date: _____
Yacine Chakhchoukh, Ph.D.

Department Administrator: _____ Date: _____
Joseph D. Law, Ph.D.

Abstract

An accurate synchronous generator model plays a crucial role in planning and predicting the dynamic performance of the power system in order to maintain its stability and reliability. In current practice, offline tests are conducted to determine synchronous generator parameters. However, removing the generator from service can cause lost revenue and increase the stress on other generators. Furthermore, these tests can degrade the insulation of the synchronous generator, and some are impractical to conduct, such as the short circuit test.

This thesis explores online estimation techniques and chooses the unscented Kalman filter (UKF) method. A simulated synchronous generator model was developed to test the UKF. This research also performs the sensitivity analysis on different aspects of the online estimation method. In other words, it investigates the performance of the UKF in the presence of innovation and observation outliers. These outliers can be due to uncertainties such as inaccuracies of the model parameters or the measurement noise. The thesis presents and compares generalized maximum-likelihood- combined with unscented Kalman filter (GM-UKF) and the regular UKF in the presence of Gaussian and non-Gaussian noise.

The thesis is extended to determine the parameters of a laboratory synchronous generator using UKF. The IEEE 115 recommended tests were conducted to obtain reference values and to show the performance of the filter. Frequency and load angle tracking methods were developed to obtain the synchronous reference frame (Park transform) components during steady-state and transient conditions.

Acknowledgements

I would like to start by thanking God for all the blessings I have received so far. I also would like to express my sincere gratitude to my major professor, Dr. Brian Johnson, for offering me the opportunity to work on this topic at the University of Idaho. I am very grateful for his patience, guidance, and immense knowledge. My sincere thanks also go to my committee members, Dr. Joseph D. Law and Dr. Yacine Chakhchoukh, for their valuable time, insightful comments, and questions, which motivated me to improve my thesis. Additionally, special thanks to Dr. Normann Fischer and Schweitzer Engineering Laboratories for sponsoring this work.

Dedication

This work is dedicated to my beloved family for their love, kindness, and support. Without them, I would have never gotten this far.

Table of Contents

List of Tables

List of Figures

List of Abbreviations

General List

IEEE	Institute of Electrical and Electronics Engineers.
WECC	Western Electricity Coordinating Council.
NERC	North American Electric Reliability Corporation.
KF	Kalman Filter.
UKF	Unscented Kalman Filter.
EKF	Extended Kalman Filter.
GM-UKF	Generalized Maximum-Likelihood-type Unscented Kalman Filter.
LSE	Least Squares Estimation.
PMU	Phasor Measurement Unit.

Machine list

v_a, v_b, v_c	Stator voltages in phases a, b, and c.
i_a, i_b, i_c	Stator currents in phases a, b, and c.
v_{fd}, i_{fd}, ψ_{fd}	Voltage, current, and flux in the field winding.
v_d, i_d, ψ_d	Stator voltage, current, and flux in the direct-axis.
v_q, i_q, ψ_q	Stator voltage, current, and flux in the quadrature-axis.
v_D, i_D, ψ_D	Voltage, current, and flux in the direct-axis damper winding.
v_Q, i_Q, ψ_Q	Voltage, current, and flux in the the quadrature-axis damper winding.
r_s	Resistance in stator winding.
r_{fd}	Resistance in field winding.
r_Q	Resistance in quadrature-axis damper winding.
r_D	Resistance in direct-axis damper winding.
X_q, L_q	Stator self reactance and inductance in the quadrature-axis.
X_d, L_d	Stator self reactance and inductance in the direct-axis.
X_{mq}, L_{mq}	Magnetizing reactance and inductance in the quadrature-axis.
X_{md}, L_{md}	Magnetizing reactance and inductance in the direct-axis.
X_{ls}, L_{ls}	Stator winding leakage reactance and inductance.
X_{lfd}, L_{lfd}	Field winding leakage reactance and inductance.
X_{lQ}, L_{lQ}	Damper bar leakage reactance and inductance in the quadrature-axis winding.
X_{lD}, L_{lD}	Damper bar leakage reactance and inductance in the direct-axis winding.
T_m	Mechanical torque applied on the rotor.
T_e	Electrical torque.
δ	Load angle.
ω_s	Synchronous angular speed.
J	Total moment of inertia of the rotor mass

1. Introduction

Having knowledge of power system model parameters is crucial for performing accurate stability and post-mortem instability analysis. Despite the rapid increase in wind and photovoltaic generation, synchronous generators still play a significant role in the operation of power systems. Even 90 years after the first publications in modeling synchronous generators [5,6], the topic of determining parameters in an accurate and efficient manner is still challenging and attracts many researchers.

1.1 Background and Motivation

Having an accurate dynamic model of a synchronous generator is essential for accurate system modeling and simulation for maintaining stable operation. In addition, accurate models play a vital role in post-mortem instability analysis. For example, in the 2003 blackout, inaccurate generator parameters frustrated the investigators who were trying to develop accurate simulations of the event [7]. Further, the analysis of the blackout of August 10, 1996, has shown the importance of accurate synchronous generator modeling, which could have prevented undesirable tripping of the generators and avoid cascading failure in that situation [8, 9]. Using machine model parameters from commissioning can result in discrepancies between the actual and simulated dynamic behavior of the generator in response to disturbances [10, 11]. As a result, the Western Electricity Coordinating Council (WECC) issued a policy stating that every generator rated at 20 MVA and larger has to be characterized to validate model data [12]. Therefore, synchronous generator owners are routinely adjusting the manufacturer's parameters based on offline field testing.

However, offline testing is associated with several drawbacks, for instance, lost revenue due to downtime, increased stress on other generators, and time-consuming test procedures. It is important to note that offline parameter identification methods do

not account for parameter deviations that could occur due to loading and temperature changes. In order to address these challenges, online estimation techniques can determine the machine parameters during normal operation or normal startup without taking machines offline, avoiding the cost of needing a generator outage for parameter testing. This approach can offer a more economical and reliable solution to determine and refine the machine parameters. It should be noted that in practice, there are many uncertainties that would affect the online estimation method, such as inaccuracies of the model parameters and the measurement noise [1,13]. Therefore, It is essential to assess the sensitivity of the online estimation method to the deviations from model and measurement noise.

1.2 Literature Review

Many researchers have developed and contributed to both online and offline parameter identification techniques. This section reviews the literature and explores the challenges and the advantages of each technique. Research on frequency and load angle measurement is also discussed.

1.2.1 Offline Parameter Identification

In past decades, there have been many developed methods for synchronous machine parameter identification. In 1931, S. Wright discussed test methods for determining synchronous machine parameters, such as slip test, locked zero-sequence reactance test, and sudden three-phase short circuit test [5]. In [14] Karapetoff discussed the drawbacks of assuming a constant armature leakage reactance in a synchronous machine model, which can cause noticeable discrepancies between the model outputs and field measurement. Another research focused on leakage reactance determination test that was proposed by L. A. March and S. B. Crary [15]. They showed that the

Potier reactance is approximately equal to the leakage reactance when the terminal voltage is at 1.6 pu, i.e., the applied field current is at 4 pu to 5 pu. This method has a high-risk level which could damage the machine windings, due to the overvoltage required between the leakage reactance and Potier reactance. There are a few standards that show detailed procedures for offline machine parameters identification, for instance, IEEE standard 115 and IEC standard 34-4 [16, 17].

Overall, some tests have a high level of risk on the machine, such as a sudden three-phase short circuit test, and others are accurate and do not impose any risk on the machine, such as the standstill frequency response test (SSFR). A major disadvantage of the SSFR test is that it is considered an intensive and time-consuming method. E. C. Bortoni and J. A. Jardini showed a mathematical approach to determine $X_d, X'_d, X''_d, T'_{d0}, T''_{d0}, X_q, X''_q, T''_{q0}$ using load rejection tests [18]. They implemented their proposed method on a real machine with two different operating points to obtain both q-axis and d-axis parameters. All in all, the load rejection test and standstill frequency response test (SSFR) have gained prominence among other tests due to their low level of stress imposed on the generator during the test and the accuracy of the obtained data. [18–22].

1.2.2 Online Parameter Identification

Based on the literature review, there are two major methods for online generator parameter estimation: Kalman filter-based estimation methods and least-squares error (LSE)-based estimation methods. In the following subsections, both estimation methods are explored.

1.2.2.1 Least Squares

Least squares error (LSE)-based estimation is one of the oldest techniques of power system estimation. This method is based on regression analysis, which approximates

the system solution by minimizing the sum of the squares of the residuals, where the residual is the difference between the measurement and estimated measurement.

Several papers have implemented this technique to determine the parameters of a synchronous generator [23, 24]. In fact, one of the previous master's students who was working on this project has investigated the limitation of this method in the field of synchronous generator parameter estimation [25].

1.2.2.2 Kalman Filter Method

In the late 1950s, the Kalman filter (KF) was initially developed for linear systems by R. Rudolf Kalman. KF consists of two stages, the prediction stage and the update stage. The prediction stage computes the predicted state from the mathematical model that represents the system, whereas the update stage corrects the state based on the collected measurement.

Dynamic power systems, especially synchronous generators, are considered nonlinear models and can not be estimated using linear KF. Therefore, there are two techniques to deal with nonlinearity. The extended Kalman Filter (EKF) method is considered a solution for the nonlinearity. It uses a Taylor expansion to linearly approximate a nonlinear function. Various researchers have contributed to the subject of generator parameters and state estimation using EKF [26–28].

Another solution for the nonlinearity is using a deterministic sampling approach proposed by Julier and Uhlman known as the unscented Kalman filter (UKF) [29]. The EKF only achieves the first-order accuracy where UKF accurately captures up to the third order for any nonlinearity [30]. Table 1.1 summarizes the estimated parameters, known parameters, and estimator methods that have been studied.

A PNNL report has shown tested field data collected from phasor measurement units (PMUs) exhibits non-Gaussian noise, which raises an issue since the EKF and UKF are only optimal under the Gaussian noise assumption. [1, 13]. Therefore, al-

Table 1.1: Summary on the parameter estimation methods.

Ref.	Model Order	System Type	Estimator Input	Estimator Output	Estimated Parameter	Known Parameter	Estimator Method
[31]*	4th	Simulated	V_{dq0}, P_m	P_e, Q_e	H, X'_d	D, T'_{d0}, T'_{q0}	CIUKF
[23]*	4th	Simulated	V_{dq0}, P_m V_{fd}	P_e, Q_e	H, X'_d, X'_q	D, T'_{d0}, T'_{q0}	LSE
[32]*	2nd	Simulated	V_{abc}, θ	P_e, Q_e	X'_d, H	D	EKF
[33]*	2nd	Simulated	I_{abc}, P_e Q_e	V_{abc}, θ	H, D, P_m, X'_d	-	EKF
[34]	4th	Actual	V_{dq0}, V_{fd} ω_m, δ	I_{dq0}, I_{fd}	X_{md}, X_{mq}, r_{fd}	X_{ls}, r_s	UKF
[24]	4th	Simulated	-	I_{dq0}, V_{dq0}	X_{md}, X_{mq}, r_{fd}	M_f, L_0, r_s	LSE
[35]*	2nd	Simulated	V_{abc}, θ, P_m	P_e, Q_e	X'_d, H, D	-	EKF
[34]	7th	Simulated	V_{dq0}, V_{fd} T_m	I_{dq0}, I_{fd}	X_{lD}, X_{lQ1}, X_{lQ2}, r_{lD}, r_{lQ1}, r_{lQ2}	H X_{md}, X_{mq},	UKF
[36]	6th	Simulated	V_{dq0}, V_{fd} T_m, ω_m	I_{dq0}, I_{fd} ω_m	X_{lD}, X_{lQ}, r_{lD}, r_{lQ}	H, X_{ls}, X_{lf} r_s, r_{fd}	UKF

ways assuming Gaussian noise in the PMU measurement is no longer valid. Figure 1.1 shows voltage and current magnitudes which follow bimodal Gaussian mixture distribution noise. Note that in practice, it is not common to use PMUs to collect generator measurements. It is more convenient to use a relay device such as SEL-400G to capture the measurement at higher sample rates than the PMU.

All papers marked with * in Table 1.1 assumed that the measurements are collected using PMUs with Gaussian noise, which raises concerns that will be explored in this thesis.

It should be noted that all papers in Table 1.1 assumed perfect known parameters while estimating the unknown parameters. In practice, known parameters will be associated with a margin of error. This thesis tests the performance of UKF in the presence of non-Gaussian noise and explores the sensitivity analysis under incorrect model parameters. It is important to note that in literature the inaccuracy of known parameter can be characterized as innovation outliers where the measurement noise

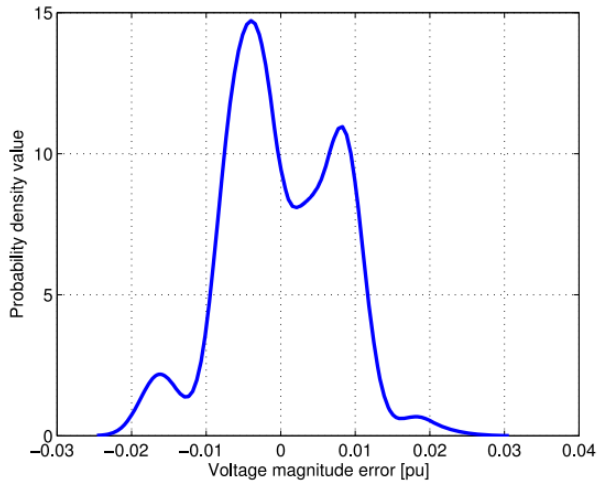

(a)

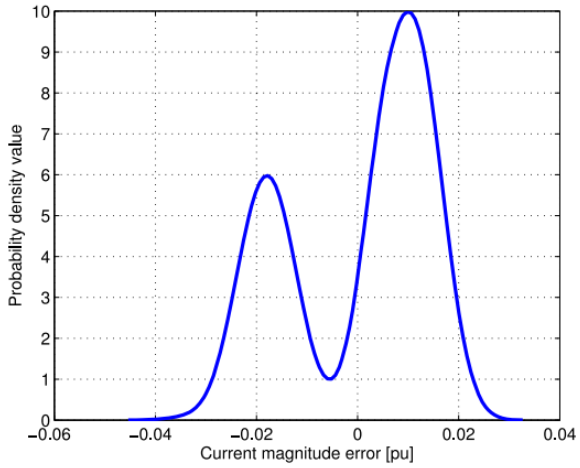

(b)

Figure 1.1: (a) Probability density of the phasor voltage magnitude error (b) Probability density of the phasor current magnitude error [1].

known as observation outliers [37]. Note that this thesis is a continuation of work by previous master's students Michael West and Andrew Miles [25, 38].

1.2.3 Frequency and Load Angle Tracking

The estimation of synchronous generator parameter needs a fast and accurate frequency tracking method. Frequency is a critical measurement in transient conditions, where it is used to compute the synchronous reference frame (dq0) components of the terminal measurements. Several researchers have developed different techniques to

estimate the power system frequency, which can be characterized into two different types:

1. Frequency-domain methods.

2. Time-domain methods.

The discrete Fourier transform (DFT) is one of the frequency-domain methods. It is considered to be the most commonly used technique in frequency-domain methods due to its low computational burden [39]. However, the major problem with this technique is low accuracy in the presence of spectrum leakage that can be due to asynchronous sampling [40]. Another technique that is characterized under frequency-domain methods is the Wavelet transform [41]. This approach has accuracy limitations based on the selection of basis wavelets and with scale resolution [42].

The second type of technique for estimating power system frequency uses time-based methods. A phase-locked loop-based approach is widely used due to its high accuracy and fast response [42]. The zero-crossings method is another example of a time-domain method. It has high precision in the presence of harmonics as long as the signal does not have either extra asymmetrically shifted zero crossings that come from heavy distortions such as switching [43, 44]. In [4], a new approach for tracking frequency known as B-function was developed. It uses a periodic waveform integration concept to find the waveform period and look at when the integrated function is equal to zero. Interpolation methods are commonly applied in the zero-crossings and B-function methods. Zero-crossings and phase-locked loop methods have been developed and are compared with the B-function in Chapter 6.

The load angle of the synchronous generator is a crucial measurement in parameter estimation. It is used to calculate the dq0 components relative to the terminal measurement. In some cases, the load angle is used as an input or measurement vector of the estimator. Load angle tracking can be characterized into two main methods:

direct methods and indirect methods. The direct method in which a physical sensor is installed on the rotor or in the air gap. In [45], an optical encoder was used to track the rotor position. In this method, the load angle can be computed by using the rotor position and terminal voltage. In [46], an air gap sensor was installed to detect the rotor position. Various indirect methods have been developed to determine the load angle [47–50] The indirect methods use parameters and measurements from the machine to compare a calculated angle with its estimated outputs.

In this thesis, an optical encoder was used to determine the load angle. Further explanation is provided in Chapter 6

1.3 Thesis Objectives

The objectives of this thesis are as follows:

- Conduct a literature study of the most used estimators for machine parameterization.
- Implement an unscented Kalman filter and a Generalized Maximum-Likelihood type UKF (GM-UKF) for machine parameterization.
- Develop a simulated synchronous machine model to test the effectiveness of the chosen estimator.
- Investigate the performance of the UKF in the presence of innovation outliers, in this thesis inaccuracy of known parameters was considered.
- Compare the performance of the UKF and GM-UKF in the presence of observation outliers.
- Conduct a literature study of synchronous machines testing.

- Determine the parameters of laboratory synchronous generators using the IEEE 115 standard.
- Estimate a laboratory synchronous generator's steady-state parameters using a UKF.
- Develop methods to track both frequency and load angle during steady-state and transient conditions.

1.4 Thesis Organization

This thesis is divided into the following chapters: Chapter 1 provides a general background and motivation for the thesis work. It also discusses an overview of previous literature related to the scope of the research and presents the thesis objectives and structure. Chapter 2 discusses the synchronous generator modeling in both ABC and dq0 domains. Also, it presents discrete-time state-space forms of the synchronous generator. A simulated synchronous generator model is described in this chapter. Chapter 3 presents the offline testing results that were conducted on a laboratory synchronous generator. It also further explores the accuracy of these tests. Chapter 4 explains the UKF and the GM-UKF algorithms. The results of UKF performance on a simulated synchronous generator are presented in that chapter. Chapter 5 performs a sensitivity analysis of using the UKF for synchronous generator parameter estimation. It presents the results of testing the UKF in the presence of observation or innovation outliers such as noise in the measurement vector or inaccuracy of the system function for the generator where the UKF was applied. In Chapter 6, the unscented Kalman filter (UKF)-based approach is applied to estimate the parameters of the laboratory generator. Development of frequency and load angle tracking methods are presented in Chapter 6. Lastly, the estimated parameters are validated against IEEE 115 tests. Finally, Chapter 7 concludes the thesis and discusses future work.

2. Synchronous Machine Modeling

This chapter discusses synchronous generator modeling in both ABC and dq0 domains. Discrete-time state-space forms of the synchronous generator are presented in this chapter. Also, a simulated synchronous generator model is described.

2.1 Mathematical Description of the Synchronous Machine

Normally, a three-phase synchronous machine can be modeled as a lumped circuit that consists of three stator windings and three rotor circuits, as illustrated in Figure 2.1.

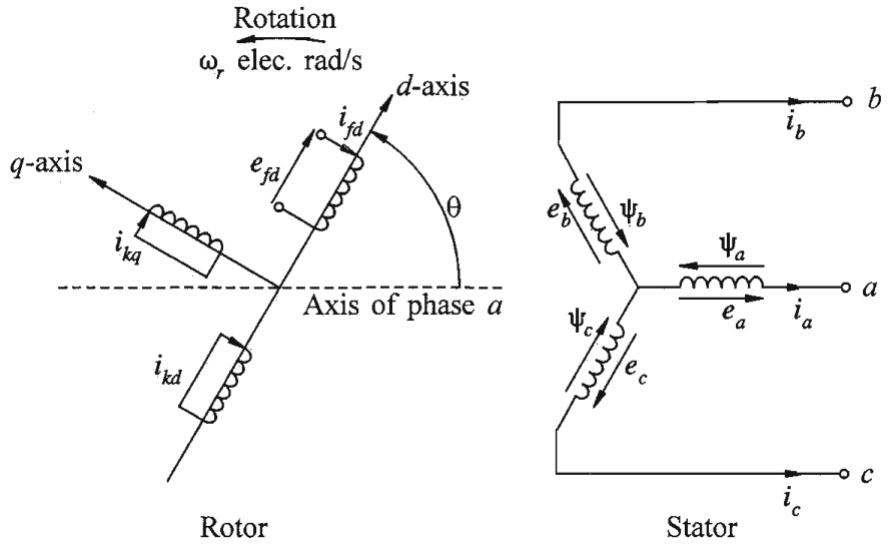

Figure 2.1: Stator and rotor circuits of a synchronous machine [2].

The stator has sinusoidally distributed three-phase windings. The three-phase windings are spaced 120 electrical degrees to induce a three-phase balanced voltage. The rotor model consists of three circuits, where two circuits are placed in the direct axis (d-axis), the field winding, and one amortisseur winding, while one amortisseur winding is placed in the quadrature axis (q-axis). The subscripts of the electrical quantities in rotor circuits f, kd, and kq are denoted for the field, amortisseur windings

in the direct axis, and amortisseur windings in the quadrature axis, respectively. Note that different rotor representations in terms of different numbers of circuits are used in various researches [2]. For the purposes of generator parameter estimation, three-rotor circuits are assumed.

Applying a direct current (DC) to the field winding produces a magnetic flux that penetrates the stator windings. Since the rotor rotates, the magnetic flux will vary with time; as a result, an emf is induced. Equations (2.1)-(2.6) describe the synchronous generator voltage equations of both rotor and stator [2].

Stator voltage equations (2.1)-(2.3):

$$v_a = \frac{d\psi_a}{dt} - i_a r_a \tag{2.1}$$

$$v_b = \frac{d\psi_b}{dt} - i_b r_b \tag{2.2}$$

$$v_c = \frac{d\psi_c}{dt} - i_c r_c \tag{2.3}$$

Rotor voltage equations (2.4)-(2.6):

$$v_{fd} = \frac{d\psi_{fd}}{dt} - i_{fd} r_{fd} \tag{2.4}$$

$$0 = \frac{d\psi_D}{dt} - i_D r_D \tag{2.5}$$

$$0 = \frac{d\psi_Q}{dt} - i_Q r_Q \tag{2.6}$$

Where ψ is the linkage flux, v is the voltage, i is the current, and r is the winding resistance. Equation (2.7) shows the stator flux linkage in phase a winding; a similar

concept will apply in phase b and c.

$$\psi_a = -l_{aa}i_a - l_{ab}i_b - l_{ac}i_c + l_{afd}i_{fd} + l_{aD}i_D + l_{aQ}i_Q \tag{2.7}$$

It is important to note that the inductance is directly proportional to the permeance, and it varies as the rotor rotates. Therefore, the self-inductance can be expressed in terms of rotor position.

$$\begin{aligned} l_{aa} &= L_{al} + L_{g0} + L_{aa2}cos(2\theta) \\ &= L_{aa0} + L_{aa2}cos(2\theta) \end{aligned} \tag{2.8}$$

Where L_{al} is the leakage inductance that accounts for the leakage flux that did not cross the air-gap, L_{g0} is the inductance that accounts for the constant component of the air-gap permeance, L_{aa2} is the inductance that accounts for the variation of the permeance with rotor position, and θ is the rotor position in electrical degrees. Figure 2.2 illustrates the behavior of the phase a self-inductance.

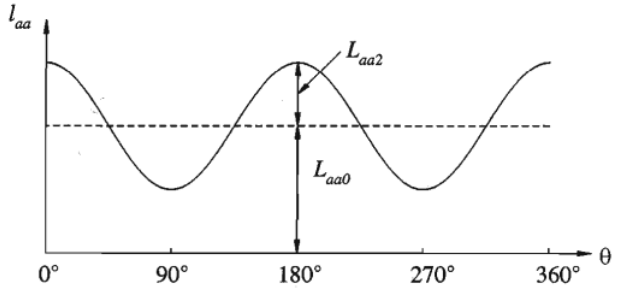

Figure 2.2: Phase a stator self-inductance variation with rotor angle [2].

As equation (2.7) indicates, other phases induce mutual fluxes in phase a; for example, the mutual inductance between phase a and b can be expressed as follows:

$$l_{ab} = l_{ba} = -L_{ab0} + L_{ab2}cos(2\theta - \frac{2\pi}{3}) \tag{2.9}$$

similarly for

$$l_{bc} = l_{cb} = -L_{ab0} + L_{ab2}cos(2\theta) \tag{2.10}$$

$$l_{ac} = l_{ca} = -L_{ab0} + L_{ab2}cos(2\theta + \frac{2\pi}{3}) \tag{2.11}$$

As mentioned previously, there is also mutual linkage flux between the rotor and the stator, which can be written as follows:

$$l_{af} = l_{fa} = L_{af}cos(2\theta) \tag{2.12}$$

$$l_{bf} = l_{fb} = L_{af}cos(2\theta - \frac{2\pi}{3}) \tag{2.13}$$

$$l_{cf} = l_{fc} = L_{cf}cos(2\theta + \frac{2\pi}{3}) \tag{2.14}$$

The equations above describe the behavior of a synchronous machine. However, it can be seen that the inductances between stator windings and stator rotor winding are mutually coupled. This coupling depends on the rotor position, which in turn varies with time. Therefore, it creates nonlinear complexity and challenges in understanding the synchronous machine and for estimating its parameters.

2.2 Park Transformation and the dq0-System Modeling

As a solution to the coupling and time-varying, a mathematical transformation is used to simplify the analysis. The Park's transformation that was proposed in [51] transforms quantities from a coupled stationary reference frame (ABC domain) to rotating reference frame (dq0). As a result, there will be no inductance variation

with rotor position. Equation (2.15) shows the Park's transformation. Where f_{abcs} is a vector of the stator quantities in ABC domain such as current and voltage, f_{dq0s} is the transformed stator quantities to dq0 domain. Lastly, θ_r is the angular position of the reference frame which can be defined as shown in equation (2.16). The ω_s is angular frequency of the stator, and δ is the load angle which can be defined as shown in Figure 2.3.

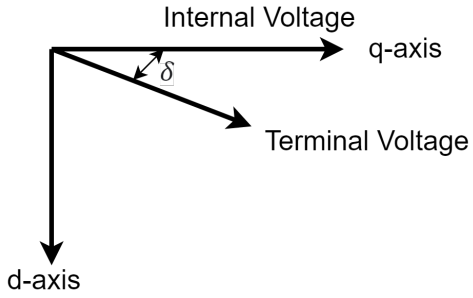

Figure 2.3: Voltage vector diagram.

$$\begin{bmatrix} f_{ds} \\ f_{qs} \\ f_0 \end{bmatrix} = \frac{2}{3} \begin{bmatrix} cos(\theta_r) & cos(\theta_r - \frac{2\pi}{3}) & cos(\theta_r + \frac{2\pi}{3}) \\ -sin(\theta_r) & -sin(\theta_r - \frac{2\pi}{3}) & -sin(\theta_r + \frac{2\pi}{3}) \\ \frac{1}{2} & \frac{1}{2} & \frac{1}{2} \end{bmatrix} \begin{bmatrix} f_{as} \\ f_{bs} \\ f_{cs} \end{bmatrix} \tag{2.15}$$

$$\theta_r = \omega_s t + \delta - \frac{\pi}{2} \tag{2.16}$$

Using the Park's transformation, equations (2.1)-(2.6) can be written as described in (2.17)-(2.22).

Stator voltage equations (2.17)-(2.19):

$$v_d = \frac{d\psi_d}{dt} - \psi_q \omega_r - r_s i_d \tag{2.17}$$

$$v_q = \frac{d\psi_q}{dt} + \psi_d \omega_r - r_s i_q \tag{2.18}$$

$$v_0 = \frac{d\psi_0}{dt} - r_s i_0 \tag{2.19}$$

Rotor voltage equations (2.20)-(2.22):

$$v_{fd} = \frac{d\psi_{fd}}{dt} + r_{fd} i_{fd} \tag{2.20}$$

$$v_D = 0 = \frac{d\psi_D}{dt} + r_D i_D \tag{2.21}$$

$$v_Q = 0 = \frac{d\psi_Q}{dt} + r_Q i_Q \tag{2.22}$$

Based on the above equations, equivalent circuits can be constructed, as illustrated in Figure 2.4. With these equivalent circuits, the analysis of synchronous machines is much simpler than in Figure 2.1. All the inductances are decoupled into two axes in these circuits without angle dependent variation, making it easier to estimate them.

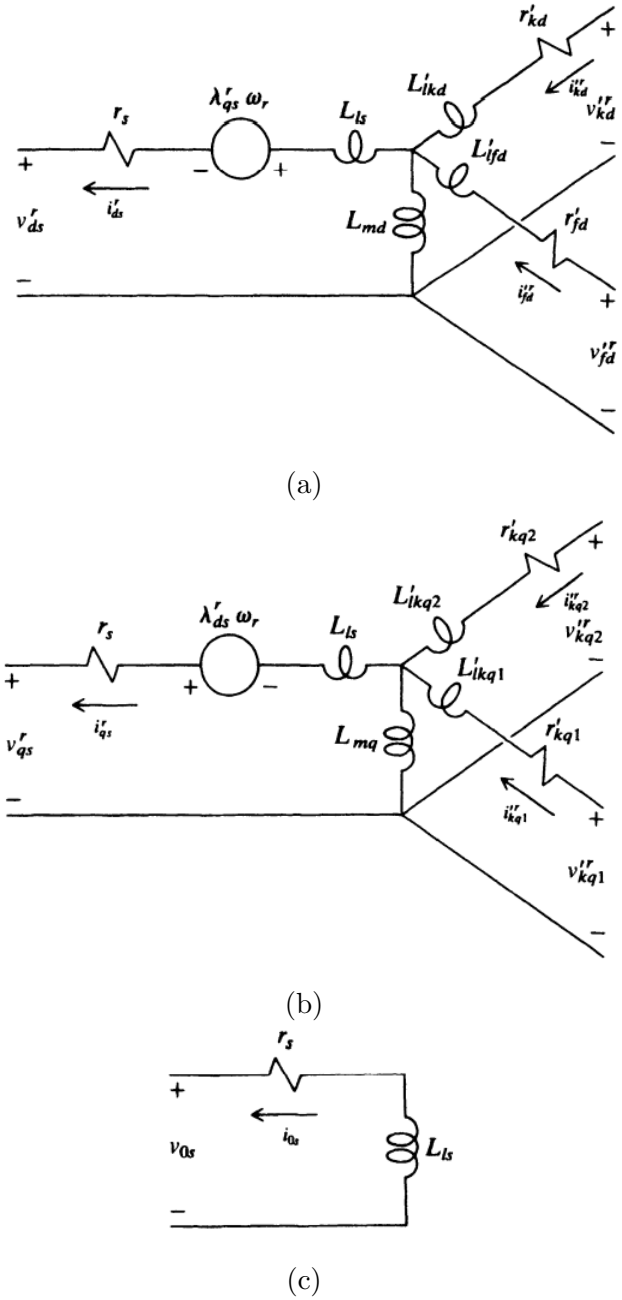

Figure 2.4: DQ0-equivalent circuits of a synchronous machine [3]: (a) Direct axis generator model equivalent circuit. (b) Quadrature axis generator model equivalent circuit. (c) Zero-sequence generator model equivalent circuit.

2.3 State-Space Synchronous Machine Model

Normally, a dynamic system can be represented by a discrete-time state-space, which can be written as

$$x_k = f(x_{k-1}, u_k) + w_k \tag{2.23}$$

$$z_k = h(x_k) + v_k \tag{2.24}$$

Where x_k and z_k are the state vector and the measurement vector at time sample k, respectively; f and h are nonlinear system and the measurement functions; v_k and w_k are the measurement and the system process noise.

As demonstrated in the literature review section, machine models of different orders can be used to estimate the machine parameters. Each choice has its own advantages and disadvantages. Using a 2^{nd}-order function to represent the machine, similar to [32, 33, 35], can reduce the number of known parameters in the system and measurement functions, but other parameters that are not accounted for can not be estimated. In this thesis, two different state-space synchronous machine models are considered. A 4^{th}-order system is considered to estimate the steady-state parameters, while the transient parameters are estimated using a 6^{th}-order system. Note that the order of the model in this thesis means the number of windings used to represent the machine. Equations (2.17)-(2.22) can be re-arranged to represent the system function.

$$\dot{\psi}_q = v_q - \omega\psi_d + \frac{r_s}{L_{ls}}(\psi_{mq} - \psi_q) \tag{2.25}$$

$$\dot{\psi}_d = v_d + \omega\psi_q + \frac{r_s}{L_{ls}}(\psi_{md} - \psi_d) \tag{2.26}$$

$$\dot{\psi}_0 = v_0 + \frac{r_s}{L_{ls}}\psi_0 \tag{2.27}$$

$$\dot{\psi}_{fd} = v_{fd} + \frac{r_{fd}}{L_{lfd}}(\psi_{md} - \psi_{fd}) \tag{2.28}$$

$$\dot{\psi}_Q = v_Q + \frac{r_Q}{L_{lQ}}(\psi_{mq} - \psi_Q) \tag{2.29}$$

$$\dot{\psi}_D = v_D + \frac{r_D}{L_{lD}}(\psi_{md} - \psi_D) \tag{2.30}$$

Where

$$\psi_{mq} = X_{aq}(\frac{\psi_q}{L_{ls}} + \frac{\psi_Q}{L_{lQ}}) \tag{2.31}$$

$$\psi_{md} = X_{ad}(\frac{\psi_d}{L_{ls}} + \frac{\psi_{fd}}{L_{lfd}} + \frac{\psi_D}{L_{lD}}) \tag{2.32}$$

$$X_{aq} = (\frac{1}{L_{mq}} + \frac{1}{L_{ls}} + \frac{1}{L_{lQ}})^{-1} \tag{2.33}$$

$$X_{ad} = (\frac{1}{L_{md}} + \frac{1}{L_{ls}} + \frac{1}{L_{lfd}} + \frac{1}{L_{lD}})^{-1} \tag{2.34}$$

Note that the change of linkage of flux with respect to time is denoted by $\dot{\psi}$.

To obtain a fully observable system, the deviations of both the angular frequency and load angle are included in the system function.

$$\dot{\omega} = \frac{1}{J}(T_m - T_e) \tag{2.35}$$

$$\dot{\delta} = \omega - \omega_s \tag{2.36}$$

In this thesis, terminal and field currents are used as the measurement function.

$$i_q = \frac{1}{L_{ls}}(\psi_{mq} - \psi_q) \tag{2.37}$$

$$i_d = \frac{1}{L_{ls}}(\psi_{md} - \psi_d) \tag{2.38}$$

$$i_0 = \frac{1}{L_{ls}}\psi_0 \tag{2.39}$$

$$i_{fd} = \frac{1}{L_{lfd}}(\psi_{fd} - \psi_{md}) \tag{2.40}$$

Equations (2.41) and (2.42) are the system and measurement functions that are used to estimate the steady-state parameters, whereas equations (2.43) and (2.44) are the input and measurement vectors of the UKF. In the case of transient parameter estimation, equations (2.45)-(2.48) are used as the system function, measurement function, input vector, and measurement vector, respectively. Further details of the online estimation are discussed in Chapter 4

$$f_{Steady-State}(x,u) = \begin{bmatrix} \dot{\psi}_d \\ \dot{\psi}_q \\ \dot{\psi}_0 \\ \dot{\psi}_{fd} \end{bmatrix} = \begin{bmatrix} v_d + \omega_r\psi_q + (r_s/L_{ls})(\psi_{md} - \psi_d) \\ v_q - \omega_r\psi_d + (r_s/L_{ls})(\psi_{mq} - \psi_q) \\ v_0 - (r_s/L_{ls})\psi_0 \\ v_{fd} + (r_{fd}/L_{fd})(\psi_{md} - \psi_{fd}) \end{bmatrix} \tag{2.41}$$

$$h_{Steady-State}(x) = \begin{bmatrix} i_d \\ i_q \\ i_0 \\ i_{fd} \end{bmatrix} = \begin{bmatrix} \frac{1}{L_{ls}}(\psi_{md} - \psi_d) \\ \frac{1}{L_{ls}}(\psi_{mq} - \psi_q) \\ \frac{1}{L_{ls}}\psi_0 \\ \frac{1}{L_{lfd}}(\psi_{fd} - \psi_{md})) \end{bmatrix} \tag{2.42}$$

$$u_{Steady-State} = \begin{bmatrix} v_d & v_q & v_0 & v_{fd} \end{bmatrix} \tag{2.43}$$

$$z_{Steady-State} = \begin{bmatrix} i_d & i_q & i_0 & i_{fd} \end{bmatrix} \tag{2.44}$$

$$f_{Transient}(x,u) = \begin{bmatrix} \dot{\psi}_d \\ \dot{\psi}_q \\ \dot{\psi}_0 \\ \dot{\psi}_{fd} \\ \dot{\psi}_D \\ \dot{\psi}_Q \\ \dot{\omega} \\ \dot{\delta} \end{bmatrix} = \begin{bmatrix} v_d + \omega_r\psi_q + (r_s/L_{ls})(\psi_{md} - \psi_d) \\ v_q - \omega_r\psi_d + (r_s/L_{ls})(\psi_{mq} - \psi_q) \\ v_0 - (r_s/L_{ls})\psi_0 \\ v_{fd} + (r_{fd}/L_{fd})(\psi_{md} - \psi_{fd}) \\ v_D + (r_D/L_{lD})(\psi_{md} - \psi_D) \\ v_Q + (r_Q/L_{lQ})(\psi_{mq} - \psi_Q) \\ (1/J)(T_m - T_e) \\ \omega - \omega_s \end{bmatrix} \tag{2.45}$$

$$h_{Transient}(x) = \begin{bmatrix} i_d \\ i_q \\ i_0 \\ i_{fd} \\ \omega \\ \delta \end{bmatrix} = \begin{bmatrix} \frac{1}{L_{ls}}(\psi_{md} - \psi_d) \\ \frac{1}{L_{ls}}(\psi_{mq} - \psi_q) \\ \frac{1}{L_{ls}}\psi_0 \\ \frac{1}{L_{lfd}}(\psi_{fd} - \psi_{md})) \\ \omega \\ \delta \end{bmatrix} \tag{2.46}$$

$$u_{Transient} = \begin{bmatrix} v_d & v_q & v_0 & v_{fd} & T_m \end{bmatrix} \tag{2.47}$$

$$z_{Transient} = \begin{bmatrix} i_d & i_q & i_0 & i_{fd} & \omega & \delta \end{bmatrix} \tag{2.48}$$

2.4 Synchronous Machine Modeling in EMTP-RV

A built-in synchronous generator model from the Electromagnetic Transient Program -Revised Version (EMTP-RV) is used to represent a real machine's response and test the online estimation techniques. To fully represent the generator response, exciter

and governor models were included. Figure 2.5 shows the system model that is used in this thesis. The generator model considered in this thesis is used to represent a single generator and focus on a single generator response during steady-state and transient conditions, whereas in a large power plant multiple generators will respond differently during disturbances, the simpler case is considered here. Two switches were connected in parallel to perform the load rejection conditions for estimating the transient parameters, which will be discussed later in Chapter 4. Tables 2.1 and 2.2 list the ratings of the simulated synchronous generator and its parameters. IEEE type 3 governor model parameters and exciter parameters are listed in Tables 2.3 and 2.4. The EMTP-RV schematic of the system is illustrated in Appendix A.

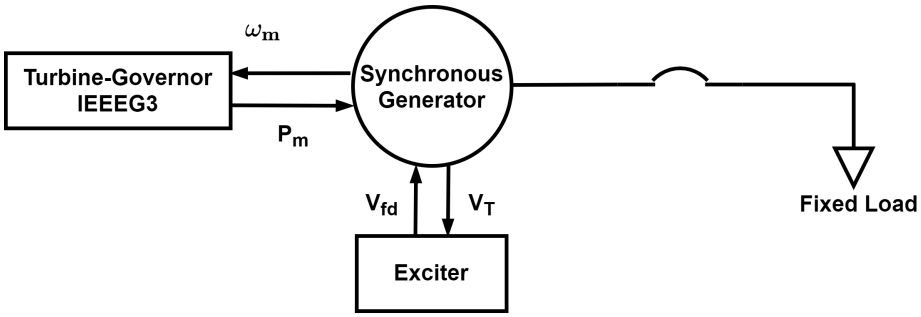

Figure 2.5: System model.

Table 2.1: Simulated generator nameplate data.

Symbol	Description	Value	Unit
$S_{3\theta}$	Apparent power	175	MVA
V_T	L-L terminal voltage	14.7	kV
I_L	Line current	3.8732	kA
I_{DC}	Field current base	1	kA

The online estimation techniques are implemented in MATLAB. Therefore, a set of measurements is exported from EMTP-RV in MAT format. The measurements are defined as follows:

$$Measurements = [V_{dq0}, I_{dq0}, V_{abc}, I_{abc}, V_{fd}, I_{fd}, \omega_{rotor}, \delta, T_m]$$

Table 2.2: Simulated generator model parameters.

Parameter	Value (pu)	Parameter	Value (pu)
R_a	0.0015	L_{lD}	0.2
X_d	1.13	L_{lq}	0.122
X_q	0.66	r_D	0.0212
X_l	0.1	r_q	0.015
X_{lf}	0.25	r_{fd}	5.77×10^{-4}

Table 2.3: IEEE type 3 governor model parameters.

Symbol	Description	Value	Unit
T_G	Time constant	0.2	s
T_P	Time constant	0.01	s
T_R	Time constant	2	s
$SIGMA$	Permanent droop	0.06	pu
DELTA	Temporary droop	0.2	pu
U_0	Maximum opening velocity	0.2	pu/s
U_C	Maximum closing velocity	-0.1	pu/s
P_{MAX}	Maximum value opening	0.9	pu
P_{min}	Minimum value opening	0.2	pu

Where V_{abc} and I_{abc} are the instantaneous voltages and currents in the ABC domain, V_{dq0} and I_{dq0} are the instantaneous voltages and currents in the dq0 domain, and V_{fd} and I_{fd} are the field voltage and current. The rotor angular frequency and load angle are denoted by ω_{rotor}, δ. Lastly, the mechanical torque of the generator is denoted by T_m.

Table 2.4: Exciter model parameters.

Symbol	Description	Value	Unit
K	Gain	100	pu
T_E	Time constant	0.05	s
E_{MAX}	Maximum exciter output	5	pu
E_{MIN}	Minimum exciter output	-5	pu

3. Determination of Synchronous Generator Parameters Using Off-line Testing

This chapter presents the offline testing results that were conducted on a synchronous laboratory generator. The objective of the test is to find the steady-state and transient parameters. In this chapter, suspected error of tested parameters are discussed.

3.1 Synchronous Generator Nameplate Data

Figure 3.1 shows the motor-generator set used in this thesis. A 1200 rpm, 13.5 kVA synchronous generator is driven by a 15 hp dc motor.

Figure 3.1: Motor-generator set with synchronous generator driven by a DC motor.

The synchronous generator has a rating of 13.5kVA and two terminal voltage ratings, 120V and 220V, based on the connection of the windings. Table 3.1 shows the rating information for the tested synchronous generator. The same synchronous generator will be tested for an online estimation, which will be presented in Chapter 6.

Table 3.1: Generator nameplate data.

Symbol	Description	Value	Unit
$S_{3\theta}$	Apparent power	13.5	kVA
V_T	L-L terminal voltage	220	V
I_L	Line current	35.4	A
V_{DC}	Excitation voltage	74.4	V
I_{DC}	Excitation current	8	A

3.2 Off-Line Testing

The following testings were conducted on synchronous laboratory generator:

- Open-Circuit and Short-Circuit Tests.
- Slip Test.
- Load Rejection Test.

3.2.1 Open-Circuit and Short-Circuit Tests

The open circuit is obtained by operating the generator at rated speed and open-circuited stator windings with the field excited to produce different terminal voltages. Terminal voltage and field voltage are recorded for different voltage sets. As the IEEE 115 standard recommends, a minimum of six readings were taken to obtain open-circuit characteristics [16]. The readings are distributed as follows:

- Six readings must be taken below 0.6 pu of the rated voltage, including one reading at zero excitation.
- Ten readings must be taken from 0.6 pu to 1.1 pu with 0.05 pu increments.
- Two of the readings are above 1.1 pu, including one reading at 1.2 pu

From the above readings, the open circuit characteristic (OCC) curve can be plotted with the air-gap line, which is defined as a linear line that has the maximum slope of the OCC curve, as shown in Figure 3.2.

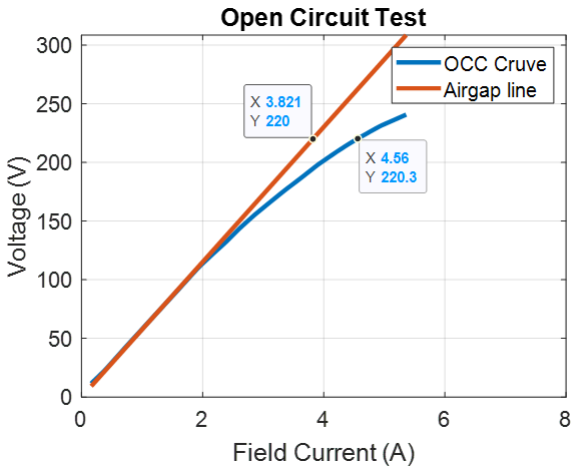

Figure 3.2: Open-circuit saturation curve.

The short-circuit test is considered complementary to the open-circuit test. The short circuit test is conducted by operating the generator at rated speed with the short-circuited stator windings. As the IEEE standard recommended, a minimum of five terminal and field currents readings must be taken starting at approximately 1.25 pu, 1 pu, 0.75 pu, 0.5 pu, and 0.25 pu of rated current. Figure 3.3 shows the short-circuit saturation curve (SCSC) of the tested generator.

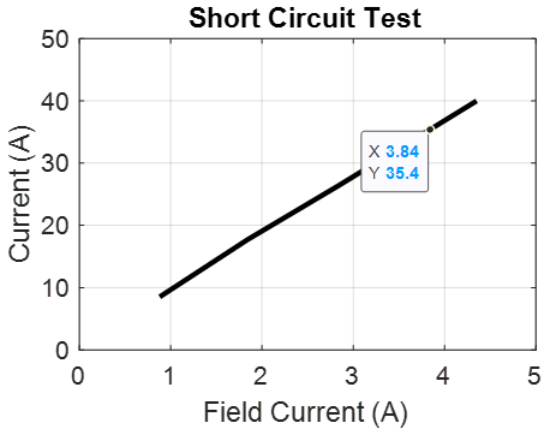

Figure 3.3: Short-circuit saturation curve.

From Figures 3.2 and 3.3, the unsaturated direct axis synchronous reactance can be obtained as follows:

$$X_{du} = \frac{I_{FSI}}{I_{FG}} = \frac{3.84\ A}{3.821\ A} = 1.005\ pu \tag{3.1}$$

Where X_{du} is the per-unit unsaturated synchronous reactance, I_{FSI} is denoted for the field current that produces the base terminal current on the short-circuit saturation curve, and I_{FG} is the field current that produces the rated terminal voltage on the air-gap line.

3.2.2 Slip Test

The slip test is implemented to determine the saliency ratio, which is defined as X_q/X_d. After that, the X_{du}, the value from OCSC, can be multiplied by this ratio to obtain X_q. As IEEE 115 recommends, the slip test was conducted by operating the rotor at a speed slightly different from the synchronous speed, typically less than 1%, with open an circuited field winding. Then, a three-phase voltage was applied to the terminal. Terminal voltage and current are recorded for several tests with different terminal voltage points, then the average X_{qu} was calculated. Figure 3.4 shows one case of slip test where the oscillation of both terminal current and voltage can be seen. More tests are illustrated in Appendix B. When the direct axis of the rotor is in line with the stator magnetomotive force, the current will be at its minimum. Also, when the quadrature axis of the rotor is in line with the stator magnetomotive force, the current will be at its maximum. This is because X_d is larger than X_q in salient pole synchronous generators. Equation (3.2) is used to calculate X_q.

$$X_{qu} = X_{du}\frac{E_{min}}{E_{max}}\frac{I_{min}}{I_{max}} \tag{3.2}$$

Where E_{min} and E_{max} are denoted for the minimum and maximum value of the

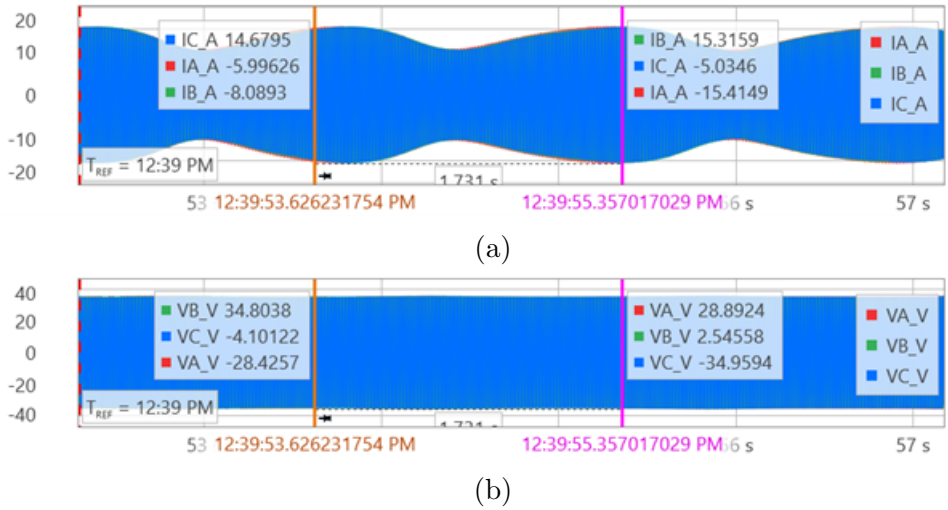

Figure 3.4: Slip test results: (a) Terminal current (b) Terminal voltage.

line to neutral terminal voltage, I_{min} and I_{max} are the minimum and maximum value of terminal current, and X_{du} is the per-unit unsaturated synchronous reactance. The average value of X_q from multiple slip tests is 0.65 pu.

3.2.3 Load Rejection Test

The load rejection test is performed by opening the main circuit breaker with the generator loaded. The load rejection can be conducted to determine both q-axis and d-axis parameters with different operating points. In this thesis, a capacitive load rejection was performed to determine the d-axis transient and sub-transient parameters. At this condition, the load angle was approximately equal to zero. Hence the active power is zero. The speed was kept constant, and DC voltage was set to be constant during the load rejection. The terminal voltage can be expressed as follows:

$$V_t = V_q = V_0 - [X_d - (X_d - X'_d)e^{\frac{-t}{T'_{d0}}} - (X'_d - X''_d)e^{\frac{-t}{T''_{d0}}}]I_0 \tag{3.3}$$

Where V_t is the peak time-variant magnitude of the terminal voltage, V_0 and I_0 are the initial magnitudes value of the terminal voltage and current before opening the breaker, and X_d, X'_d , and X''_d denote direct-axis synchronous, transient, and

sub-transient reactances. Lastly, T'_{d0} and T''_{d0} are the direct-axis transient and sub-transient open-circuit time constants.

Equation (3.3) can be re-written as follows:

$$V_t = V_{q\infty} + V'_{q0}e^{\frac{-t}{T'_{d0}}} + V''_{q0}e^{\frac{-t}{T''_{d0}}} \tag{3.4}$$

where $V_{q\infty}$ is the steady state voltage after circuit breaker is opened and V'_{q0} and V''_{q0} are the initial values of the transient and sub-transient voltage. It is important to note that the generator was operated under-excited to obtain the unsaturated parameters. The terminal voltage, terminal current, field voltage, and field current were collected using the data acquisition testbed described in Chapter 6. After that, all the measurements were imported to MATLAB to transform the terminal measurements from the ABC domain to the dq0 domain using the zero-crossings method, which will also be described in Chapter 6. A finite impulse response low pass filter with a 90 Hz cut-off frequency was used. Figure 3.5 shows zoomed-in waveforms of the q-axis voltage and the d-axis current during the load rejection.

A nonlinear least-squares solver was used on equation (3.4) to find the $V_{q\infty}$, V'_{q0}, V''_{q0}, T'_{d0}, and T''_{d0}. The voltage of q-axis (V_q) was used as measurement for the solver to find the best curve fit that satisfied equation (3.4). Figure 3.6 shows the filtered and the raw V_q measurements plotted with the best fit data, which is the result from the solver.

It can be seen from Figure 3.6 that the fitted curve and filtered V_q are at the center of the raw V_q. The oscillation in the V_q is due to the slightly unbalanced condition on the generator. As a result, negative sequence currents appear in addition to the dominant positive sequence current. The negative sequence current and voltage appear as a double frequency (120 Hz in this case) ripple in the positive sequence rotation synchronous reference frame.

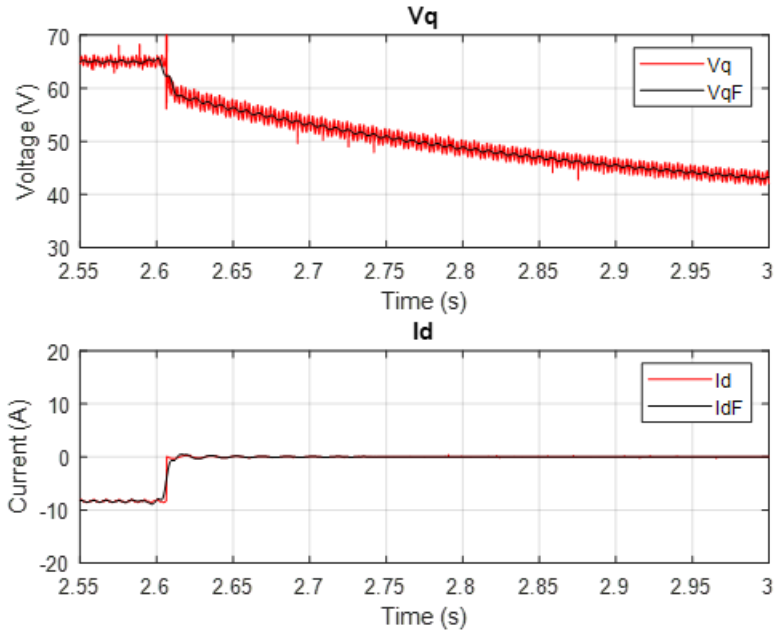

Figure 3.5: Comparison between the raw and filtered q-axis voltage and the d-axis current.

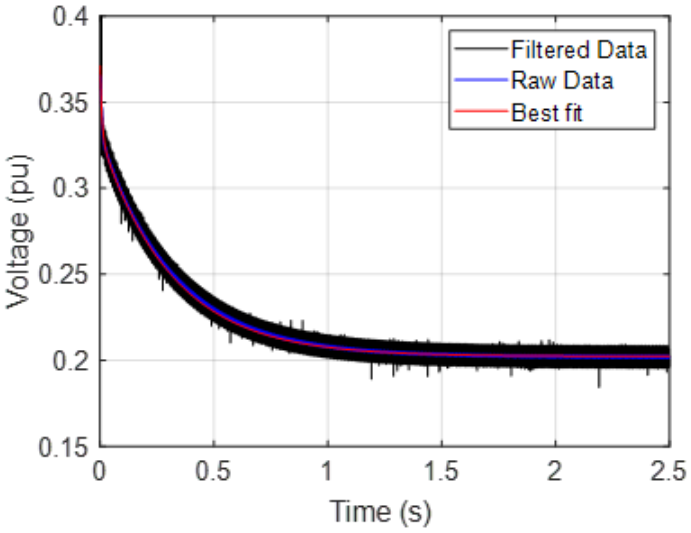

Figure 3.6: Magnitude of the terminal voltage response during load rejection of a purely capacitive load.

According to the IEEE 115 standard, the direct-axis synchronous, transient, and sub-transient reactance can be obtained as follows:

$$\begin{aligned} X_d &= \frac{V_0 - V_{q\infty}}{I_0} \\ X'_d &= X_d - \frac{V'_{q0}}{I_0} \\ X''_d &= X'_d - \frac{V''_{q0}}{I_0} \end{aligned} \tag{3.5}$$

Table 3.2 presents the d-axis steady-state, transient, and sub-transient parameters from the load rejection test.

Table 3.2: Load rejection test result.

Symbol	Description	Value	Unit
X_d	Direct-axis synchronous reactance	0.993	pu
X'_d	Direct-axis transient reactance	0.225	pu
X''_d	Direct-axis sub-transient reactance	0.015	pu
T'_{d0}	Direct-axis transient open-circuit time constants	0.3145	s
T''_{d0}	Direct-axis sub-transient open-circuit time constant	0.008	s

Note that X_d obtained from open-and short-circuit tests is very close to the X_d from the load rejection test. From these parameters, the fundamental parameters such as X_{ls} and X_{lfd} can be calculated using mathematical relations as shown in [52].

3.3 Accuracy of Off-Line Testing

The parameters from the test result of Section 3.2 have their margins of error. X_d and X_q vary depending on the saturation level the machine operates at. The saturated values will be less than the unsaturated parameters from the test. Table 3.3 shows a comparison of the manufacturer and tested parameters for three large machines. This result was presented in IEEE 1110 to show the expected accuracy of the offline

testing [53].

Table 3.3: Comparison of manufacturer and tested parameters.

Parameter	S/G 1			S/G 2			S/G 3		
	Mea (pu)	Manuf (pu)	Error (%)	Mea (pu)	Manuf (pu)	Error (%)	Mea (pu)	Manuf (pu)	Error (%)
X_d	1.02	1.14	10.44	1.1	1	10.4	1.31	1.32	1.14
X_q	0.54	0.63	14.13	0.42	0.62	32.9	0.47	0.8	40.75

Since the synchronous laboratory generator has no manufacturer parameters available, a second method is used to determine the q-axis synchronous reactance to compare the X_q from the slip test result. The encoder is used to calculate the load angle, as will be discussed in detail in Chapter 6. The load angle can then be used with the voltage and current measurement to determine X_q as shown in equation (3.6)

$$\delta = \arctan \frac{X_q I_a \cos(\phi)}{V_a + X_q I_a \sin(\phi)} \tag{3.6}$$

A comparison of the two methods for calculating q-axis synchronous reactance is illustrated in Table 3.4. As can be seen, the percentage difference of X_q changes as the operation points change. The calculated X_q from the encoder has a smaller difference relative to the X_q from slip test in the case of leading power factor. A balanced three-phase set of stator currents is assumed in equation (3.6). However, the tested generator produces a slightly unbalanced three-phase current. For example, case 1 has the following peak currents:

$$I_a = 32.64\,A \qquad I_b = 34\,A \qquad I_c = 35.96\,A \tag{3.7}$$

A source of error in the slip test is the current induced in the amortisseur winding. The slip test does induce a current in the amortisseur winding, but if the slip frequency is extremely low, the error can be minimized. However, the standing unbalanced condition on the generator also induces an additional current in the amortisseur

winding, which contributes to degrading the accuracy of the test result.

Table 3.4: Comparison of two methods of calculating q-axis synchronous reactance.

X_q	Case 1 $\delta = 65.5°$ pf = 0.89 leading		Case 2 $\delta = 47°$ pf = 0.994 lagging		Case 3 $\delta = 21.1°$ pf = 0.999 unity		Case 4 $\delta = 20.78°$ pf 0.9151 leading	
Slip Test (pu)	Using Encoder (pu)	difference (%)	Using Encoder (pu)	difference (%)	Using Encoder (pu)	difference (%)	Using Encoder (pu)	difference (%)
0.65	0.71	8.33	0.87	25.1	0.83	22.1	0.74	11.82

Varying harmonic content was seen in the current waveform from the slip test, unlike the typical behavior observed during the other slip tests in the literature. Figure 3.7 shows the current waveform during the slip test. It is noticeable that harmonics effect the magnitude of the current which will degrade the accuracy of the X_q determination. Figure 3.8 show a zoomed-in figure of the current waveform.

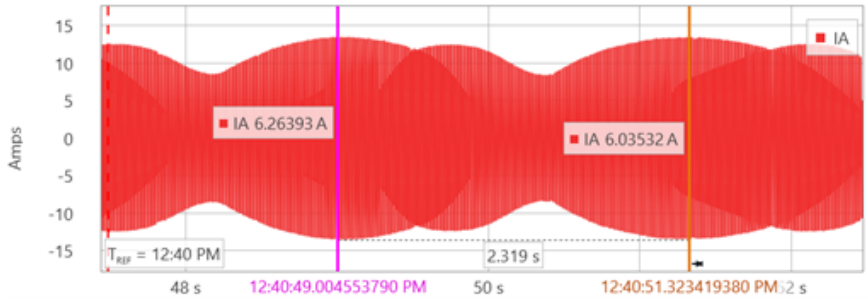

Figure 3.7: Slip test current waveform

Another source of error in the load rejection test is neglecting the voltage drop across the stator resistance in equation (3.3). Usually, the large machine has very small stator resistance relative to the reactance terms; the voltage across the stator resistance is not significant. However, the synchronous laboratory generator has a significant stator resistance, and neglecting the stator resistance will contribute to the load rejection test error. Also, the assumption of a load angle of zero and insignificant stator terminal real power during the capacitive load rejection is no longer valid. As a result, a slightly noticeable change in the frequency was seen during the load rejection.

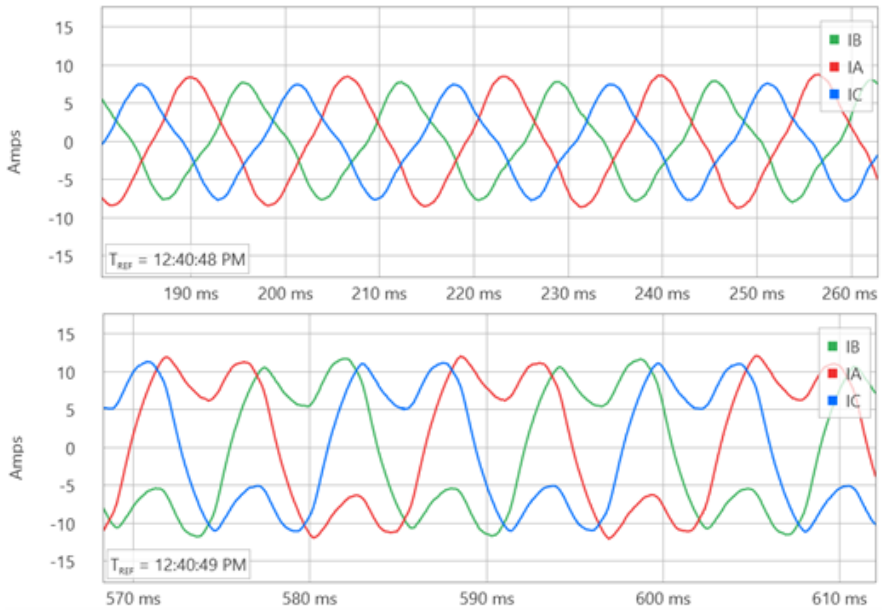

Figure 3.8: Slip test zoomed-in current waveform

3.4 Summary

The nameplate data of a synchronous laboratory generator that was used in this thesis was presented. The results of several offline tests conducted to determine the parameters of the laboratory synchronous generator were presented. This chapter explores the accuracy of these tests. The aforementioned generator will be used in the online estimation technique.

4. Online Parameter Identification

Various researchers have proposed online parameter identification methods for synchronous generators. The unscented Kalman filter (UKF) has shown optimistic results in the field of parameter estimation. This chapter presents the algorithm of the UKF as well as the Generalized Maximum-Likelihood-type UKF (GM-UKF). In this chapter, the performance of the UKF in parameter estimation was tested using a simulated synchronous machine.

4.1 The Unscented Kalman Filter

The UKF is a recursive discrete-time filter used to solve estimation problems represented in the following form:

$$x_k = f(x_{k-1}, u_k) + w_k \tag{4.1}$$

$$z_k = h(x_k) + v_k \tag{4.2}$$

Where x_k and z_k are the state vector and the measurement vector at time sample k, respectively; f and h are nonlinear system and the measurement functions; v_k and w_k are the measurements and the system process noise with zero mean and uncorrelated covariance matrices R_k and Q_{k-1} [30]. In other words, the noise is assumed Gaussian, independent, and identically distributed. The UKF is based on a deterministic sampling technique known as the unscented transformation, which uses a selected set of sample points named sigma points. Under the Gaussian noise assumption, the sigma points are propagated through the non-linear system model and the measurement functions to determine the posterior state mean and its covariance. Therefore, the Jacobian matrix calculation is not needed, and higher linearization order can be obtained.

The UKF algorithm consists of three major steps: sigma point calculation, state prediction, and state correction.

4.1.1 Sigma Point Calculation

After initializing the $n \times 1$ state vector, x, and its $n \times n$ covariance matrix, P, the sigma point can be calculated as described in (4.3)-(4.5).

$$X_{k-1}^{0} = x_{k-1} \tag{4.3}$$

$$X_{k-1}^{n+i} = x_{k-1} - (\sqrt{(n+\lambda)P_{k-1}})_i, \quad i = 1, ..., n \tag{4.4}$$

$$X_{k-1}^{n+i} = x_{k-1} + (\sqrt{(n+\lambda)P_{k-1}})_i, \quad i = 1, ..., n \tag{4.5}$$

Equations (4.3)-(4.5) can be constructed in compact form as follows:

$$X_{k-1}^{-} = [x_k^- \ ... \ x_k^-] + \sqrt{c}[0 \ \sqrt{P_k^-} \ - \sqrt{P_k^-}] \tag{4.6}$$

Where $c = \lambda + n$, and λ is defined as $\lambda = \alpha^2(n + \kappa) - n$. The parameter κ is used to reduce the higher-order errors of the estimation, with default values of $3 - n$ or zero [54]. The α is a scaling parameter that determines the spread of the sigma points around the state mean with typical range of 0.001 - 1 p.u. Note that the matrix $\sqrt{P_k}$ is obtained from the Cholesky factorization technique.

4.1.2 State Prediction

The calculated sigma points are propagated through the prediction function, also known as a system function, defined in (4.7).

$$\hat{X}_k = f(X^i_{k-1}, u_k) \tag{4.7}$$

After that, the predicted state mean vector and predicted covariance matrix are computed as follows:

$$\tilde{x}^-_k = \sum_{i=0}^{2n} W^m_i \hat{X}^i_k \tag{4.8}$$

$$P^-_k = \sum_{i=0}^{2n} W^c_i [(\hat{X}^i_k - \tilde{x}^-_k)(\hat{X}^i_k - \tilde{x}^-_k)^T] + Q_{k-1} \tag{4.9}$$

Where the weights W^m and W^c can be computed as in equations (4.10)-(4.11).

$$W^m_0 = \frac{\lambda}{n+\lambda}, W^c_0 = \frac{\lambda}{n+\lambda}(1 - \alpha^2 + \beta) \tag{4.10}$$

$$W^m_i = W^c_i = \frac{\lambda}{2(n+\lambda)} \tag{4.11}$$

The parameter β has a typical value of two [54].

4.1.3 State Correction

In this step, the sigma points are re-generated using the predicted state mean vector and its covariance from the previous step. Next, these sigma points are propagated through the measurement function as shown in (4.12)

$$\hat{Y}^{i-}_k = h(X^{-i}_k) \tag{4.12}$$

The calculated measurement mean vector is obtained as follows:

$$\tilde{y}_k = \sum_{i=0}^{2n} W^m_i \hat{Y}^{-i}_k \tag{4.13}$$

Then, the covariance matrix of the measurement and the cross-covariance of the

state and measurement are computed as follows:

$$S_k = \sum_{i=0}^{2n} W_i^c [(\hat{Y}_k^{i-} - \tilde{y})(\hat{Y}_k^{i-} - \tilde{y})^T] + R_k \tag{4.14}$$

$$C_k = \sum_{i=0}^{2n} W_i^c [(\hat{X}_k^{-i} - \tilde{x}_k^-)(\hat{Y}_k^{-i} - \tilde{y}_k)^T] \tag{4.15}$$

Lastly, the filter gain vector, K_k, the corrected state vector, x_k, and the state covariance matrix, P_k, are calculated as follows:

$$K_k = C_k S_k^{-1} \tag{4.16}$$

$$x_k = \tilde{x}_k^- + K_k[z_k \ - \tilde{y}_k] \tag{4.17}$$

$$P_k = P_k^- + K_k S_k K_k^T \tag{4.18}$$

4.2 Generalized Maximum-Likelihood-Type UKF

Several robust state estimation methods have recently been developed to replace dynamic estimators such as the Extended Kalman Filter (EKF) and the UKF, and to compensate for their shortcomings [55–58]. Both EKF and UKF assume Gaussian probability distributions for the process and observation noise. However, conducted studies raise a question about the validity of that assumption, where non-Gaussian errors were measured from PMU devices [1,13]. The Generalized Maximum-Likelihood-Type UKF (GM-UKF) proposed in [55] has proven its robustness against outliers and the effect of non-Gaussian noise. This section presents the GM-UKF algorithm. The following four major steps describe the GM-UKF algorithm:

- Step 1: Construct a Batch-Mode Regression Form.
- Step 2: Pre-whitening the Noise.
- Step 3: Regression State Estimation.
- Step 4: Updating the Error Covariance Matrix.

4.2.1 Construct a Batch-Mode Regression Form

The batch-mode regression form can be obtained using the predicted state mean vector and the calculated measurement mean vector combined with the measurement vector.

$$\begin{bmatrix} z_k + H_k\tilde{x}_k^- - \tilde{y}_k \\ \tilde{x}_k^- \end{bmatrix} = \begin{bmatrix} H_k \\ I \end{bmatrix} x_k + \begin{bmatrix} v_k + \nu_k \\ \delta_k \end{bmatrix} \tag{4.19}$$

$$H_k = C_k^T P_k^{-1} \tag{4.20}$$

Where δ_k is denoted for the prediction error, v_k for the measurement error, and ν_k for the statistical linearization error.

For simplicity, the equation (4.19) can be rewritten in a compact form as follows:

$$\tilde{z}_k = \tilde{H}_k x_k + \tilde{e}_k \tag{4.21}$$

4.2.2 Pre-whitening the Noise

In this step, the state prediction error is uncorrelated by multiplying both sides of equation (4.21) by S^{-1} as shown in equation (4.22) which can be re-written in a compact form as shown in (4.23). Where S can be obtained from equation (4.24) using the Cholesky decomposition technique.

$$S_k^{-1}\tilde{z}_k = S_k^{-1}\tilde{H}_k x_k + S_k^{-1}\tilde{e}_k \tag{4.22}$$

$$y_k = G_k x_k + \xi_k \tag{4.23}$$

Where $E[\xi_k \xi_k^T] = \mathrm{I}$.

$$E(\tilde{e}_k \tilde{e}_k^T) = \begin{bmatrix} \Sigma_k & 0 \\ 0 & P_k \end{bmatrix} = S_k S_k^T \tag{4.24}$$

4.2.3 Regression State Estimation

First, the weights are calculated by applying the Projection Statistics (PS) method to a 2-dimensional matrix. The PS method was proposed in [59], where it showed its effectiveness to detect outliers. The 2-dimensional matrix can be constructed as follows:

$$M_k = \begin{bmatrix} z_{k-1} - h(\tilde{x}_{k-1}^-) & z_k - h(\tilde{x}_k^-) \\ \tilde{x}_{k-1}^- & \tilde{x}_k^- \end{bmatrix} \tag{4.25}$$

Where the first row is innovation vectors, and the second row is the predicted state vector. Equation (4.26) expresses the mathematical form of PS.

$$PS_j = \max_{||\mu||=1} \frac{l_j^T\ \mu - med_i\ (l_i^T\ \mu)}{1.4826\ \ med_k\ |l_k^T\ \mu - med_i\ (l_i^T \mu)|} \quad i, j, k = 1, 2, ..., m+n. \tag{4.26}$$

Where l_j^T is denoted for the jth row vector of M_k and μ denotes a set of directions originating from the M_k coordinate-wise median. A pre-defined statistical threshold is compared with the PS data points to detect the outliers as shown in equation (4.27).

$$\bar{w} = min(1, d^2/PS_i^2) \tag{4.27}$$

Next, the GM-estimator is used, which minimizes the following function:

$$J = \sum_{i=1}^{m+n} \bar{w}_i^2 \rho(r_{S_i}) \tag{4.28}$$

$$r_{S_i} = \frac{r_i}{s\bar{w}} \tag{4.29}$$

Where $r_i = y_i - g_i^T \tilde{x}_k^-$, g_i^T is the i^{th} row vector of the matrix G_k and s is a robust scale estimate, which is defined as $s = 1.4826 \cdot b_m \cdot median_i|r_i|$. A correction factor denoted by b_m is used to obtain unbiasedness [59]. In this thesis, the convex Huber-ρ function is used.

$$\rho(r_{s_i}) = \begin{cases} \frac{1}{2} r_{s_i}^2, & \text{for } |r_{s_i}| < c_m \\ c_m |r_{s_i}| - c_m^2/2, & \text{else} \end{cases} \tag{4.30}$$

Where the Huber threshold parameter is denoted by c_m, and it has a typical value between 1.5 to 3. The partial derivative is taken with respect to x_k in (4.28) and setting to zero, results in:

$$\frac{\partial J(x_k)}{\partial x_k} = \sum_{i=1}^{m+n} \frac{\bar{w}_i c_m}{s} \psi(r_{s_i}) = 0 \tag{4.31}$$

$$\psi(r_{s_i}) = \frac{\partial \rho(r_{s_i})}{\partial r_{s_i}} \tag{4.32}$$

Equation (4.31) can be rearranged by multiplying and dividing r_{s_i} on both sides to obtain the following equation:

$$G_k^T \hat{Q}(y_k - G_k x_k) = 0 \tag{4.33}$$

Where $\hat{Q} = diag(\psi(r_{s_i}))/(r_{s_i})$.

Iteratively reweighted least squares method (IRLS) is used on equation (4.35) to solve for x_k.

$$x_k^{j+1} = (G_k^T \bar{Q}^j)^{-1} G_k^T \bar{Q}^j y_k \tag{4.34}$$

Where the algorithm convergence can be set as $||x_k^{j+1} - x_k^j|| < 10^{-2}$.

4.2.4 Updating the Error Covariance Matrix

Last step is updating the state covariance matrix which is obtained as:

$$P_k = 1.0369(G_k^T G_k)^{-1}(G_k^T Q_{\bar{w}} G_k)(G_k^T G_k)^{-1} \tag{4.35}$$

Where $Q_{\bar{w}} = diag(\bar{w_i}^2)$

The 1.0369 factor is used if c_m is set to be 1.5. More details on updating the state covariance matrix are provided in [60]

4.3 UKF Algorithm Results

First, all the required measurements were imported from the EMTP-RV model to MATLAB, where the UKF is developed to estimate both steady-state and transient parameters of the synchronous generator simulated in EMTP-RV. A 4^{th}-order state-space generator model is used to estimate the steady-state parameters, while a 6^{th}-order state-space generator model is implemented to estimate the transient parameters. Both models were derived in Chapter 2.

4.3.1 Estimating Steady-State Parameters

The steady-state measurement was collected from the EMTP-RV model to be used as input and output vectors of the UKF. Table 4.1 shows an operating condition for the simulated synchronous generator.

Table 4.1: Simulated generator operating condition.

V_d (kV)	V_q (kV)	I_d (kA)	I_q (kA)	Power Factor	Load Angle (Degrees)
5.993	10.399	4.243	7.363	Unity	29.95

In this thesis, the UKF covariance matrices for estimating the generator steady-state parameter were set as shown in equations (4.36) - (4.38).

$$Q = diag([10^{-9}\ \ 10^{-9}\ \ 10^{-9}\ \ 10^{-9}\ \ 10^{-9}\ \ 10^{-9}]) \tag{4.36}$$

$$R = diag([10^{-9}\ \ 10^{-9}\ \ 10^{-9}\ \ 10^{-9}]) \tag{4.37}$$

$$P = diag([10^{-8}\ \ 10^{-8}\ \ 10^{-8}\ \ 10^{-7}\ \ 10^{-8}\ \ 10^{-8}]) \tag{4.38}$$

Where the states and the output vectors are ordered as:

$$x = [\psi_d; \psi_q; \psi_0; \psi_{fd}; L_{md}; L_{mq}]; \tag{4.39}$$

$$z = [i_d; i_q; i_0; i_{fd}]; \tag{4.40}$$

In this case, both the stator and field leakage inductances are kept as constants since they are immune from the saturation effect. Therefore, only L_{md} and L_{mq} were estimated as steady-state parameters due to their dependence on the saturation effect. Figures 4.1 and 4.2 show the estimated fluxes versus time. A fast convergence can be

seen in Figure 4.3, where both L_{md} and L_{mq} converged to their actual value after 0.02 s. Figures 4.4 and 4.5 show the calculated measurement from the estimated states. Table 4.2 shows a summary of the steady-state parameter estimation. It can be seen that the UKF shows its effectiveness under conditions with high-accurate system and measurement functions.

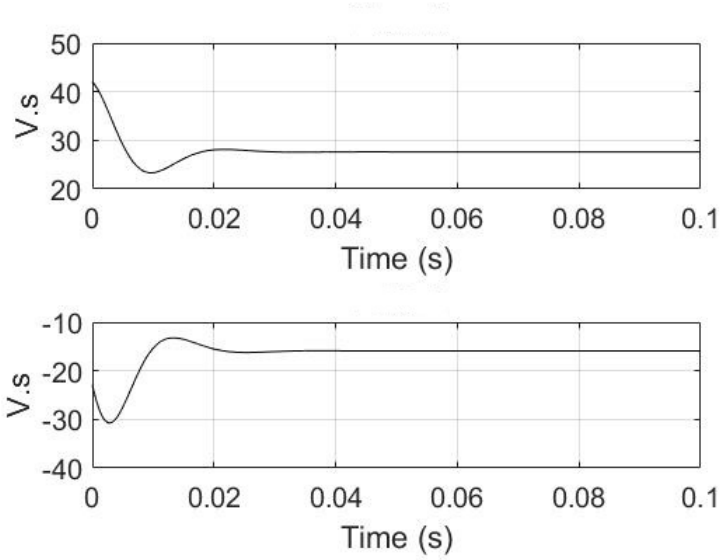

Figure 4.1: State estimation results for ψ_d (upper traces) and ψ_q (lower traces).

Table 4.2: Steady-state parameter estimation.

Parameter	L_{md}	L_{mq}
Initial Guess Error	50%	50%
Actual Value	3.374mH	1.834mH
Estimated Values	3.375mH	1.835mH
Error (%)	0.0296	0.0545

4.3.2 Estimating Transient Parameters

A 6^{th}-order model is used to obtain the transient parameters. In order to observe the transient parameters, the synchronous generator must be subjected to a transient event. In this case, a load rejection was simulated to imitate a scenario that can

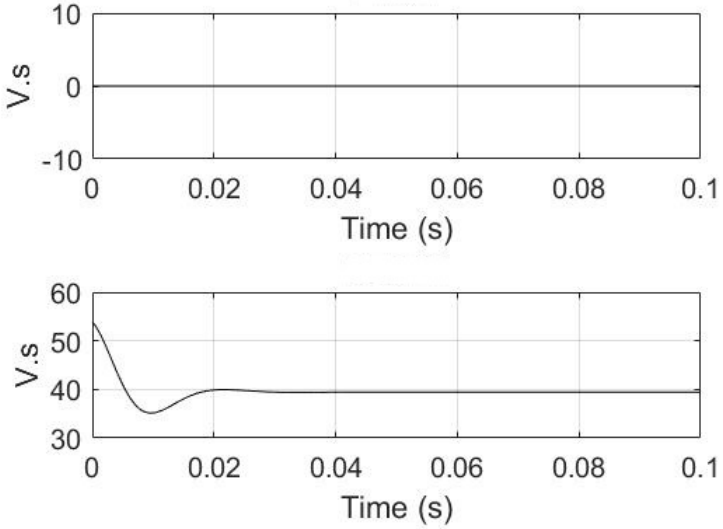

Figure 4.2: Steady-state estimation results for ψ_0 (upper traces) and ψ_{fd} (lower traces).

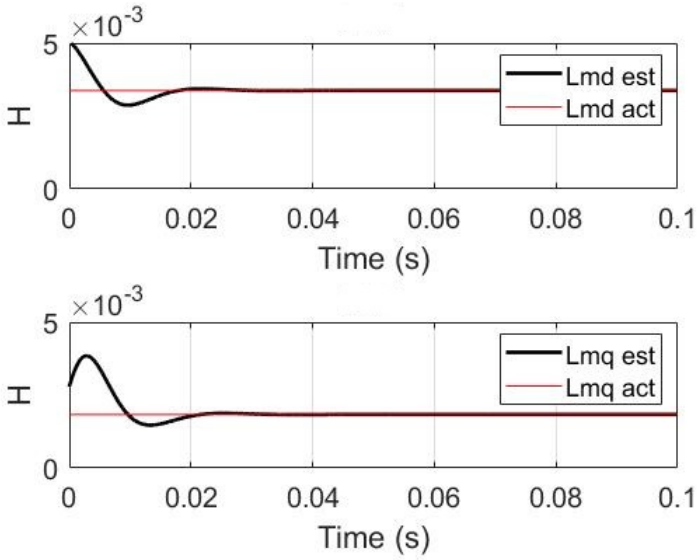

Figure 4.3: Comparing true and estimated parameters for magnetizing inductances in d-and q-axes.

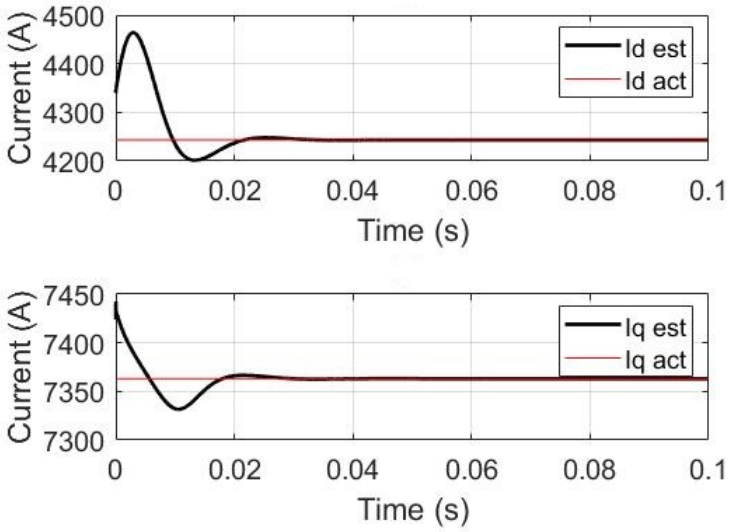

Figure 4.4: Comparing measured current to calculated current from estimated parameters for stator d-and q-axes currents.

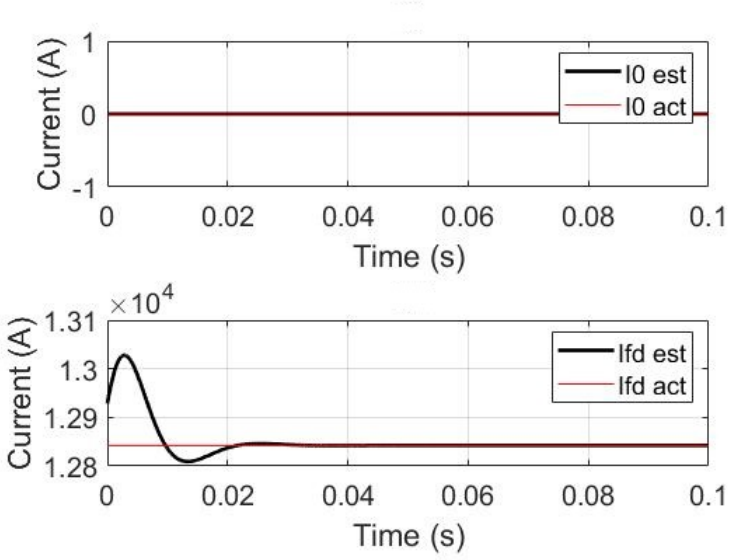

Figure 4.5: Comparing measured current to calculated current from estimated parameters for the zero-sequence and the field currents.

be implemented in the laboratory generator or in the field. The circuit breaker was opened at 0.5 s and re-closed at 1.2 s starting from the steady-state operating condition in previous subsection. The measurements were acquired with 50 kilo-samples per second (kSamp/s) and stepped-down to 8.33 kSamp/s. The covariance matrices were set as follows:

$$P = diag([10^{-9}\ \ 10^{-7}\ \ 10^{-10}\ \ 10^{-4}\ \ 10^{-5}\ \ 10^{-8}\ \ 10^{-5}\ \ 10^{-5}\ \ 10^{-6}\ \ 10^{-6}\ \ 10^{-6}\ \ 10^{-6}]) \tag{4.41}$$

$$R = diag([10^{-10}\ \ 10^{-9}\ \ 10^{-9}\ \ 10^{-9}\ \ 10^{-9}\ \ 10^{-9}]) \tag{4.42}$$

$$Q = diag([10^{-8}\ \ 10^{-6}\ \ 10^{-9}\ \ 10^{-9}\ \ 10^{-9}\ \ 10^{-6}\ \ 10^{-8}\ \ 10^{-8}\ \ 10^{-14}\ \ 10^{-16}\ \ 10^{-14}\ \ 10^{-16}]) \tag{4.43}$$

$$\alpha = 0.1\ \ ,\ \ \beta = 2\ \ ,\kappa = 0 \tag{4.44}$$

Where the states and the output vectors are ordered as:

$$x_0 = [\psi_d; \psi_q; \psi_0; \psi_Q; \psi_{fd}; \psi_D; \omega; \delta; r_D; L_{lD}; r_Q; L_{lQ}]; \tag{4.45}$$

$$z = [i_d; i_q; i_0; i_{fd}; \omega; \delta]; \tag{4.46}$$

Figures 4.6 - 4.8 show the state estimation for the fluxes. The estimation time is 50 seconds. However, a 20-seconds window of time is demonstrated in this subsection to observe the transient response clearly. The 50-seconds time window estimation

can be found in Appendix C. It can be seen in Figures 4.9 - 4.11 that the calculated measurements follow the actual measurements, which is an indication of a successful convergence. Note that the angular frequency has increased linearly during the load rejection with a slope of 37.9 rad/s per second, i.e. 6 Hz/s. The estimated transient parameters are displayed in Figures 4.12 and 4.13. It is noticeable that the transient parameters can only be observable during the transient response, where the state parameters converged after the circuit breaker opened. Table 4.3 summarizes the UKF results, where the initial guess error is the initial estimated parameters value relative to the actual value, and the actual value is the true value that was used in the simulated model, the estimated value is the final converged value of the estimated parameters, and the error is the difference between the final estimated value relative to the actual value.

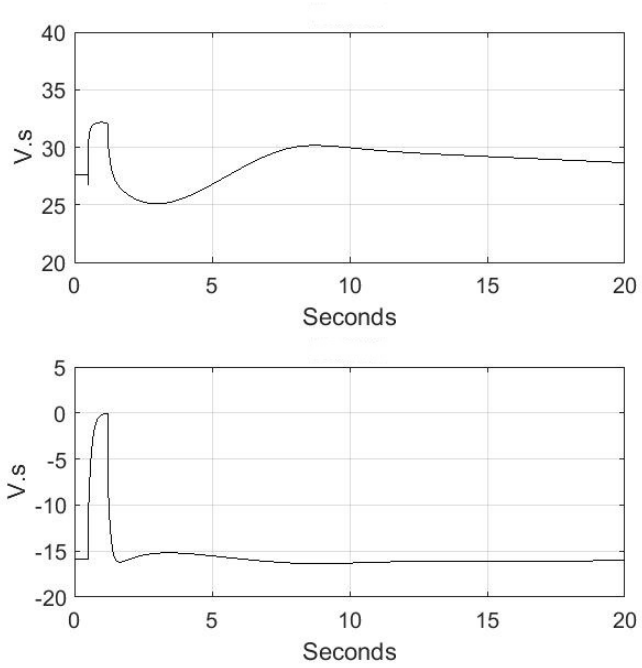

Figure 4.6: State Estimation of ψ_d (upper traces) and ψ_q (lower traces).

It should be noted that the accuracy of the estimation depends on Kalman gains and the covariance matrices. The error of the estimated parameters can vary with

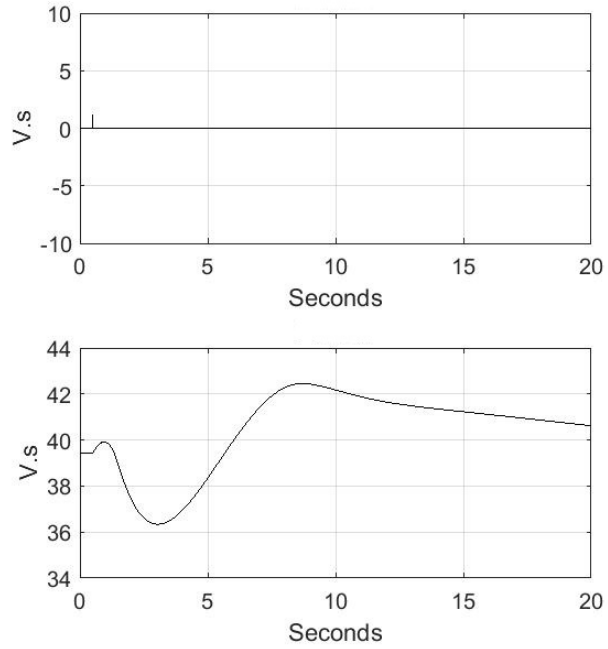

Figure 4.7: State estimation of ψ_0 (upper traces) and ψ_{fd} (lower traces).

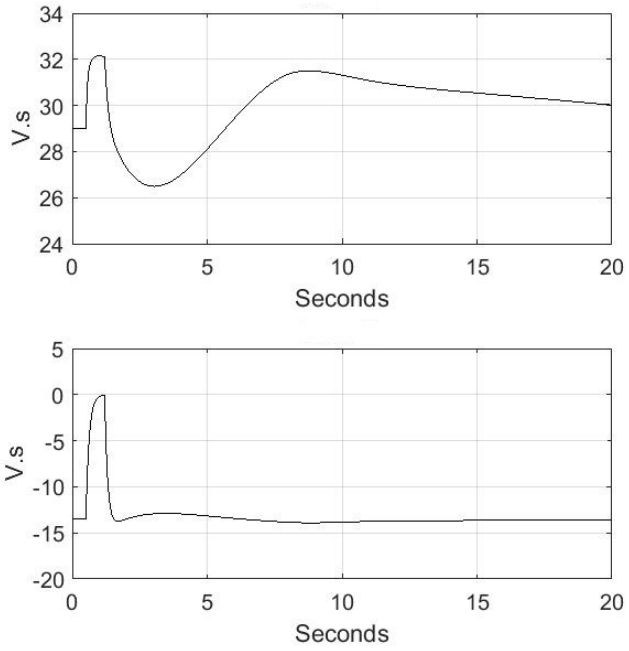

Figure 4.8: State estimation results of ψ_D (upper traces) and ψ_Q (lower traces).

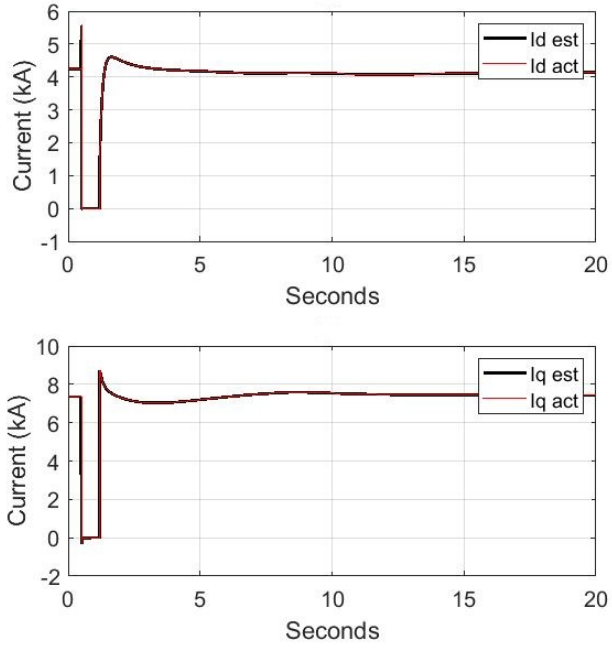

Figure 4.9: Comparing measured current to current calculated from estimated parameters for stator d-and q-axes currents.

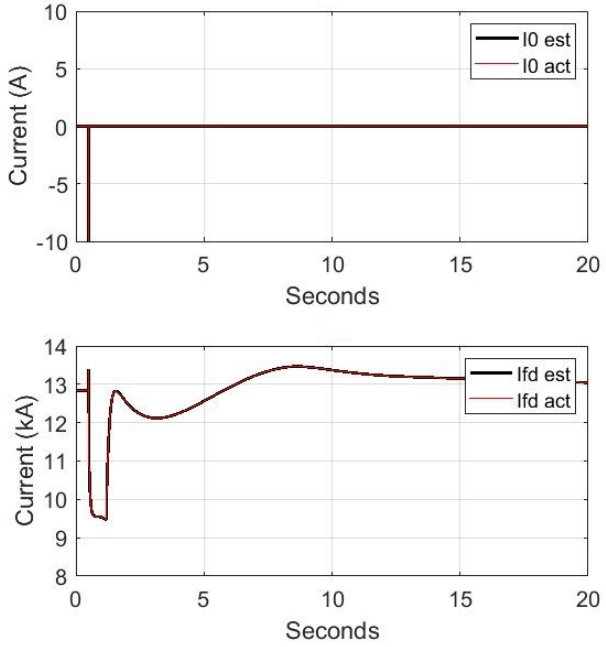

Figure 4.10: Comparing measured current to calculated current from estimated parameters for the zero-sequence and the field currents.

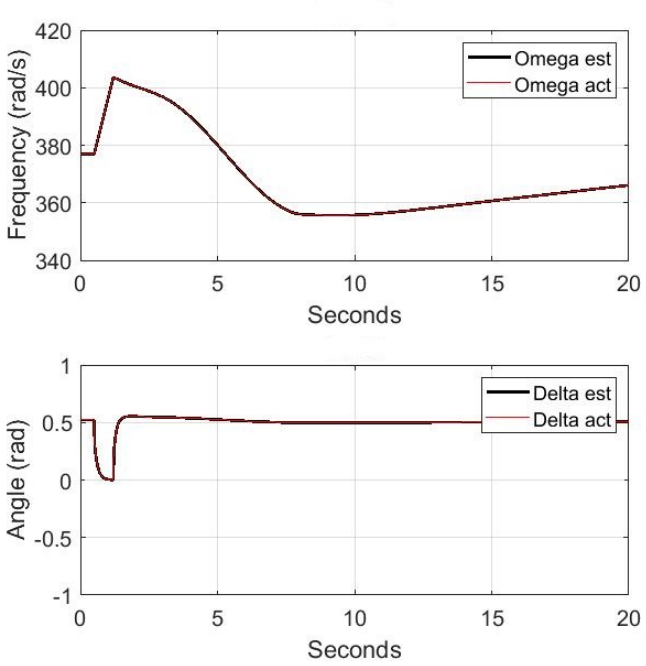

Figure 4.11: Measurement estimation and verification of system measurements angular frequency and load angle.

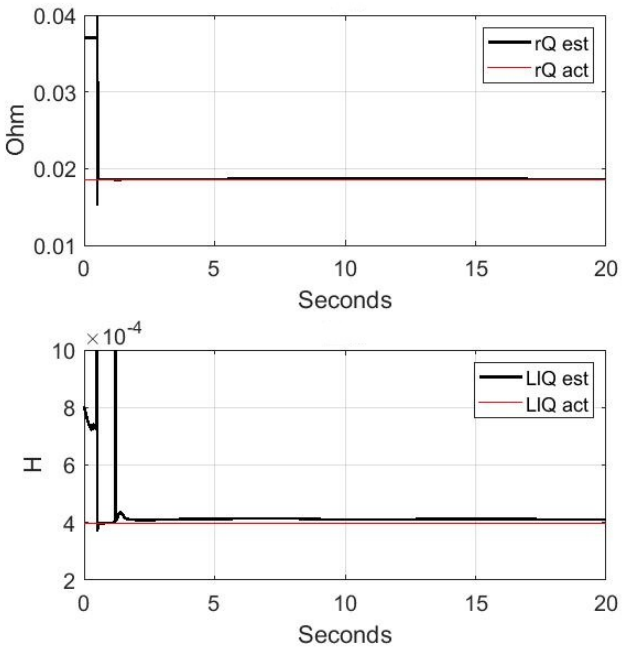

Figure 4.12: Comparing true and estimated parameters for resistance and leakage inductance of the Q-axis damper winding, r_Q and L_{lQ}.

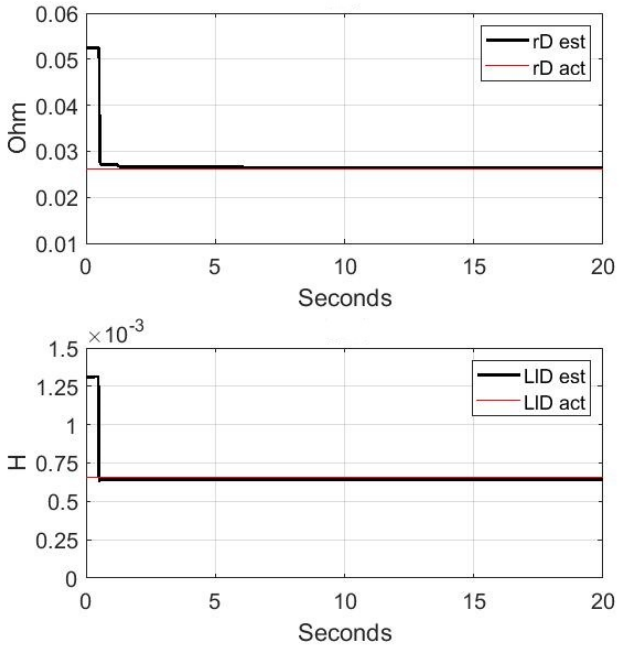

Figure 4.13: Comparing true and estimated parameters for resistance and leakage inductance of the D-axis damper winding, r_D and L_{lD}.

Table 4.3: Transient parameter estimation.

Parameter	L_{lD}	L_{lQ}	r_D	r_Q
Initial Guess Error	100%	100%	100%	100%
Actual Value	0.655mH	0.399mH	0.0262 ohm	0.0185ohm
Estimated Values	0.638mH	0.41mH	0.0266 ohm	0.0186 ohm
Error (%)	2.6	2.8	1.5	0.5

different covariance matrices.

With the knowledge of the actual parameter values, these matrices are usually tuned to minimize the error of the estimated parameters. However, the objective of estimating the parameters in the synchronous generator is to find the unknown parameters. Moreover, it can be noted from the above figures that the UKF has estimated the transient parameters accurately under the assumption of a perfect function model of the generator and zero-percent error for the known parameters. In practice, there is a margin of error in every known parameter. Chapter 5 will explore more the sensitivity analysis of the known parameter during the estimation.

4.4 Summary

This chapter has described the UKF and the GM-UKF algorithms implemented in this research. The UKF method was tested on the simulated synchronous generator that was described in Chapter 2. Both steady-state and transient parameters were estimated accurately without any outliers such as noise or inaccuracy of the model function. In Chapter 5, the GM-UKF and UKF will be tested and compared in the presence of the observation noise.

5. Sensitivity Analysis

This chapter will perform a sensitivity analysis of using the UKF for synchronous generator parameter estimation. It presents the results of testing the UKF in the presence of observation or innovation outliers such as noise in the measurement vector or inaccuracy of the system function for the generator where the UKF was applied. Inaccuracy of the known parameters of the system function can be due to the aging of the generator, saturation effects, and temperature changes.

5.1 Innovation Outliers

The authors of the papers summarized in Table 1.1 tested their methods using a perfect system function where all the known parameters are accurate and have zero percent error. However, known parameters will be associated with a margin of error. As a consequence, the performance of the estimator may change. This section investigates the performance of the UKF applied to generator parameter estimation in the presence of inaccuracy of the known parameters. This chapter uses the same operating point and the same sample rate as used in Section 4.3. It is important to note that the error percentage of the estimated parameter was calculated as defined in equation 5.1. The known parameters were changed by an increment of positive and negative values relative to their actual values.

$$\text{Percentage error of the parameter} = \frac{\text{Actual} - \text{Estimated}}{\text{Actual}} \tag{5.1}$$

5.1.1 Steady-State Parameters

The variation of the parameters L_{md} and L_{mq} due to saturation depends on the generator's operating conditions, whereas both the stator and field leakage inductance are

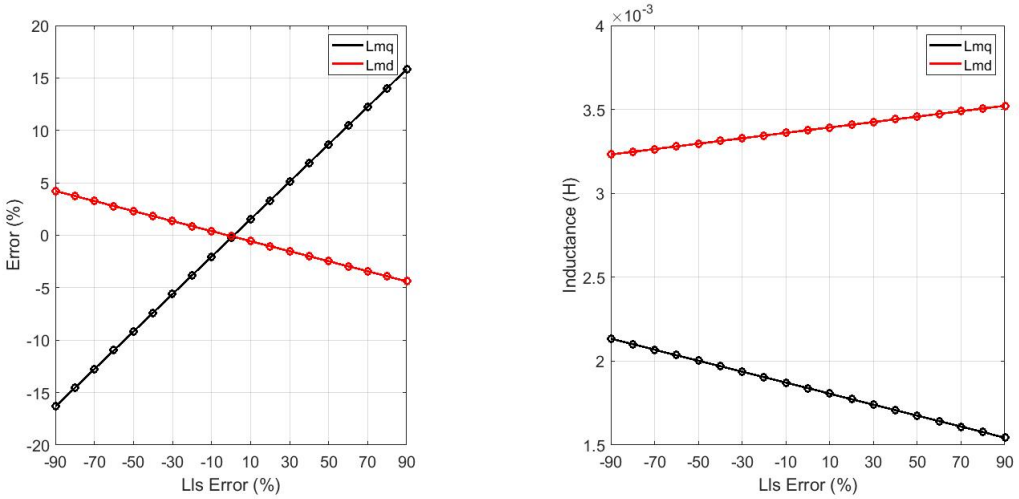

(a) (b)

Figure 5.1: Sensitivity analysis on the variation of stator leakage inductance in generator steady-state parameters estimation; (a) the percentage error of the estimated parameters versus the percentage error of known parameter; (b) the estimated parameter values versus the percentage error of known parameter.

immune from the saturation effect. Therefore, the sensitivity of the state estimation to L_{md} and L_{mq} when other known parameters have error is analyzed.

5.1.1.1 Stator Leakage Inductance

Nineteen simulations were conducted to investigate the effect of variation of the stator leakage inductance on estimated L_{md} and L_{mq} results. In each simulation, the error of stator leakage inductance value is increased by an increment of 10%. In all cases the estimated results converged to positive and stable values. Figure 5.1 shows two subplots; the right subplot shows the error percentage of the leakage inductance versus the estimated value of the L_{md} and L_{mq} in Henries; the left subplot shows the error percentage of the leakage inductance versus the error percentage of the L_{md} and L_{mq}.

Note that the measurement function used the estimated L_{md} to calculate i_{fd} and i_d, which then compared with the measurement vector, z. On the other hand, the estimated L_{mq} was used only to calculate i_q. As a result, the error in the stator leakage

inductance has affected the estimated L_{mq} more than the estimated L_{md}. Keep in mind that the L_{mq} value is smaller than L_{md}, which means the error percentage with the same deviation will be larger in L_{mq} than L_{md}. Another observation is that the error percentages of both L_{md} and L_{mq} are symmetrical. In other words, a positive 30% error of the leakage inductance will produce the same estimate error of L_{md} and L_{mq} as the negative 30% error of the leakage inductance. Overall, the error of the leakage inductance has a low impact on the estimated values.

Usually, when the transient parameters are estimated, L_{md} and L_{mq} are considered known parameters. The critical question is, will the 15% error of the estimated L_{md} and L_{mq} introduce a more significant error in estimated transient parameters? This question will be answered later in this chapter.

5.1.1.2 Field-to-Stator-Turns Ratio

The field-to-stator-turns ratio $N_f N_s$ is an important parameter to estimate the physical parameters of the synchronous generator in units. This parameter was varied by an increment of 10% while estimating L_{md} and L_{mq} to examine the sensitivity of the estimation. A total of 17 simulations were performed and converged to positive values. Figure 5.2 summarizes the result of these simulations.

It can be seen from the figure that L_{md} is very sensitive to field-to-stator-turns ratio. However, L_{mq} is not sensitive to the $N_f N_s$. This can be seen from the mathematical relationship between $N_f N_s$ and L_{md} in the following equation:

$$N_f N_s = \frac{1.5 \times (i_a)_{peak}}{(i_{fd})_{base} \times L_{md}} \tag{5.2}$$

Where $(i_{fd})_{base}$ is the required field current to have rated terminal voltage under an open circuit condition. Figure 5.2 shows that a positive percentage error of $N_f N_s$ will cause an approximately double effect on the estimated L_{md} than a negative percentage

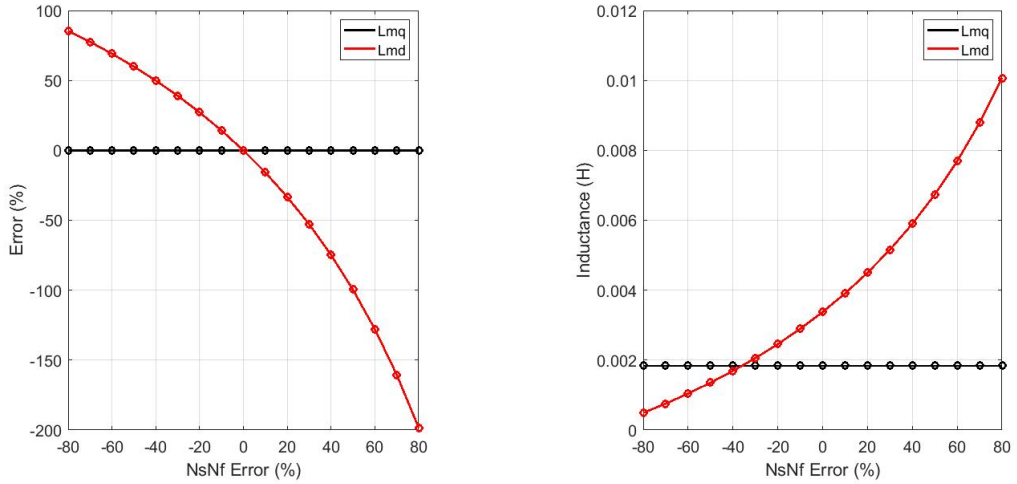

(a) (b)

Figure 5.2: Sensitivity analysis on the variation of field-to-stator-turn ratio in generator steady-state parameters estimation; (a) the percentage error of the estimated parameters versus the percentage error of known parameter; (b) the estimated parameter values versus the percentage error of known parameter.

error of $N_f N_s$. In other words, a positive 80% error in the known parameter $N_f N_s$ will cause the estimated L_{md} to be off by 200%, whereas a negtive 80% error in the known parameter $N_f N_s$ will cause the estimated L_{md} to be off by 90%.

5.1.1.3 Load Angle

The load angle is a critical parameter in the UKF estimation, where an error in the load angle will cause an error in I_{dq0} and V_{dq0}. These measurements are used as input and measurement vectors for the UKF. Figure 5.3 shows the effect of the load angle error in the L_{md} and L_{mq} estimation. It is noticeable that the L_{mq} is more sensitive to the load angle than L_{md}. This also can be seen in equation (5.3).

$$\delta = \arctan \frac{X_q I_a \cos(\phi)}{V_a + X_q I_a \sin(\phi)} \tag{5.3}$$

Where ϕ is the power factor angle, I_a and V_a is phase A terminal current and voltage.

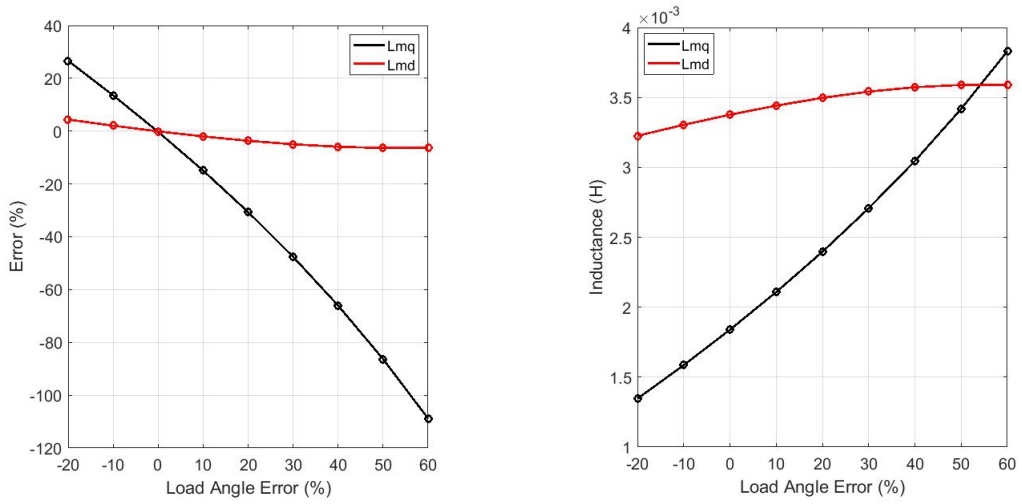

(a) (b)

Figure 5.3: Sensitivity analysis on the variation load angle in generator steady-state parameters estimation; (a) the percentage error of the estimated parameters versus the percentage error of known load angle; (b) the estimated parameter values versus the percentage error of known load angle.

It is important to note that the filter was unusable when the known parameter δ was set below -20% relative to its actual value. However, the filter was stable when the known angle δ was set above +20% relative to its actual value. This can be resolved by re-tuning the filter covariance matrices. However, the objective of this chapter is to observe the effect of the error of the known parameters on the UKF results while maintaining the same covariance matrices for all cases since in practice the error is not known and the covariance matrices can't be re-tuned to correct for it.

5.1.1.4 Sensitivity to Other Parameters

Other parameters were varied to test the performance of the UKF result. The stator resistance was varied over a range of error from -90% to $+90\%$ error. However, the estimated L_{md} and L_{mq} values are immune to the variation of the stator resistance. Therefore, an accurate stator resistance value does not affect steady-state parameters

estimation. Another parameter that was investigated is the variation of field leakage inductance. The field leakage inductance has no impact on the L_{md} and L_{mq}, since the inductance behaves as a short circuit in DC.

5.1.2 Transient Parameters

The transient parameters L_{lD}, L_{lQ}, r_D, and r_Q represent the rotor equivalent circuits. These parameters may change over time due to the aging of the synchronous generator, temperature, or broken damper bars. Therefore, in order to implement an online estimation method to determine the transient parameters, the estimator method must distinguish between the deviation because of the actual machine condition which the owners would want to detect and the error in the system function of the estimator. In this subsection, the deviation of the transient parameters due to the accuracy of system function is explored.

5.1.2.1 Stator Leakage Inductance

The error of leakage inductance value is increased by an increment of 0.1% on each simulation case. Figure 5.4 shows the results of 18 cases of estimation of the transient parameters. It can be seen from the figure that the leakage inductance has more impact on the L_{lD} and r_D than on L_{lQ} and r_Q. Note that the -0.9% and -1% cases were not plotted because the filter was unstable in these cases. As mentioned before, the UKF states can converge to reasonable and positive values but not correct values. Therefore, without the knowledge of the actual parameters, the result might be misleading.

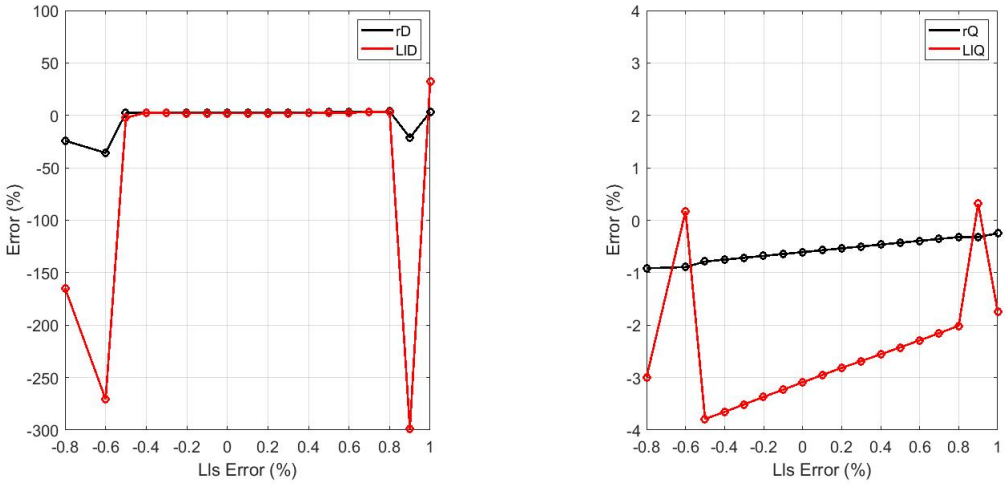

(a) (b)

Figure 5.4: Sensitivity analysis on the variation of stator leakage inductance in generator transient parameters estimation; (a) the percentage error of the estimated parameters L_{lD} and r_D versus the percentage error of known parameter L_{ls}; (b) the percentage error of the estimated parameter values L_{lQ} and r_Q versus the percentage error of known parameter L_{ls}.

5.1.2.2 Field Leakage Inductance

Unlike in the steady-state parameter estimation, the field leakage inductance has an effect on the estimated transient parameters. Figure 5.5 shows 14 cases results of the transient parameters estimation while changing the L_{lfd} with an incremental increase of 2% on each estimation. As discussed in Chapter 3, the offline tested parameters may vary from the manufacturer parameters by 40%. Therefore, having a 10% error of the field inductance may be considered to be satisfactory. As a result, UKF may converge to an incorrect value, as shown in the Figure 5.5. Note that some cases were not included in the figure, for example, ±12%, ±14%. Some of these points settled to a negative value or diverged; hence there were removed. Overall, the d-axis damper widening parameters are more sensitive to the variation of the L_{lfd} than the q-axis damper winding parameters.

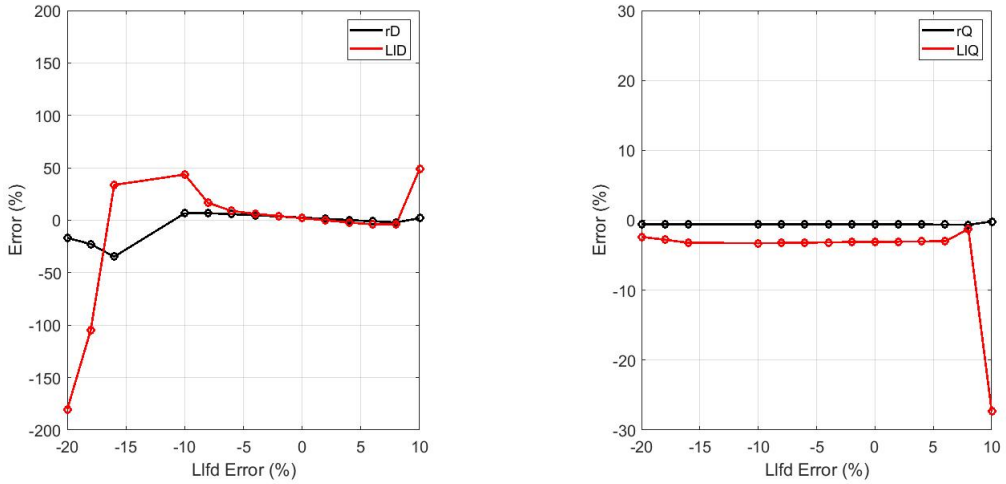

(a) (b)

Figure 5.5: Sensitivity analysis on the variation of field leakage inductance in generator transient parameters estimation; (a) the percentage error of the estimated parameters L_{lD} and r_D versus the percentage error of known parameter L_{lfd}; (b) the percentage error of the estimated parameter values L_{lQ} and r_Q versus the percentage error of known parameter L_{lfd}.

5.1.2.3 Field-to-Stator-Turns Ratio

In this case, the $N_f N_s$ parameter was varied by 0.2% while estimating transient parameters. A total of 17 estimation results are illustrated in Figure 5.6. It can be seen that the L_{lD} is more sensitive than other estimated parameters. Unlike the steady-state case, there is no specific pattern that can be noticed, but without knowing the true value of $N_f N_s$, the estimated results of the UKF could be misleading.

5.1.2.4 Direct-Axis Magnetizing Inductance

The following two subsections will answer the question about whether a low estimated error of steady-state L_{md} has a significant impact on subsequent estimation of the transient parameters. Figure 5.7 presents the estimation results of estimated transient parameters; for each estimation L_{md} was changed by 0.01%. It can be observed that the L_{lD} parameter is more sensitive than other transient parameters. There were a

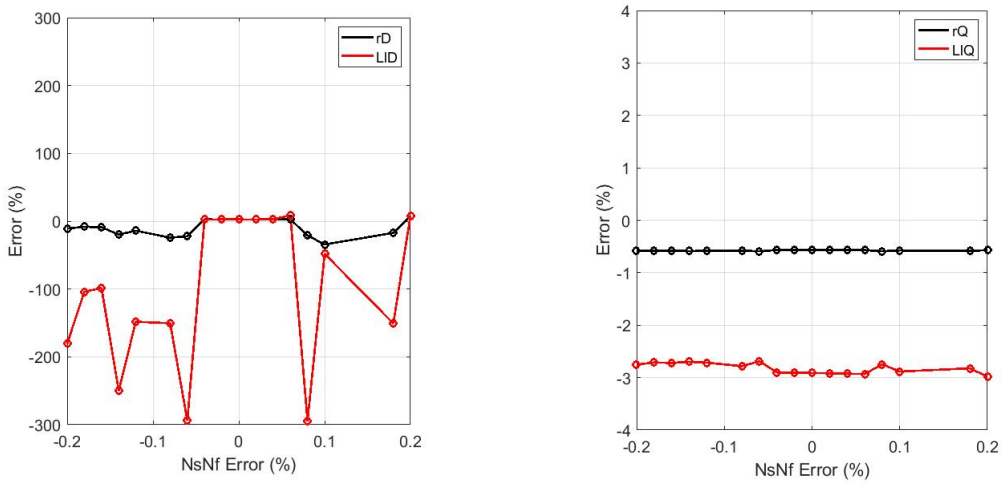

(a) (b)

Figure 5.6: Sensitivity analysis on the variation of field-to-stator-turn ratio in generator transient parameters estimation; (a) the percentage error of the estimated parameters L_{lD} and r_D versus the percentage error of known parameter $N_f N_s$; (b) the percentage error of the estimated parameter values L_{lQ} and r_Q versus the percentage error of known parameter $N_f N_s$.

few estimation cases that converged to a negative value or diverged; hence, there were removed.

5.1.2.5 Quadrature-Axis Magnetizing Inductance

Unlike the L_{md}, the L_{mq} was varied over a smaller range due to the high sensitivity of the transient parameters to its variation. Figure 5.8 shows that the L_{lD} is vulnerable to the minor variation of the L_{mq}. Having no knowledge of the true value of transient parameters and in the presence of minors errors in the known parameters, the unknown parameters in UKF may converge to incorrect values. For example, -0.02% error in the L_{mq} will cause the L_{lD} and r_D to converge to values that are off by 84% and 34%, respectively.

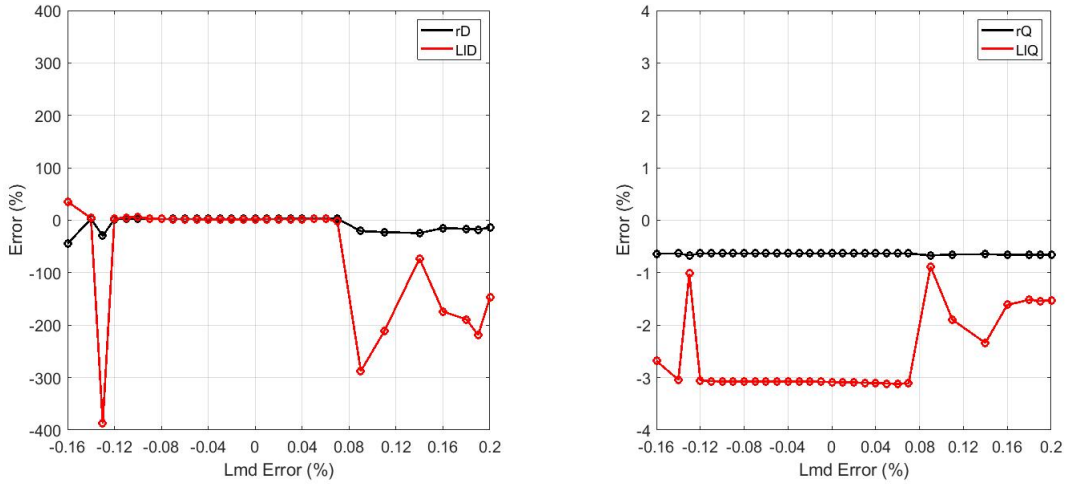

(a) (b)

Figure 5.7: Sensitivity analysis on the variation of d-axis magnetizing inductance in generator transient parameters estimation; (a) the percentage error of the estimated parameters L_{lD} and r_D versus the percentage error of known parameter L_{md}; (b) the percentage error of the estimated parameter values L_{lQ} and r_Q versus the percentage error of known parameter L_{md}.

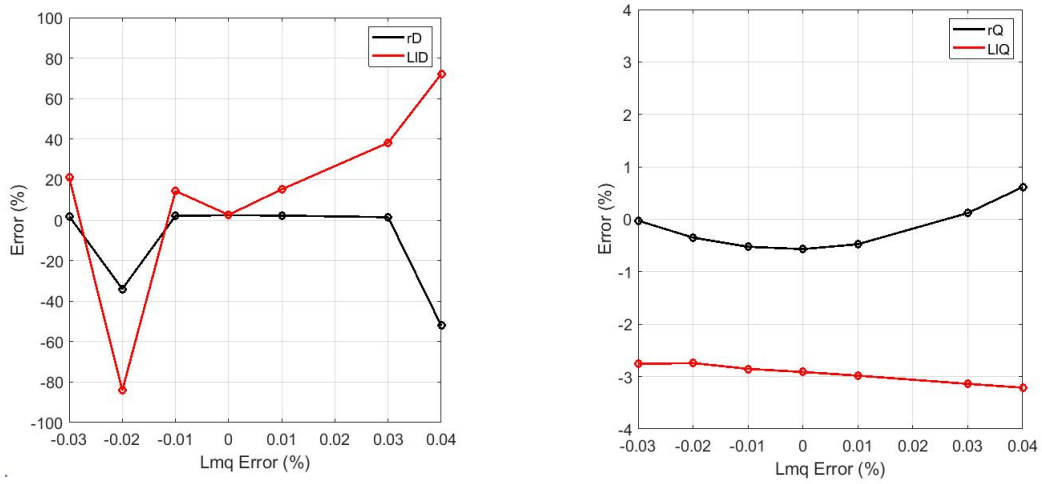

(a) (b)

Figure 5.8: Sensitivity analysis on the variation of q-axis magnetizing inductance in generator transient parameters estimation; (a) the percentage error of the estimated parameters L_{lD} and r_D versus the percentage error of known parameter L_{mq}; (b) the estimated parameter values L_{lQ} and r_Q versus the percentage error of known parameter L_{mq}.

5.1.2.6 Sensitivity to Other Parameters

The moment of inertia of the rotor mass is considered one of the known parameters. It is used to calculate the deviation angular frequency, as shown in equation (5.4).

$$\dot{\omega} = \frac{1}{J}(T_m - T_e) \tag{5.4}$$

After varying the known value for the J parameter by -80% to +80% while estimating the transient parameters, we concluded that the J does not affect the estimated parameters. This lack of sensitivity is because of how the measurement and the system covariance were tuned. The angular frequency was used as a measurement and compared with the calculated measurement. The measurement covariance for the angular frequency was set to be 10^{-9}, whereas the covariance value for the estimated angular frequency was set to be 10^{-8}. In other words, the filter relies more on the angular frequency measurement than the estimated angular frequency. Similarly, when the mechanical torque was varied, there were minor changes in the estimated parameters.

However, when the covariance value for the estimated angular frequency was set to be 10^{-10}, which is smaller than the covariance of measurement, and with a 3% error of the mechanical torque, the estimated L_{lD} converges to a positive value with a 65% error relative to the true value.

Any variation in the load angle will cause the UKF to be unstable. This is because any error in the load angle will cause an error in the dq0 components. It requires re-tuning the covariance matrices. As mentioned before, the covariance matrices of the UKF could minimize the error of the mechanical torque. The mechanical torque corresponds to a single state. On the other hand, the load angle was used in three states and three measurements as input and measurement vectors of the filter.

With the chosen filter, downsampling the measurements below 8 kHz will require

re-tuning the system covariance matrix Q. Nevertheless, the UKF result accuracy will be degraded, and it will cause some of the estimated parameters to be unstable. In [61], the Iterated UKF (IUKF) method was used to estimate the transient parameters at a low sample rate of 60 Samp/s. It can be concluded from the above tests that the UKF result is highly dependent on its covariance matrices, and without knowing the actual value of the parameters, which is the case in practice, the UKF can converge to an incorrect solution.

5.2 Observation Outliers

Impulsive communication noise measurement, instrument failures, or infrequent calibration in PMU can cause an observation outlier [1], [13]. These outliers may come in the form of non-Gaussian noise. This section will test the UKF performance in the presence of non-Gaussian noise in the measurement vector. Also, a comparison between the robust GM-UKF and UKF will be presented.

5.2.1 Gaussian Noise

Most UKF implementations have assumed that the error of the measurements follows a Gaussian distribution form. Gaussian noise with zero mean and variance of 10^{-4} was assumed for the measurement vector of the UKF, as shown in Figure 5.9. In this case, the same condition and configuration as in Section 4.3.1 were used. The Gaussian noise was added starting at 0.25 s until 0.8 s to test the performance of the estimators. Figure 5.10 shows the performance of both estimators in the presence of Gaussian noise. It can be seen that both estimators converged to the true value of L_{md} and L_{mq}. Note that the GM-UKF has taken a longer time to converge, which might be reduced with re-tuning its gains.

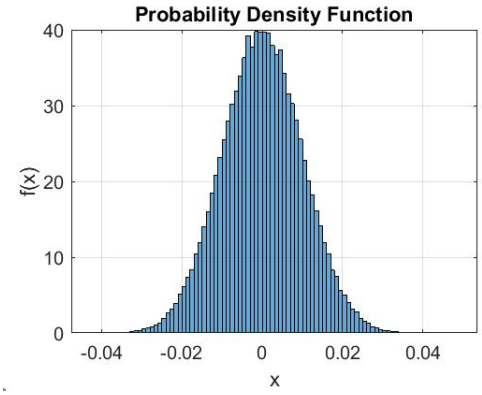

Figure 5.9: Gaussian noise

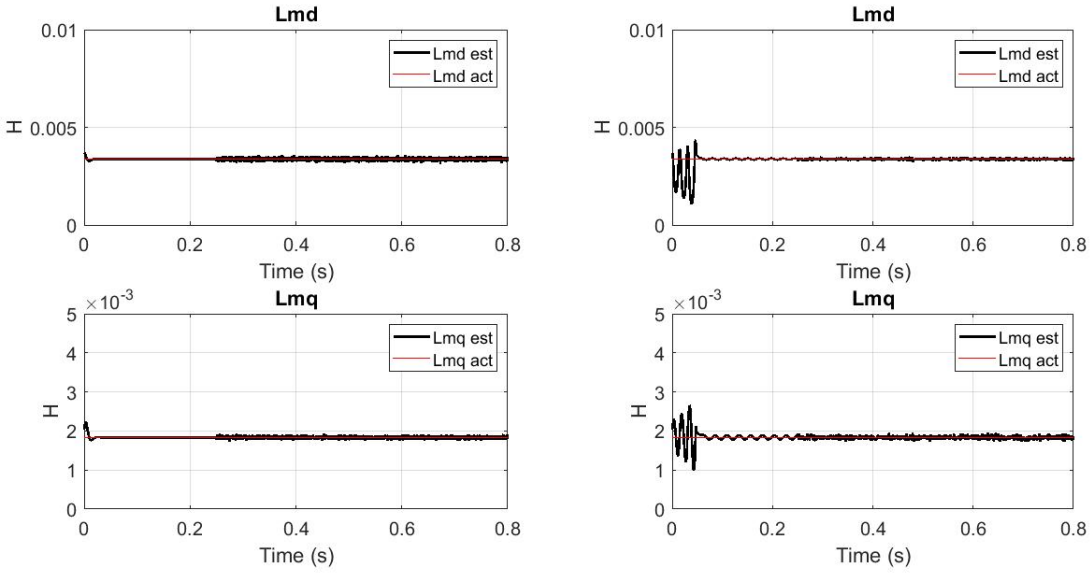

(a) UKF (b) GM-UKF

Figure 5.10: Steady-state parameters estimation in the presence of Gaussian noise

5.2.2 Non-Gaussian Noise

Non-Gaussian noise was tested in the form of a bimodal Gaussian mixed distribution as well as a Laplacian distribution. To account for the noise of the measurement vector, the coviarance matrix were set as follows:

$$Q = diag([10^{-3}\ \ 10^{-3}\ \ 10^{-9}\ \ 10^{-5}\ \ 10^{-10}\ \ 10^{-10}]) \tag{5.5}$$

$$R = diag([10^{-3}\ \ 10^{-3}\ \ 10^{-3}\ \ 10^{-3}]) \tag{5.6}$$

$$P = diag([10^{-8}\ \ 10^{-8}\ \ 10^{-8}\ \ 10^{-7}\ \ 10^{-8}\ \ 10^{-8}]) \tag{5.7}$$

Figure 5.11 shows bimodal Gaussian mixture noise with zero means, a variance of 10^{-4} and 10^{-3}, and weights of 0.9 and 0.1. This noise was added to the measurement vector at 0.25 s until 2 s. The results of both GM-UKF and UKF are plotted in Figure 5.12. It can be seen that the UKF diverged at 0.25 s, whereas GM-UKF was able to cope with bimodal Gaussian noise. Similarly, 7% of the measurement was corrupted with Laplacian noise starting at 0.25 and ending at 2 s. Figure 5.13 shows the performance of both UKF and GM-UKF in estimating the steady-state parameters under Laplacian noise. Note that the UKF could not handle Laplacian noise. By contrast, GM-UKF exhibits robustness against this situation.

5.3 Overall Analysis of the Results

In this chapter, the UKF was tested against innovation and observation outliers. For the innovation outliers, the known parameters were varied individually in both steady-state and transient estimations. The steady-state analysis has shown a pattern in each case. For example, the variation of the load angle error has more impact on

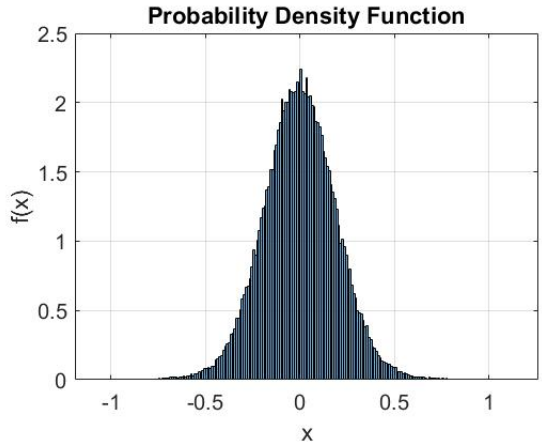

Figure 5.11: Bimodal Gaussian mixture distribution noise.

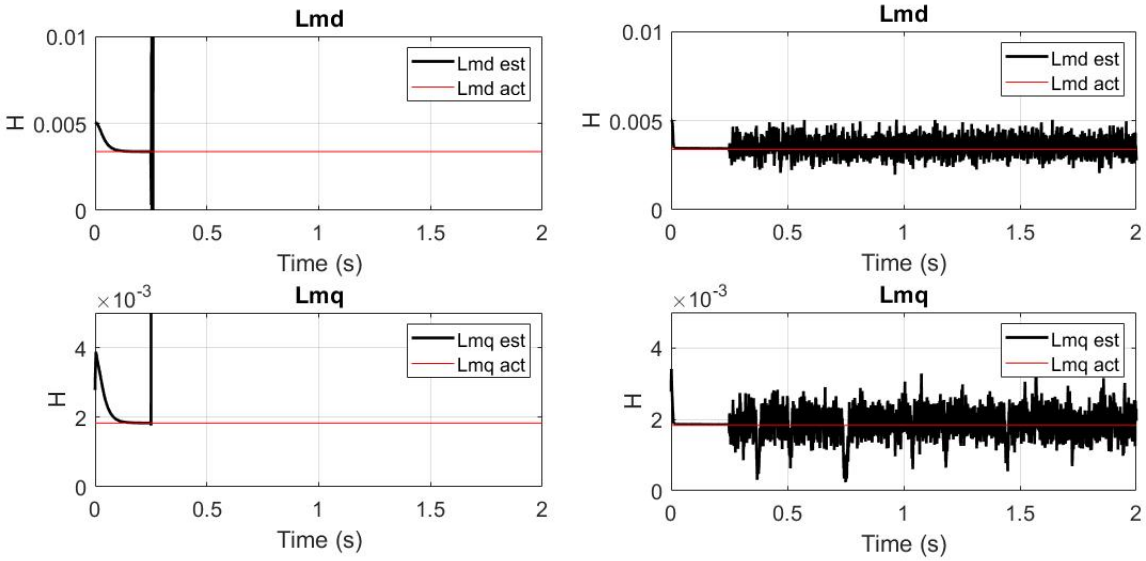

(a) UKF

(b) GMUKF

Figure 5.12: Steady-state parameters estimation in the presence of bimodal Gaussian noise

the L_{mq} than L_{md}, whereas the L_{md} is more sensitive to the error of the field-to-stator-turn ratio. The stator leakage inductance has minimal effect on both L_{mq} and L_{md}.

In the transient estimation, there was no pattern in the variations. However, the convergence of the estimated transient parameters using UKF does not mean it reaches the correct states. It should be noted that the setting of the system covariance

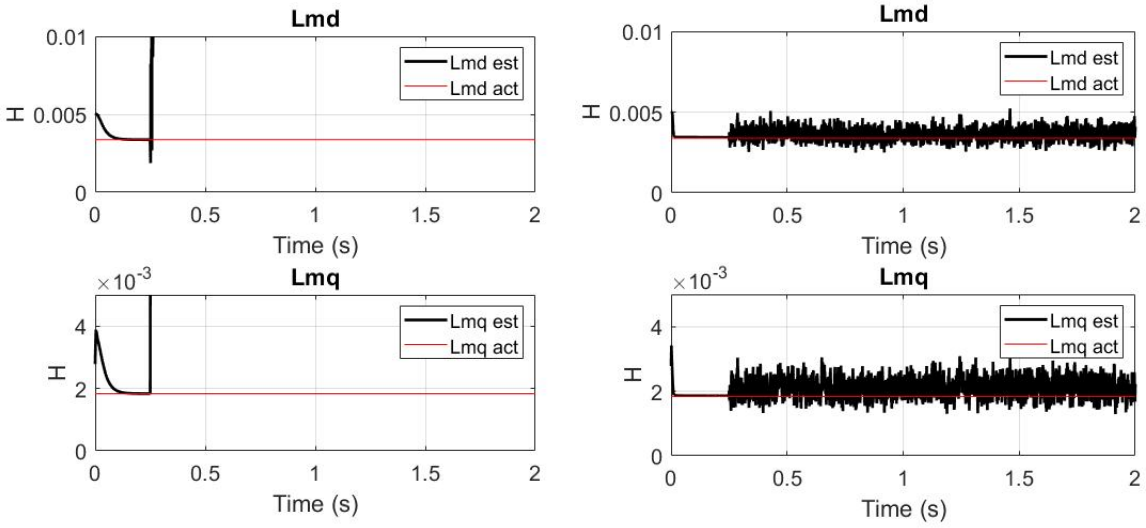

(a) UKF (b) GM-UKF

Figure 5.13: Steady-state parameters estimation in the presence of Laplacian noise.

matrix may cause a different response. For example, in this case, it can be noticed that the d-axis damper winding parameters are more sensitive to the variation of the known parameters than the q-axis damper winding parameters, even with a minor error in the known parameter. This is because of the filter covariance matrices setting. Recall the setting value for the ψ_Q was tuned to be smaller than ψ_D, as defined in equation (4.43). Therefore, re-tuning the filter may result in a better estimation, and usually, the re-tuning is done while observing the error of the estimated parameters relative to the true parameters. In practice, the true parameters are unknown, and the objective of the estimation is to find them, which makes it very challenging to know whether the converged value represents the actual parameter of the machine or the estimator converges to different values due to the effect of the error in known parameters. It is important to keep in mind that the manufacturer provided parameters have their error, and the parameters may vary over time due to the aging of the generator, saturation effects, and temperature changes.

The UKF was tested with different types of the noise distribution. It was clear that the UKF could not cope with a non-Gaussian noise, whereas GM-UKF proved

its robustness against non-Gaussian noise.

Overall, the steady-state parameters can be estimated using UKF instead of implementing the offline tests. The UKF has the advantage of estimating these parameters on different conditions, whereas the offline testing is only calculating the unsaturated parameters. Keep in mind that the UKF estimated the steady-state parameters with certain errors due to the error in the known parameters. Finally, note that the testing in this chapter only introduced error in one parameter at a time. In practice, all of the known parameters may have some degree of error.

6. Laboratory Generator Online Parameter Estimation

In this chapter, the unscented Kalman filter (UKF) based approach is applied to estimate the parameters of the laboratory generator that was presented in Chapter 3. Also, frequency and load angle tracking methods are developed to support the parameter estimation in this chapter. Finally, the estimated parameters are validated against the data from the IEEE 115 tests.

6.1 Testbed Description

The testbed was designed to work with 60 Hz synchronous machines in a university lab with power ratings up to 20 kVA and terminal voltage ratings up to 240 V. The machines each use a motor-generator arrangement, with several machines using dc motors and one using an induction motor controlled by an adjustable speed drive. Figure 6.1 shows the system diagram for the motor-generator set used in the remainder of this chapter. A 15 hp dc motor drives a 1200 rpm, 13.5 kVA synchronous generator.

6.1.1 Data Acquisition System

The data acquisition system was implemented in a chassis with two data acquisition (DAQ) boards. Both use 16-bit Analog-to-Digital Converters (ADC) with an absolute accuracy at full scale of 1.9 mV. A remote control module and a Peripheral Component Interconnect (PCI) Express host card are used to acquire and post-process the measurements using a Windows PC. Having a common internal timebase clock enables both DAQs to be synchronized. In addition, both DAQs are triggered simultaneously with the same sample rate to fully time-align the measurements. This can be done using the Real-Time System Integration (RTSI) bus, which is located in

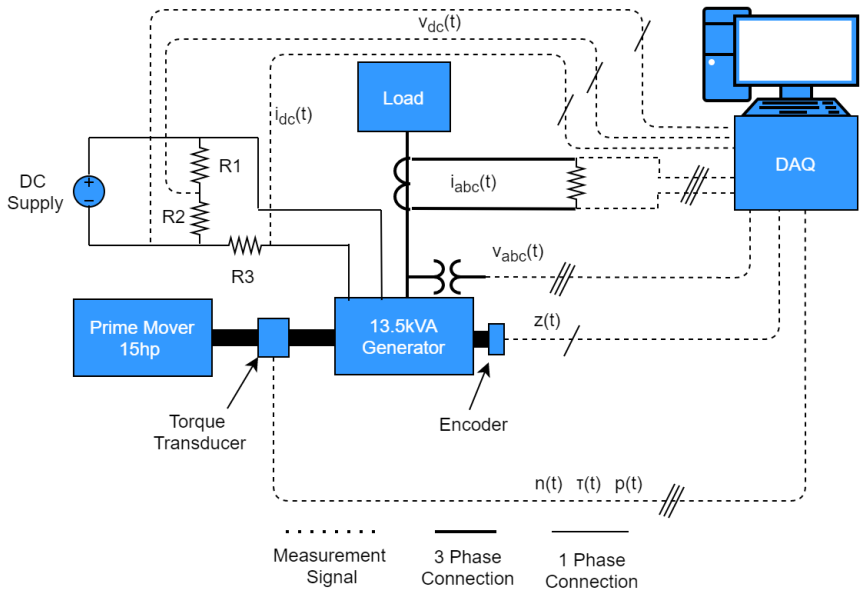

Figure 6.1: Data acquisition system topology.

the chassis backplane. The system was built in the National Instruments LabVIEW software to record and stream the acquired measurements.

6.1.2 AC and DC Measurements

Instrument transformers are used both to provide isolation and to step terminal voltage signals and line current signals down to the desired range for the DAQ. The current transformer (CT) ratio was chosen to accurately capture the measurements given the worst case operating current condition of the machine in the expected classes of normal and abnormal operating condition tests. Table 6.1 lists the peak transient current range the testbed can handle with the installed CTs, which have a CT ratio of 150A/5A. The current measurements input to the DAQ as the voltage across high precision resistive shunts, since the DAQ requires voltage inputs. Similarly, the voltage transformer (VT) ratios were chosen based on the maximum transient overvoltages. Table 6.1 lists the peak transient voltage range the testbed can handle with the installed VTs, which have a VT ratio of 230V/5V. The test result of determine the VT ratio can be found in Appendix D.

Table 6.1: Maximum measurement input ranges for the testbed.

Measurements	Maximum range	Rated range
Terminal Voltage	± 386.7 V	± 179.6 Vpk
Line current	± 300 A	± 50.1 Apk
Field voltage	± 198.5 V	74.4 V
Field current	± 100 A	8 A
Rotor speed	± 8500 rpm	1200 rpm
Mechanical Torque	± 226 N · m	35.81 N · m

Figure 6.1 shows the circuit designed to measure the dc field voltage and field current. Since the DAQ only accepts a voltage signal, R3 was used to convert the current measurement to voltage measurement. Also, a DAQ channel is connected to R2 to measure the field voltage. Both resistors were sized to acquire the maximum field current and voltage under transient conditions without exceeding the DAQ voltage range.

6.1.3 Shaft Encoder

An incremental optical encoder is installed on the rotor shaft to measure speed. This is a rotating electromechanical device with three output signals: A, B, and Z. The A and B signals have 2160 pulses per turn, where the Z signal has one pulse per turn. For load angle measurement, the Z signal is used to indicate where the rotor position is with respect to a phase A terminal voltage. This is further described in Section 6.3. As shown in Table 6.1, the testbed is rated for 1200 rpm machines but supports operation up to 8500 rpm, rotating in either direction.

6.1.4 Torque Transducer

A digital torque transducer is installed on the shaft between the motor and generator to measure torque, power, and speed with a resolution of 0.003% of ratings [62]. The torque rating for the torque transducer was chosen to account for the maximum

torque for the 13.5 kVA machine during out-of-step transient conditions. The analog port of the torque transducer outputs a DC signal with a magnitude proportional to torque, power, and speed measurements in real-time. The analog measurements were correlated with digital measurements, see Appendix D. These mechanical measurements are crucial and challenging to obtain in transient stability events. However, the developed testbed offers accurate mechanical measurements that provide an opportunity to study and develop generator protection schemes. The developed testbed can capture transient events as well as steady-state operation. Figure 6.2 presents some results of a load rejection test where the generator started in a loaded condition and then the prime mover was tripped at 2.15 seconds; thereafter, the generator behaves as a synchronous condenser. Table 6.1 shows the maximum torque measurement input range for the testbed and the rated measurement for the generator in this thesis.

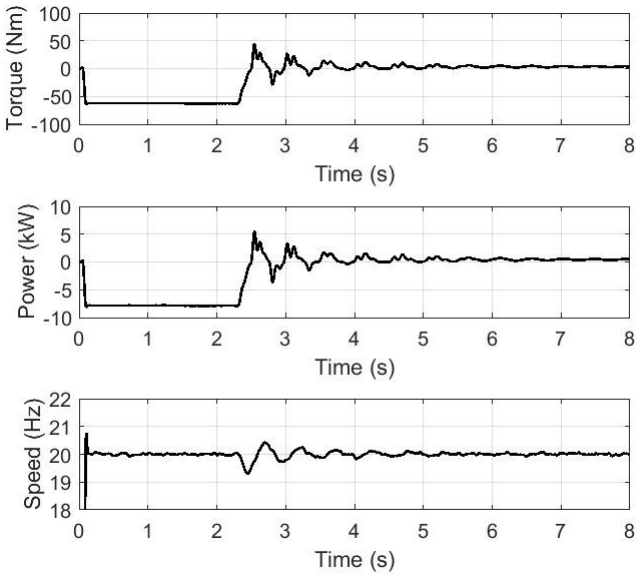

Figure 6.2: Mechanical torque, power, and speed of the shaft for a load rejection test.

6.2 Park's Transformation

In order to compute the dq0 components, both load angle and angular velocity ωt must be tracked. This thesis has chosen two time domain frequency tracking methods: zero-crossings and phase-locked loop. Both methods can track frequency and ωt. The development and comparison of both methods are presented in the following subsections.

6.2.1 Zero-crossings Method

The zero-crossings method is a common method for tracking the frequency in the power system. The negative and positive zero-crossings detection method was implemented in this work to track the power frequency. Three phase-simulated signals were generated to test the zero-crossings method. Each signal has frequency ramp with slope of 15 Hz/s, as shown in Figure 6.3. The zero-crossings method interpolates these signals and converts every element in the array to 1, -1, and 0. If the element is a positive value, then it is converted to 1. If the element is a negative value, then it is converted to -1. Lastly, if the element is zero, it will return zero. After that, the differences between adjacent elements of the converted signals are calculated, more details of the code are added in Appendix F. Figure 6.3 shows that the calculated frequency from the zero-crossings method, which is in red is following the true frequency, which is in black.

Figure 6.4 shows phase A of the simulated signals with the measured ωt from the zero-crossings method. It assigns the negative zero-crossings with π and positive zero-crossings with 2π and zero. The simulated signals have an amplitude of 180. For demonstration purposes, the simulated signal was scaled down by dividing by 20.

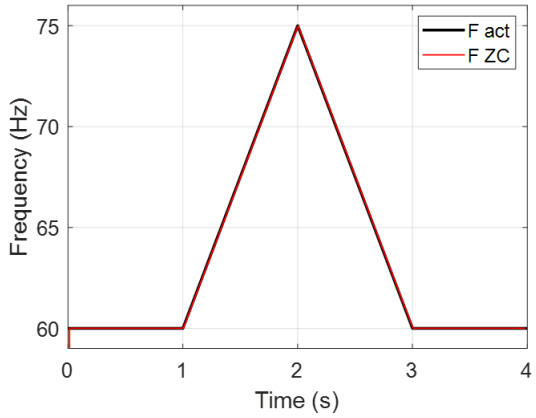

Figure 6.3: Zero-crossings method; F act is the actual frequency, F ZC is the calculated frequency from zero-crossings method.

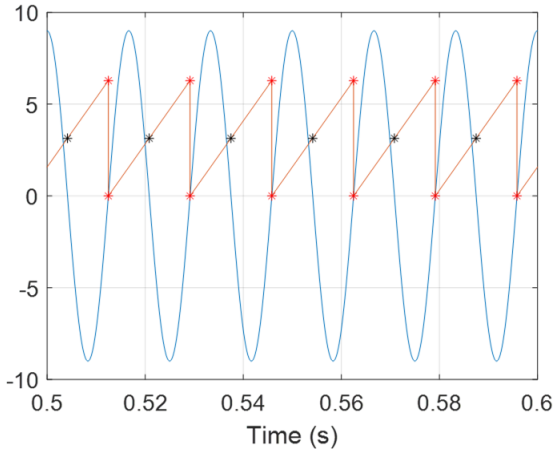

Figure 6.4: ωt tracking using zero-crossings method.

The V_{dq0} was computed to test the accuracy of the calculated ωt.

$$V_d = 0.156 = 180\ sin(0.05^\circ) \tag{6.1}$$

Assuming that the load angle is zero, the V_q will be equal to the peak of phase A, 180, as shown in Figure 6.5, whereas V_d will be equal to zero in the ideal case. The computed V_{dq0} is illustrated in Figure 6.6. It can be seen that during the frequency ramp, V_d is equal to 0.156 V, where it should be equal to zero in the ideal case. In other words, the ωt method is off by 0.05°, as shown in equation (6.1).

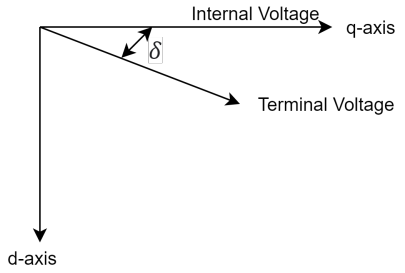

Figure 6.5: Voltage vector diagram.

6.2.1.1 Comparison Between B-function and Zero-Crossings Methods

B. Kasztenny developed a new approach of tracking frequency known as B-function, which was presented in [4]. It uses a periodic waveform integration concept. The approach looks at when the integrated function equals zero to find the waveform period. Figure 6.7(a) was presented in [4], where the top figure is the simulated input signal used for testing, and the bottom of Figure 6.7(a) is the frequency of the signal. In this thesis, a distorted simulated signal that exhibits extra zero crossings was generated to imitate the same scenario, as shown in Figure 6.7(b). It can be seen that both signals exhibit a frequency ramp with slopes of 20 Hz/s and 2.5 Hz/s. Also,

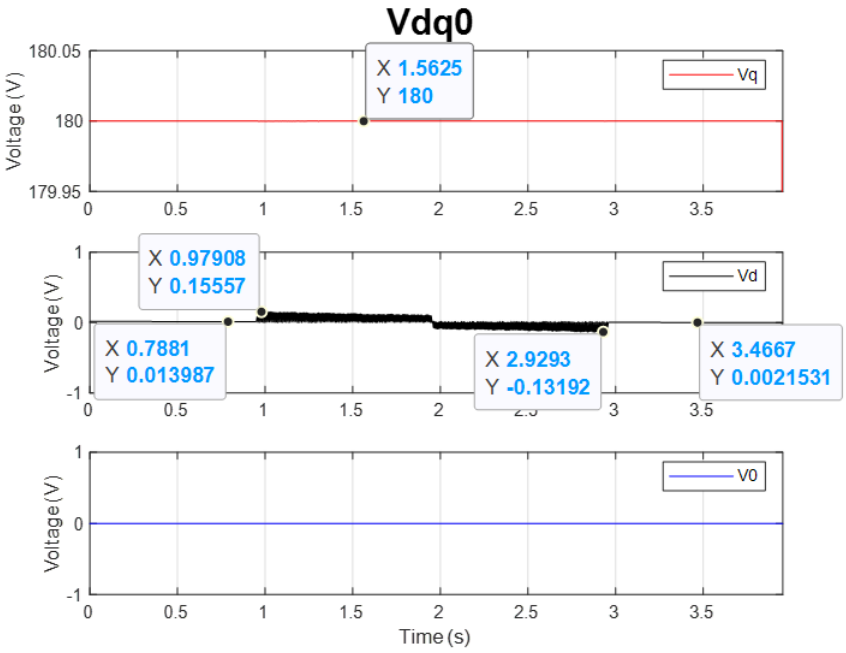

Figure 6.6: DQ0 calculation from the zero-crossings method.

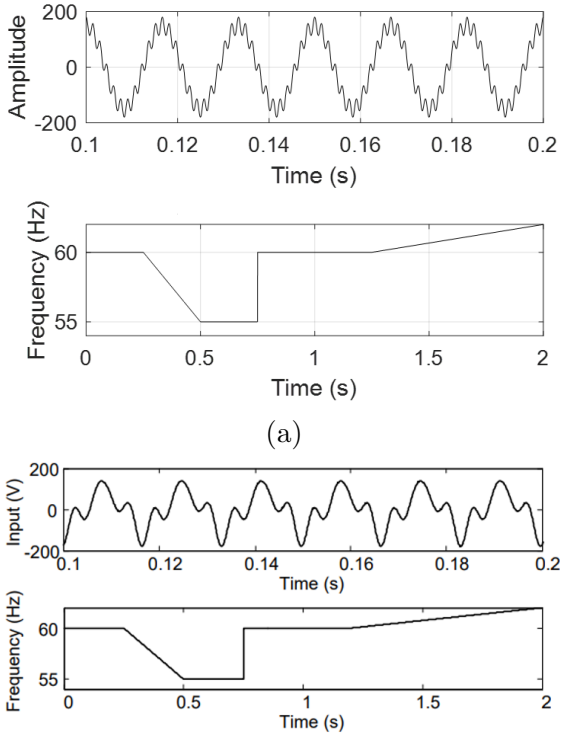

(a)

(b)

Figure 6.7: Simulated signals; (a) Simulated signal in this thesis (b) Simulated signal in [4].

it consists of a step-change which represents a switching distortion. The zero-crossings method is used to measure the frequency of the simulated signal after low-pass filtering and interpolating. It should be noted that the zero-crossings method was implemented as a post-processing technique, which means any switching distortion effect can be removed after the filtering and interpolating steps. A comparison between the two methods is illustrated in Figure 6.8. Note that the results shown in Figure 6.8(a) were taken from [4], whereas the results in Figure 6.8(b) is from the implemented zero-crossings method. It is noticeable that the zero-crossings method tracks the true frequency better than B-function. On the other hand, the B-function method has a low computation cost and can be implemented in real-time. Since there are many parameters that need to be tuned before starting generator parameter estimation algorithm, real-time tracking is not necessary for the online generator parameter estimation method.

6.2.2 Phase Locked Loop

A different scenario where both methods will perform poorly is a signal that has frequency ramp with slope of 70 Hz/s. To track the frequency in this case, a fast responding frequency tracking must be implemented. Therefore, a phase locked loop (PLL) model was developed in MATLAB-Simulink. Figure 6.9 shows the details of the PLL model. The three-phase signals were imported using the "From-Spreadsheet" block in Simulink. Then, the three-phase signals were used as input for the "MATLAB Function" block to convert the signals into the dq0 domain. The V_d signal is regulated to zero value by determining the phase angle of the rotating transformation. A proportional-integral controller was used with k_p set to 400, and k_i is set to 100E3. Three-phase simulated signals were generated that have frequency ramp with slopes of 70 Hz/s and 10 Hz/s. Figure 6.10 shows the true frequency value of the simulated signals over time and the measured frequency from the phase-locked loop. It can be

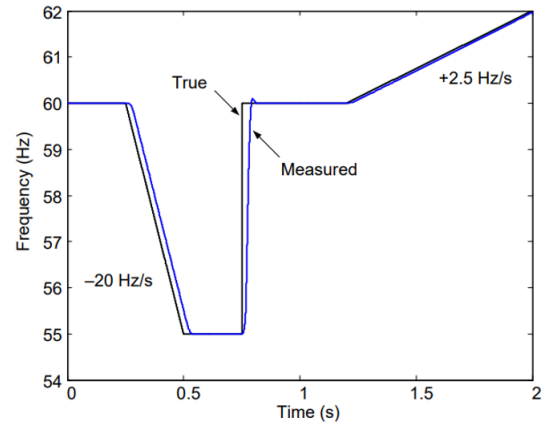

(a)

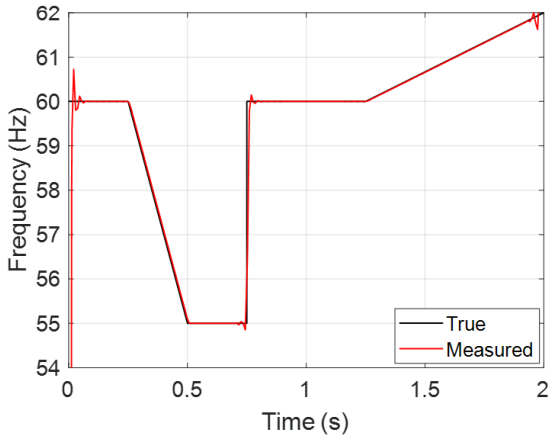

(b)

Figure 6.8: Frequency measurement; (a) the result from the B-function in [4] (b) the result from the zero-crossings method.

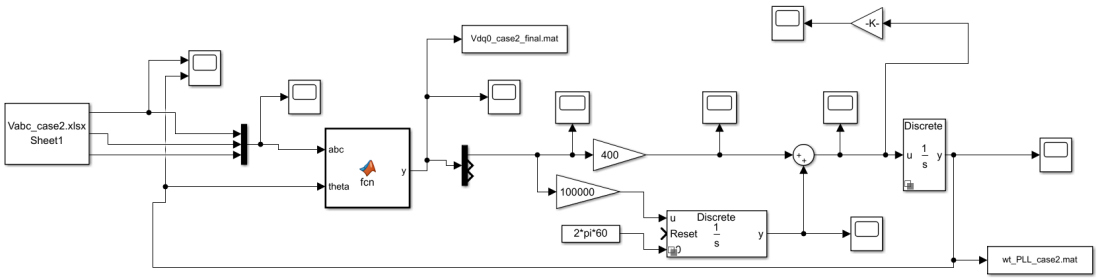

Figure 6.9: Phase locked loop model in Simulink.

seen from the figure that the PLL can track the frequency in a fast and accurate manner. The computed the V_{dq0} of the simulated signals are illustrated in Figure 6.11. Note that V_d is equal to 0.004 V, which means the PLL is off by 0.0014°

It is important to mention that both PLL and zero-crossings methods were developed to calculate the dq0 components of the laboratory synchronous generator, which has 15 Hz/s to 20 Hz/s slope during the load rejection. Therefore, It can be noted that both the zero-crossings and PLL methods are very accurate in this case.

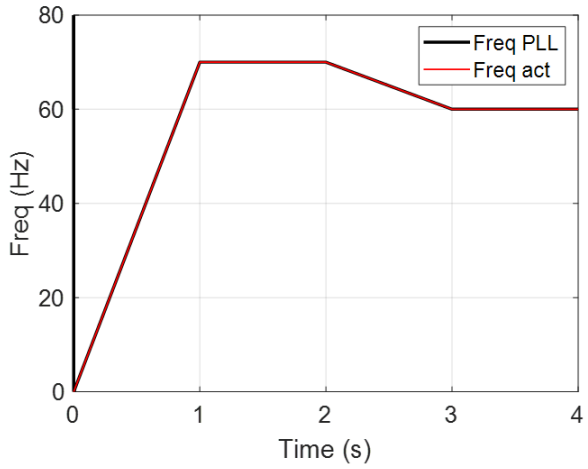

Figure 6.10: The true and the measured frequency from the PLL.

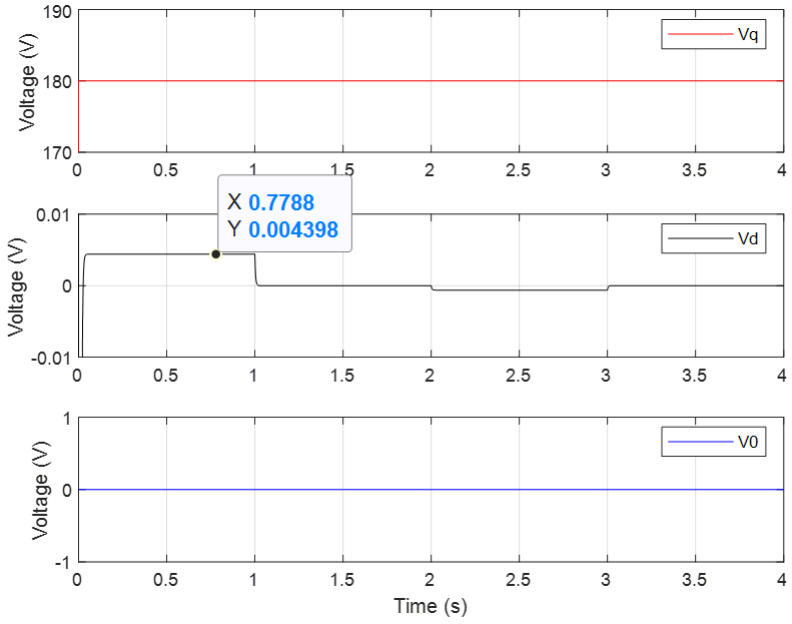

Figure 6.11: The calculated V_{dq0} using PLL.

6.3 Load Angle Tracking

In order to track the rotor angle of the generator, the angle difference between the Z signal from the shaft encoder and the falling zero crossings of phase A to neutral voltage must first be captured under a no-load condition and stored as an offset angle to measure the change in load angle under other conditions. The offset angle is calculated using formula (6.2), where T is the period of the voltage waveform, and T_{NL} is the time difference between a falling zero crossings of the phase A terminal voltage and a sequential Z pulse under no-load condition [63,64]. Similarly, the angle difference between the Z signal from the shaft encoder and the falling zero crossings of V_a under the loaded case is computed using the formula (6.3). Figure 6.12 illustrates the operation principle of load angle measurement.

$$\theta_{NL} = \frac{T_{NL}}{T} \times 360 \tag{6.2}$$

$$\theta_{UL} = \frac{T_{UL}}{T} \times 360 \tag{6.3}$$

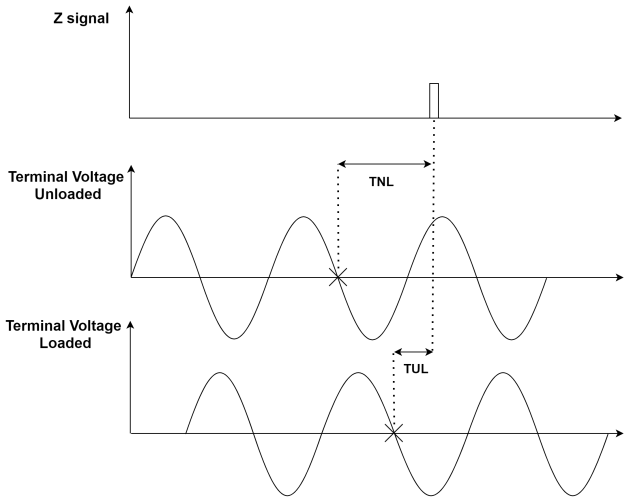

Figure 6.12: Principle of operation of load angle measuring.

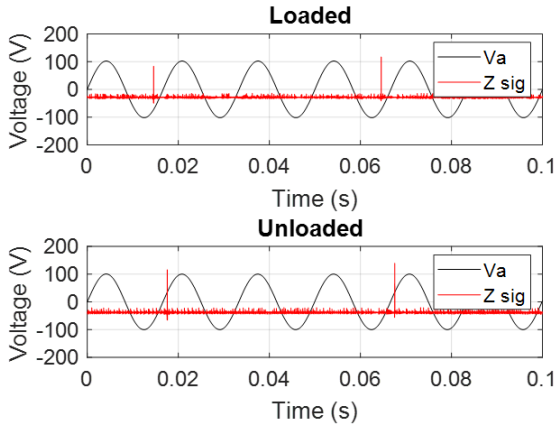

Figure 6.13: Shift of terminal voltage relative to encoder Z- signal for unloaded and loaded conditions.

The rotor angle is defined as the angle effective between the equivalent internal voltage and the phase A terminal voltage, as shown in Figure 2.3. The load angle will be zero if the internal and terminal voltages are identical in both magnitude and phase.

Figure 6.13 shows the Z signal plotted with the terminal voltage for loaded and unloaded conditions. Note that since this is a six-pole machine, there will be one Z signal pulse every three cycles. The upper traces in Figure 6.13 show the loaded condition when the generator is connected to the grid. The offset angle and the θ_{UL} were found to be 200° and 134.5°, respectively. Hence, the load angle in this case is 65.5°. This operating condition was used in the online estimation results.

A way to validate the load angle is using equation (6.4). This method is one of the recommended approaches to determine the load angle by IEEE 115 [16].

$$\delta = \arctan \frac{X_q I_a \cos(\phi)}{V_a + X q I_a \sin(\phi)} = 62^\circ \tag{6.4}$$

It is important to mention that the calculated load angle was updated every three cycles, and it was up-sampled using the built-in interpolation function in MATLAB to align it with the captured measurement sample rate, which is 80 kSamp/s.

6.4 Online Estimation of Laboratory Synchronous Generator Parameters

The testbed was used to perform a set of offline parameter identification tests, which was discussed in Chapter 3. As the IEEE 115 standard recommends, the unsaturated direct-axis synchronous reactance, X_d, was derived from the results of the open-circuit saturation and short-circuit tests. The quadrature-axis synchronous reactance was obtained from the slip test. A load rejection of a purely capacitive load was performed to calculate $X_d^{'}$ and $T_{do}^{'}$ [18,65]. Then, the fundamental parameters X_{ls} and X_{lfd} were calculated using mathematical relations, as shown in [2, 52].

The unscented Kalman filter was implemented to estimate steady-state parameters from measurements captured during generator operation using the testbed. Table 6.2 summarizes three operating condition cases with the generator synchronized to the building power supply from the power grid.

Table 6.2: Generator measurement under different power factor operation

Case	Vd (V)	Vq (V)	Id (A)	Iq (A)	Power Factor	Load Angle (Degrees)
1	92.8	41.19	30.6	37.8	0.89 leading	65.5
2	63.7	79.67	14.1	24.7	0.988 leading	38.6
3	75.3	69.5	34.6	24.5	0.992 lagging	47

In this chapter, the 4^{th}-order non-linear synchronous machine state-space model, which was derived in Chapter 2 is used, with parameters, input, and measurements as shown in (6.5)-(6.7). The transformed voltages, v_{dq0}, and the applied voltage in the field winding, v_{fd}, are used as the input vector of the UKF. Similarly, the stator current of the generator in the synchronous reference frame i_{dq0} and the current in the field winding i_{fd} were used as measurement vector of the UKF. All the measurements were captured at an 80 kHz sample rate and imported to MATLAB to estimate the steady-state parameters [66].

$$x = \{\psi_d, \psi_q, \psi_0, \psi_{fd}, L_{md}, L_{mq}, L_{ls}\} \tag{6.5}$$

$$u = \{v_d, v_q, v_0, v_{fd}\} \tag{6.6}$$

$$z = \{i_q, i_d, i_0, i_{fd}\} \tag{6.7}$$

Equations (6.8)-(6.10) define the state, system, and measurement covariance matrices P, Q and R used in the parameter estimation solution for all cases.

$$P = diag\{10^{-6}, 10^{-6}, 10^{-6}, 10^{-6}.10^{-6}, 10^{-6}, 10^{-6}\} \tag{6.8}$$

$$Q = diag\{10^{-7}, 10^{-9}, 10^{-8}, 10^{-7}.10^{-9}, 10^{-9}, 10^{-9}\} \tag{6.9}$$

$$R = diag\{10^{-6}, 10^{-7}, 10^{-10}, 10^{-6}\} \tag{6.10}$$

Figures 6.14, 6.15 and 6.16 compare the estimated steady-state machine parameters with the parameters determined from the IEEE 115-2019 testing for all cases.

It can be seen from the figures that all the steady-state parameters have successfully converged. Note that L_{md} converged to a value higher than the tested value in cases 1 and 2, whereas in case 3, L_{md} is converged to a value lower than the tested value. This is due to the operation condition. In cases 1 and 2, the generator was operated at leading power factor, and in case 3, it was operated at lagging power factor. In other words, the generator provide a reactive power which can cause X_d to saturate.

Figure 6.17 compares the measured field current and stator currents transformed

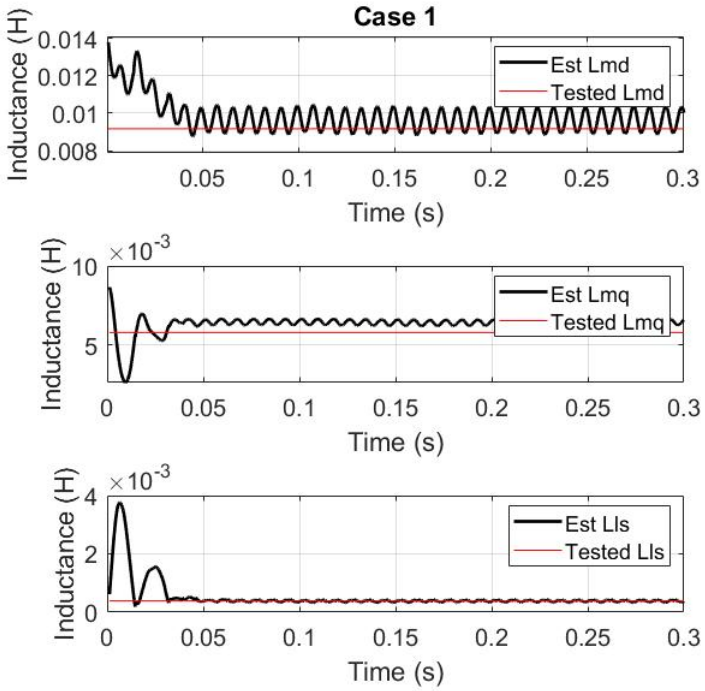

Figure 6.14: Steady-state parameter estimation results of case 1. The estimated parameter values L_{md}, L_{mq}, and L_{ls} versus time.

to the synchronous reference frame to the estimated measurements from case 1. The plots indicate that the UKF state estimator produces accurate states. The laboratory machine was operating in a slightly imbalanced state, supplying negative sequence currents in addition to the dominant positive sequence current. The negative sequence currents appear as a double frequency (120 Hz in this case) ripple on top of the constant term in the stator currents in the positive sequence reference frame.

Table 6.3 provides numerical values for the accuracy of the estimation after the UKF has converged. The estimated difference is the final converged value from the UKF result relative to the value from the IEEE 115 tests. The initial guess value for the UKF relative to the value from the IEEE 115 tests varied from 0% to 100%, and the final estimated values were found to be the same. This is true only if the initial guess of the other states are calculated using the same error in the initial guess parameters. The impact of the unbalanced machine operation leads to a noticeable

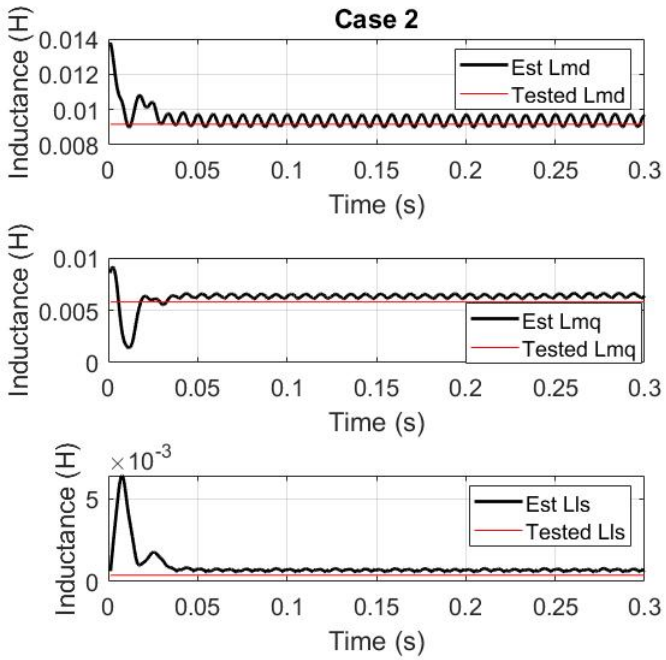

Figure 6.15: Steady-state parameter estimation results of case 2. The estimated parameter values L_{md}, L_{mq}, and L_{ls} versus time.

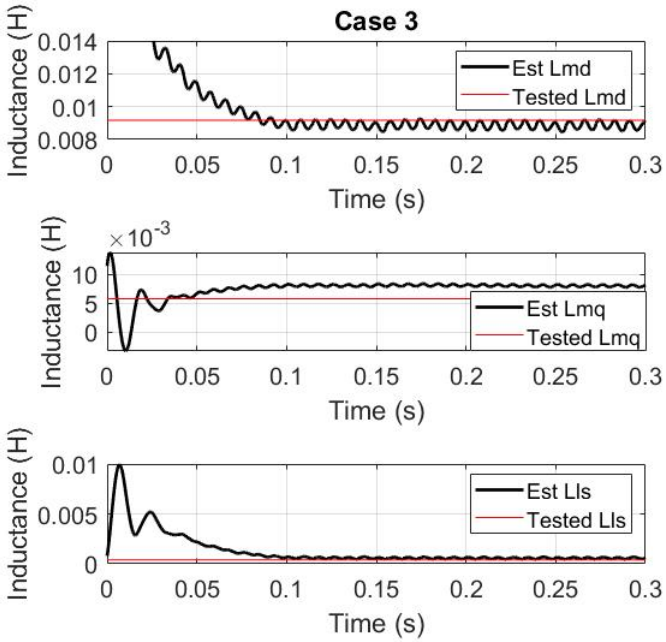

Figure 6.16: Steady-state parameter estimation results of case 3. The estimated parameter values L_{md}, L_{mq}, and L_{ls} versus time.

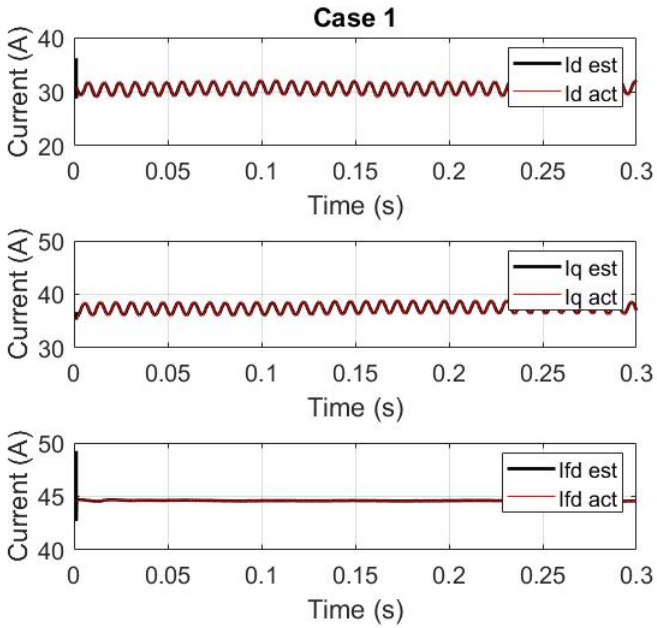

Figure 6.17: Comparison of measured currents and estimated measurements I_d, I_q, and I_{fd} from case 1

ripple in L_{md} and a smaller ripple in L_{mq} and L_{ls}. Table 6.4 presents the percent differences between the IEEE 115 tested parameters and estimated parameters of the three cases. It should be mentioned that IEEE 115 tests also potentially have a significant error, which was discussed in Chapter 3. However, they were the best option available alternative for comparison. Note that the offline test to find X_d is the most accurate test. Therefore, the parameter X_d has the lowest average differences. As discussed in literature review Section 1.2.1 and in Chapter 3, there is no accurate test to measure the stator leakage inductance. A capacitive load rejection test with a curve fitting technique were implemented to approximate the stator leakage inductance. In addition, assumptions were made in the load rejection test to approximate the L_{ls} such as neglecting the stator resistance. These factors can degrade the overall accuracy of the L_{ls}. It is important to estimate the parameters under different conditions. For example, case 1 is not the true representation of the parameter estimation accuracy. A set of online estimations of different operating points must be performed

to reflect the the parameter estimation accuracy. Overall, the UKF estimation shows satisfactory results, and it can estimate the steady-state parameters with an error margin.

6.5 Summary

In this chapter, a synchronous generator testbed was implemented to capture speed, torque, load angle, terminal current, terminal voltage, field current, field voltage, and power. The key components of the testbed were described. Methods with sufficient level of accuracy for tracking frequency and load angle in steady-state and transient conditions were developed and presented. An unscented Kalman filter-based online generator parameter estimation scheme implemented in MATLAB was fed data from the testbed and used to estimate the steady-state parameters for the generator. It was found that the parameter estimation accuracy can be tested by estimating more cases. Three operating points were used to estimate L_{md}, L_{mq} and L_{ls} and test the parameter estimation accuracy. We conclude that UKF could estimate the steady-state parameters with an error margin.

Table 6.3: Estimated parameters of the generator

Parameter	IEEE 115 tested value (mH)	Estimated value of case 1 (mH)	Estimated value of case 2 (mH)	Estimated value of case 3 (mH)
L_{md}	9.172	9.66	9.484	8.831
L_{mq}	5.786	6.435	6.358	7.971
L_{ls}	0.3859	0.4142	0.657	0.549

Table 6.4: Percent error of the parameters from all cases

Parameter	Case 1 difference (%)	Case 2 difference (%)	Case 3 difference (%)	Average difference (%)
L_{md}	-5.32	-3.4	3.72	4.15
L_{mq}	-11.22	-9.89	-37.76	19.62
L_{ls}	-7.33	-70.25	-42.26	-39.95

7. Summary, Conclusions and Future Work

7.1 Summary and Conclusions

Accurate generator models play a crucial role in maintaining stable operation of the power system. Since the parameters from generator commissioning can result in discrepancies between the generator's actual and simulated dynamic behavior in response to disturbances, the WECC requires generator models to be validated every five years through offline testing. However, offline testing has several disadvantages: lost revenue due to downtime and increased stress on other generators. To overcome the drawbacks of offline testing, online estimation techniques can be implemented to determine and refine the generator parameters.

This thesis developed and implemented an online estimation method to determine the parameters of simulated and laboratory synchronous generators. It conducted several offline tests to determine the laboratory synchronous generator parameters to be used as a reference to the performance of the online estimation. It also explores the accuracy challenges of offline testing.

A study of sensitivity analysis of the UKF using a simulated generator model was conducted. The study focuses on the performance of the UKF in the presence of innovation and observation outliers. In the innovation outliers, the known parameters were varied in both steady-state and transient parameter estimations. The steady-state sensitivity analysis has shown a pattern in each parameter variation test. It was found that the UKF estimation can be sensitive to the accuracy of some of the known parameters in the estimation process, such as load angle. As a result, the estimated parameters could converge with an error of 100%.

On the other hand, the sensitivity analysis of the transient parameters showed no pattern in the variations of the estimation results due to the variations of the known

parameters. However, it was found that the setting of the system covariance matrix may cause a different response to the estimation. Similar to the steady-state, the UKF can converge to an incorrect solution. Without knowledge of the actual parameters, which was the case for the laboratory testing, it is very challenging to know whether the converged value represents the actual parameters of the machine or whether the estimator converges to different values due to the effect of error in the known parameters. Note that even if the manufacturers parameters were used as a reference in an commercial generator, they may still have errors since they vary over time due to the aging of the generator, saturation, and temperature changes.

The UKF parameter estimation approach assumes that the measurement noise follows a Gaussian distribution. However, some measurement devices produce non-Gaussian noise. This thesis compares the performance of the UKF and GM-UKF in the presence of Gaussian and non-Gaussian noise in the measurements. It was found that the UKF did not perform well for generator parameter estimation with non-Gaussian noise added to the measurement data from an electromagnetic transients program simulation. In contrast, the GM-UKF showed its robustness against non-Gaussian noise in the measurement data.

The UKF was used to estimate steady-state parameters of a 13.5 kVA synchronous generator and practically test the filter under the condition of uncertainties of known parameters accuracy. Data from three steady-state operating conditions were used to determine the performance of the filter. It was found that performing only one estimation test is not a proper evaluation of the UKF performance. However, a set of tests with same covariance matrices can reflect the filter's accuracy in estimating the steady-state parameters. Overall, the UKF estimations show a better accuracy relative to offline testing, since it can estimate L_{md} and L_{mq}, and account for the saturation effect of different operating conditions.

7.2 Future Work

This section discusses recommendations for future research regarding online generator estimation. It can be divided into three major topic areas: UKF testing and formulations, offline testing of the laboratory generator and other techniques of online estimation.

7.2.1 UKF Testing and Formulations

Based on the results presented in this thesis, UKF performance for generator parameter estimation can not be evaluated using one operating point. Therefore, a set of measurements with different operating conditions can be collected to estimate the steady-state parameters of a large-scale synchronous generator.

The UKF is not reliable for estimating transient and sub-transient parameters, especially when several known parameters with questionable degrees of accuracy are kept constant during the estimation. Therefore, reducing the order of the state space to minimize the number of known parameters during the estimation is recommended. For example, in [33], the authors implement a second-order function to represent the generator. The estimated parameters were H, D, P_m, and X'_d, and they have not used any known parameters. Similar developments are needed to be able to estimate the remaining parameters starting either without assuming known parameters or using only trusted known parameters.

7.2.2 Offline Testing of the Laboratory Generator

In practice, the issue of generator online parameter estimation is the uncertainty of accuracy in the known parameters. In the simulated generator model, both the actual steady-state and transient parameters are known and can be used as a reference value to validate the online estimation result. As we have seen in this thesis, minor

deviation of the known parameters during the transient parameter estimation could lead to incorrect convergence, and without knowledge of the actual parameters, the estimation result can be misleading. Therefore, standstill frequency response (SSFR) tests can be implemented to determine the full equivalent circuit of the laboratory generator and validate the load rejection test result. The tested parameters from SSFR-testing can be used as reference values for the online estimation method. Future University of Idaho researchers should know about the slightly unbalance condition in amplitude and angle of the laboratory generator and the rotor eccentricity condition if they are planning to use it for testing where that would impact their results.

7.2.3 Other Techniques of Online Estimation

Most publications describing online parameter identification approaches for a synchronous generator are implemented using a simulated model to test the estimation method. However, few papers have implemented online estimation on a physical generator (both laboratory and commercial generator), and most of them only determined the steady-state parameters. Based on our literature review, which considered papers that were published after 2000, there are only two papers that conducted online parameter identification and determined the full equivalent circuits of a physical synchronous generator [67, 68]. A gas turbine synchronous machine at Ambarli natural gas combined cycle power plant in Turkey was used in [67]. The authors were able to estimate steady-state and transient parameters using linear least-squares optimization technique. In [68], a new genetic algorithm was proposed to simultaneously identify the parameters of synchronous generator using measurement data. Future researchers need to choose and implement a more robust method that is less sensitive to the inaccuracy of the system function.

Bibliography

[1] Z. Huang, N. Zhou, R. Diao, S. Wang, S. Elbert, D. Meng, and S. Lu, "Capturing Real-Time Power System Dynamics: Opportunities and Challenges," in *2015 IEEE Power Energy Society General Meeting*, 2015, pp. 1–5.

[2] P. Kundur, *Power System Stability And Control*. McGraw-Hill, 1994. [Online]. Available: https://books.google.com/books?id=v3RxH_GkwmsC

[3] P. Krause, O. Wasynczuk, S. Sudhoff, and S. Pekarek, *Analysis of Electric Machinery and Drive Systems*, ser. IEEE Press Series on Power and Energy Systems. Wiley, 2013. [Online]. Available: https://books.google.com/books?id=ocr9wSmSZEsC

[4] B. Kasztenny, "A New Method for Fast Frequency Measurement for Protection Applications (presentation)," 03 2018.

[5] L. A. Kilgore, "Calculation of synchronous machine constants- reactances and time constants affecting transient characteristics," *Transactions of the American Institute of Electrical Engineers*, vol. 50, no. 4, pp. 1201–1213, 1931.

[6] S. H. Wright, "Determination of Synchronous Machine Constants by Test Reactances, Resistances, and Time Constants," *Transactions of the American Institute of Electrical Engineers*, vol. 50, no. 4, pp. 1331–1350, 1931.

[7] N. A. E. R. Council, *Technical Analysis of the August 14, 2003, Blackout: What Happened, Why, and what Did We Learn?*, ser. Engineering case studies online. North American Electric Reliability Council, 2004. [Online]. Available: https://books.google.com/books?id=ZfJ7MwEACAAJ

[8] O. Veloza and F. Santamaria, "Analysis of major blackouts from 2003 to 2015: Classification of incidents and review of main causes," *The Electricity Journal*, vol. 29, pp. 42–49, 09 2016.

[9] D. Kosterev, C. Taylor, and W. Mittelstadt, "Model validation for the August 10, 1996 WSCC system outage," *IEEE Transactions on Power Systems*, vol. 14, no. 3, pp. 967–979, 1999.

[10] E. Kyriakides, G. T. Heydt, and V. Vittal, "Online parameter estimation of round rotor synchronous generators including magnetic saturation," *IEEE Transactions on Energy Conversion*, vol. 20, no. 3, pp. 529–537, 2005.

[11] ——, "On-Line Estimation of Synchronous Generator Parameters Using a Damper Current Observer and a Graphic User Interface," *IEEE Transactions on Energy Conversion*, vol. 19, no. 3, pp. 499–507, 2004.

[12] "Generating Unit Model Validation Policy," 2020, https://www.wecc.org/Administrative/WECC%20Generating%20Unit%20Model%20Validation%20Policy.pdf, Accessed on 14 March 2021.

[13] S. Wang, J. Zhao, Z. Huang, and R. Diao, "Assessing Gaussian Assumption of PMU Measurement Error Using Field Data," *IEEE Transactions on Power Delivery*, vol. 33, no. 6, pp. 3233–3236, 2018.

[14] V. Karapetoff, "Variable armature leakage reactance in salient-pole synchronous machines," *Journal of the A.I.E.E.*, vol. 45, no. 7, pp. 665–669, 1926.

[15] L. A. March and S. B. Crary, "Armature Leakage Reactance of Synchronous Machines," *Transactions of the American Institute of Electrical Engineers*, vol. 54, no. 4, pp. 378–381, 1935.

[16] "IEEE Guide for Test Procedures for Synchronous Machines Including Acceptance and Performance Testing and Parameter Determination for Dynamic Analysis," *IEEE Std 115-2019 (Revision of IEEE Std 115-2009)*, pp. 1–246, 2020.

[17] "Rotating Electrical Machines- Part 4: Methods for Determining Synchronous Machine Quantities from Tests," *IEC 60034-4-1*, 2018.

[18] E. da Costa Bortoni and J. Jardini, "Identification of Synchronous Machine Parameters Using Load Rejection Test Data," *IEEE Transactions on Energy Conversion*, vol. 17, no. 2, pp. 242–247, 2002.

[19] R. Wamkeue, F. Baetscher, and I. Kamwa, "Hybrid-State-Model-Based Time-Domain Identification of Synchronous Machine Parameters From Saturated Load Rejection Test Records," *IEEE Transactions on Energy Conversion*, vol. 23, no. 1, pp. 68–77, 2008.

[20] A. Belqorchi, U. Karaagac, J. Mahseredjian, and I. Kamwa, "Standstill frequency response test and validation of a large hydrogenerator," *IEEE Transactions on Power Systems*, vol. 34, no. 3, pp. 2261–2269, 2019.

[21] P. Dandeno, H. Karmaker, C. Azuaje, M. Glinkowski, I. Kamwa, S. Oliveira, S. Salon, R. Saunders, and S. Umans, "Experience with standstill frequency response (SSFR) testing and analysis of salient pole synchronous machines," *IEEE Transactions on Energy Conversion*, vol. 14, no. 4, pp. 1209–1217, 1999.

[22] F. de Mello, L. Hannett, and J. Willis, "Determination of synchronous machine stator and field leakage inductances from standstill frequency response tests," *IEEE Transactions on Power Systems*, vol. 3, no. 4, pp. 1625–1632, 1988.

[23] R. Dutta, P. Kundu, and A. Srivastava, "Dynamic State and Parameter Estimation of Distributed Generators using Constraint Recursive Least Square Al-

gorithm and μ-PMU Data," in *2020 IEEE International Conference on Power Electronics, Smart Grid and Renewable Energy (PESGRE2020)*, 2020, pp. 1–5.

[24] E. Kyriakides and G. Heydt, "An Observer for the Estimation of Synchronous Generator Damper Currents for Use in Parameter Identification," *IEEE Transactions on Energy Conversion*, vol. 18, no. 1, pp. 175–177, 2003.

[25] M. West, "Online Dynamic Parameter Estimation of Synchronous Machine," 2016.

[26] L. Fan and Y. Wehbe, "Extended Kalman filtering based real-time dynamic state and parameter estimation using PMU data," *Electric Power Systems Research*, vol. 103, pp. 168–177, 2013. [Online]. Available: https://www.sciencedirect.com/science/article/pii/S0378779613001442

[27] Z. Huang, P. Du, D. Kosterev, and B. Yang, "Application of Extended Kalman Filter Techniques for Dynamic Model Parameter Calibration," in *2009 IEEE Power Energy Society General Meeting*, 2009, pp. 1–8.

[28] D. Meng, N. Zhou, S. Lu, and G. Lin, "An Expectation-Maximization Method for Calibrating Synchronous Machine Models," in *2013 IEEE Power Energy Society General Meeting*, 2013, pp. 1–5.

[29] S. Julier and J. Uhlmann, "Unscented filtering and nonlinear estimation," *Proceedings of the IEEE*, vol. 92, no. 3, pp. 401–422, 2004.

[30] D. Simon, *Optimal State Estimation: Kalman, H∞, and Nonlinear Approaches*, 01 2006.

[31] A. Rouhani and A. Abur, "Constrained Iterated Unscented Kalman Filter for Dynamic State and Parameter Estimation," *IEEE Transactions on Power Systems*, vol. 33, no. 3, pp. 2404–2414, 2018.

[32] D. Meng, N. Zhou, S. Lu, and G. Lin, "An Expectation-Maximization Method for Calibrating Synchronous Machine Models," in *2013 IEEE Power Energy Society General Meeting*, 2013, pp. 1–5.

[33] L. Fan and Y. Wehbe, "Extended Kalman filtering based real-time dynamic state and parameter estimation using PMU data," *Electric Power Systems Research*, vol. 103, pp. 168–177, 10 2013.

[34] G. Valverde, E. Kyriakides, G. T. Heydt, and V. Terzija, "Nonlinear Estimation of Synchronous Machine Parameters Using Operating Data," *IEEE Transactions on Energy Conversion*, vol. 26, no. 3, pp. 831–839, 2011.

[35] Z. Huang, P. Du, D. Kosterev, and B. Yang, "Application of Extended Kalman Filter Techniques for Dynamic Model Parameter Calibration," in *2009 IEEE Power Energy Society General Meeting*, 2009, pp. 1–8.

[36] A. G. Miles, B. K. Johnson, and N. Fischer, "Online Characterization of a Synchronous Generator Using an Unscented Kalman Filter," in *2019 IEEE International Electric Machines Drives Conference (IEMDC)*, 2019, pp. 1485–1492.

[37] M. A. Gandhi and L. Mili, "Robust kalman filter based on a generalized maximum-likelihood-type estimator," *IEEE Transactions on Signal Processing*, vol. 58, no. 5, pp. 2509–2520, 2010.

[38] A. Miles, "Implementation of the Joint-Unscented Kalman Filter for Online Characterization of Synchronous Machines Online," 2017.

[39] H. Wen, C. Li, and W. Yao, "Power System Frequency Estimation of Sine-Wave Corrupted With Noise by Windowed Three-Point Interpolated DFT," *IEEE Transactions on Smart Grid*, vol. 9, no. 5, pp. 5163–5172, 2018.

[40] D. Belega, "Frequency estimation via weighted multipoint interpolated DFT," *IET Science, Measurement Technology*, vol. 2, pp. 1–8(7), January 2008. [Online]. Available: https://digital-library.theiet.org/content/journals/10.1049/iet-smt_20070022

[41] A. Ashrafian, M. Mirsalim, and M. A. S. Masoum, "An Adaptive Recursive Wavelet Based Algorithm for Real-Time Measurement of Power System Variables During Off-Nominal Frequency Conditions," *IEEE Transactions on Industrial Informatics*, vol. 14, no. 3, pp. 818–828, 2018.

[42] K. Sun, Q. Zhou, and Y. Liu, *IEEE Transactions on Smart Grid, title=A Phase Locked Loop-Based Approach to Real-Time Modal Analysis on Synchrophasor Measurements*, vol. 5, no. 1, pp. 260–269, 2014.

[43] X. Luo, J. Zhang, Q. Bu, Q. Zeng, Q. Zhang, D. Luo, and L. Tang, "Improved Zero-crossing Method for Power System Frequency Estimation*," in *2018 13th World Congress on Intelligent Control and Automation (WCICA)*, 2018, pp. 1403–1407.

[44] H. Cai, "Fast Frequency Measurement Algorithm based on Zero Crossing Method," in *2010 2nd International Conference on Computer Engineering and Technology*, vol. 4, 2010, pp. V4–606–V4–608.

[45] E. Barrera-Cardiel and N. Pastor-Gomez, "Microcontroller-Based Power-Angle Instrument for a Power Systems Laboratory," in *1999 IEEE Power Engineering Society Summer Meeting. Conference Proceedings (Cat. No.99CH36364)*, vol. 2, 1999, pp. 1008–1012 vol.2.

[46] M. DespalatoviÄ, M. JadriÄ, and B. TerziÄ, "Real-time power angle determination of salient-pole synchronous machine based on air gap

measurements," *Electric Power Systems Research*, vol. 78, no. 11, pp. 1873–1880, 2008. [Online]. Available: https://www.sciencedirect.com/science/article/pii/S0378779608001077

[47] T. Idzotic, G. Erceg, and D. Sumina, "Load Angle Estimation of a Synchronous Generator," vol. 3, 06 2004, pp. 893 – 896 Vol.3.

[48] E. Ghahremani, M. Karrari, and O. Malik, "Synchronous generator third-order model parameter estimation using online experimental data," *Generation, Transmission Distribution, IET*, vol. 2, pp. 708 – 719, 10 2008.

[49] A. Del Angel, P. Geurts, D. Ernst, M. Glavic, and L. Wehenkel, "Estimation of Rotor Angles of Synchronous Machines Using Artificial Neural Networks and Local PMU-based Quantities," *Neurocomputing*, vol. 70, pp. 2668–2678, 10 2007.

[50] E. P. T. Cari, L. F. C. Alberto, and N. G. Bretas, "A novel methodology for power angle estimation of synchronous generator based on trajectory sensitivity analysis," in *2009 IEEE Power Energy Society General Meeting*, 2009, pp. 1–6.

[51] R. H. Park, "Two Reaction Theory of Synchronous Machines Generalized Method of Analysis-Part I," *Transactions of the American Institute of Electrical Engineers*, vol. 48, no. 3, pp. 716–727, 1929.

[52] T. Lipo, *Analysis of synchronous machines*. Boca Raton, FL: Taylor Francis, 2012.

[53] "IEEE Guide for Synchronous Generator Modeling Practices and Parameter Verification with Applications in Power System Stability Analyses," *IEEE Std 1110-2019 (Revision of IEEE Std 1110-2002)*, pp. 1–92, 2020.

[54] S. Sarkka, "On Unscented Kalman Filtering for State Estimation of Continuous-Time Nonlinear Systems," *IEEE Transactions on Automatic Control*, vol. 52, no. 9, pp. 1631–1641, 2007.

[55] J. Zhao and L. Mili, "A Robust Generalized-Maximum Likelihood Unscented Kalman Filter for Power System Dynamic State Estimation," *IEEE Journal of Selected Topics in Signal Processing*, vol. 12, no. 4, pp. 578–592, 2018.

[56] Y. Chakhchoukh and H. Ishii, "Robust estimation for enhancing the cyber security of power state estimation," in *2015 IEEE Power Energy Society General Meeting*, 2015, pp. 1–5.

[57] Y. Chakhchoukh, V. Vittal, G. T. Heydt, and H. Ishii, "LTS-Based Robust Hybrid SE Integrating Correlation," *IEEE Transactions on Power Systems*, vol. 32, no. 4, pp. 3127–3135, 2017.

[58] J. Zhao, M. Netto, and L. Mili, "A Robust Iterated Extended Kalman Filter for Power System Dynamic State Estimation," *IEEE Transactions on Power Systems*, vol. 32, no. 4, pp. 3205–3216, 2017.

[59] L. Mili, M. Cheniae, N. Vichare, and P. Rousseeuw, "Robust state estimation based on projection statistics [of power systems]," *IEEE Transactions on Power Systems*, vol. 11, no. 2, pp. 1118–1127, 1996.

[60] J. Zhao, M. Netto, and L. Mili, "A Robust Iterated Extended Kalman Filter for Power System Dynamic State Estimation," *IEEE Transactions on Power Systems*, vol. 32, no. 4, pp. 3205–3216, 2017.

[61] A. Mitra, A. Mohapatra, and S. Chakrabarti, "Parameter Estimation of a Synchronous Generator at Moderate Measurement Sampling Rate," in *2019 IEEE PES Innovative Smart Grid Technologies Europe (ISGT-Europe)*, 2019, pp. 1–5.

[62] "Ultra Precise Shaft Torquemeters," 2018, https://www.himmelstein.com/sites/default/files/2018-10/B7409.pdf, Accessed on 14 March 2021.

[63] S. M. Hosseini, R. Abdollahi, and M. Karrari, "Inclusive Design and Implementation of Online Load Angle Measurement for Real-Time Transient Stability Improvement of a Synchronous Generator in a Smart Grid," *IEEE Transactions on Industrial Electronics*, vol. 65, no. 11, pp. 8966–8972, 2018.

[64] T. Rahman, S. Sankaran, N. Seeley, and K. Garg, "Capturing generator rotor angle and field quantities - SDGE experience and approach to using nontraditional generator measurements," 04 2016, pp. 1–9.

[65] D. Tiomo, E. Y. Kenfack, and R. Wamkeue, "Dynamic Study and Analysis of Synchronous Generator under Sudden Short Circuit and Load Rejection Tests," in *2019 IEEE/IAS 55th Industrial and Commercial Power Systems Technical Conference (I CPS)*, 2019, pp. 1–5.

[66] MATLAB, *9.8.0.1323502 (R2020a)*. Natick, Massachusetts: The MathWorks Inc., 2010.

[67] U. Karaagac and O. Tor, "On-line Parameter Identification of a Gas Turbine Generator at Ambarli Power Plant," in *2006 IEEE Power Engineering Society General Meeting*, 2006, pp. 5 pp.–.

[68] B. Zaker, G. B. Gharehpetian, M. Karrari, and N. Moaddabi, "Simultaneous Parameter Identification of Synchronous Generator and Excitation System Using Online Measurements," *IEEE Transactions on Smart Grid*, vol. 7, no. 3, pp. 1230–1238, 2016.

A. Simulated Model

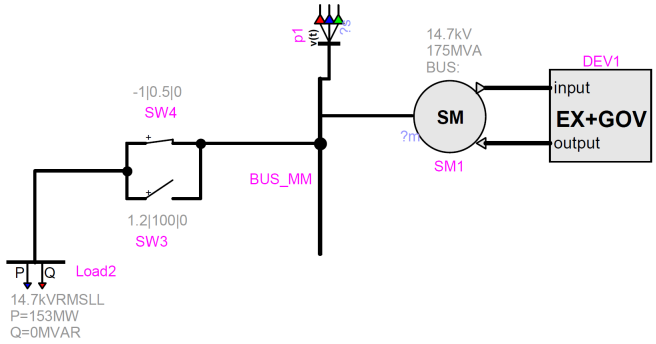

(a)

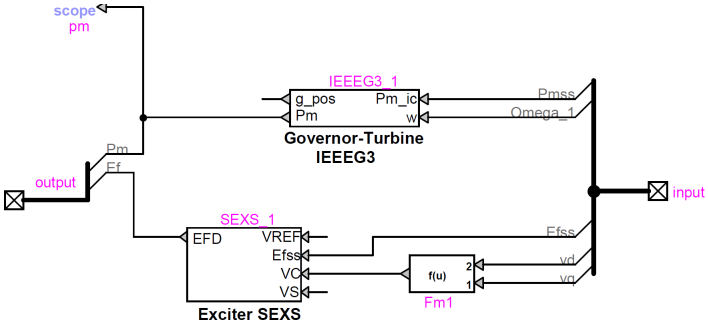

(b)

Figure A.1: System model in EMTP-RV: (a) Overview of system model. (b) The exciter and the governor model

B. Slip Test Results

Figures B.1 and B.2 present the slip results.

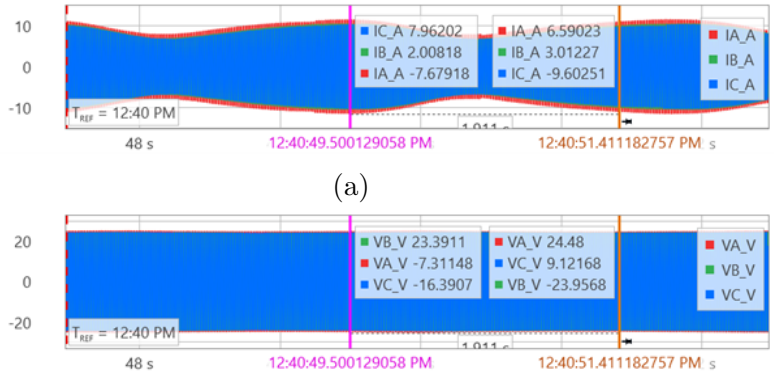

(a)

(b)

Figure B.1: Slip test results 2: (a) Terminal current (b) Terminal voltage

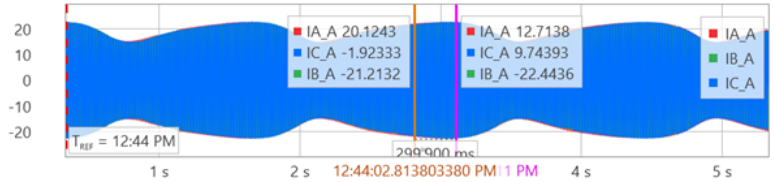

(a)

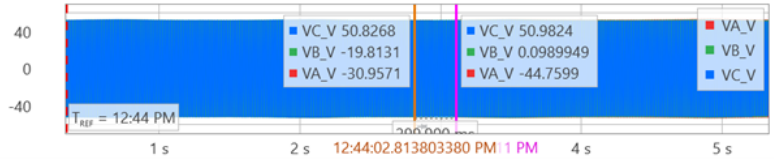

(b)

Figure B.2: Slip test results 3: (a) Terminal current (b) Terminal voltage

C. Transient Parameter Estimation - Zoomed out Version

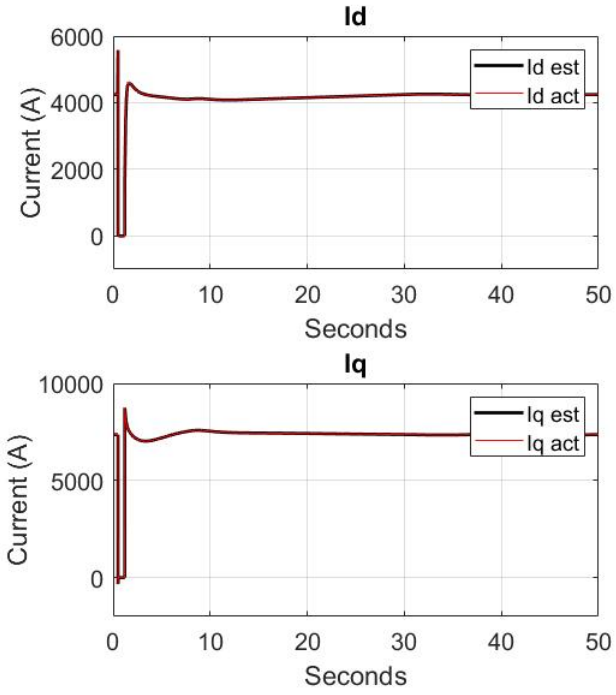

Figure C.1: Estimated measurement: the current of d and q axes - zoomed out version

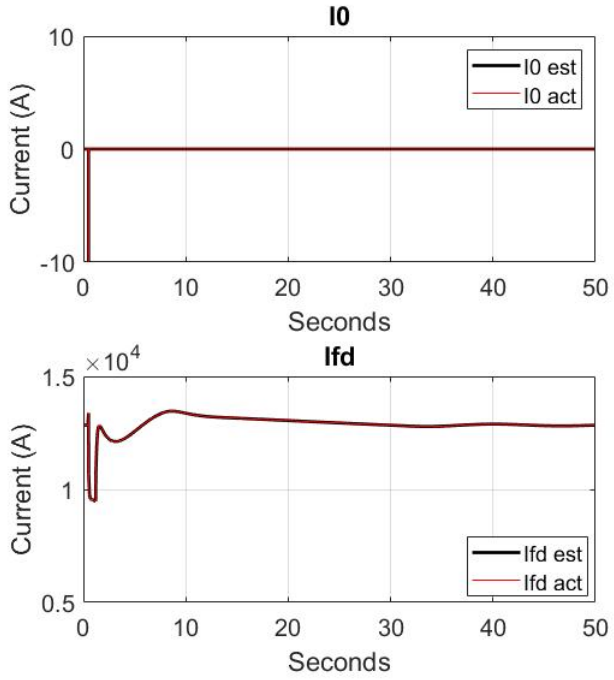

Figure C.2: Estimated measurement: zero-sequence current and the field current - zoomed out version

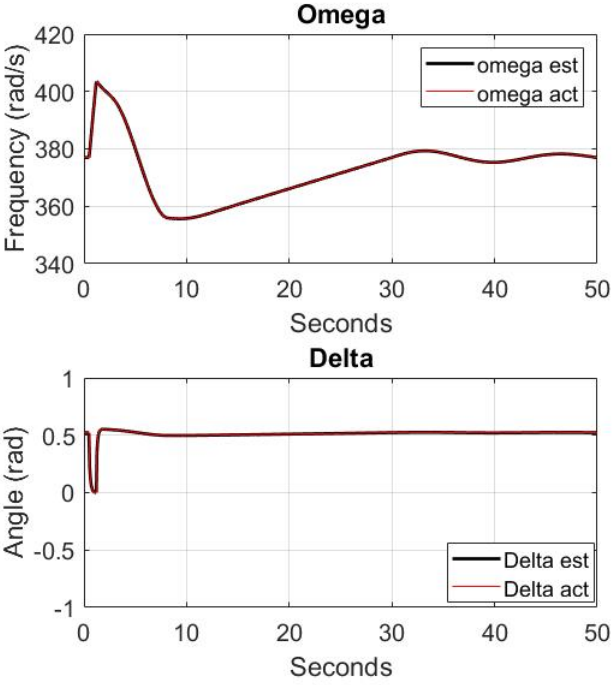

Figure C.3: Estimated measurement: the angular frequency and the load angle - zoomed out version

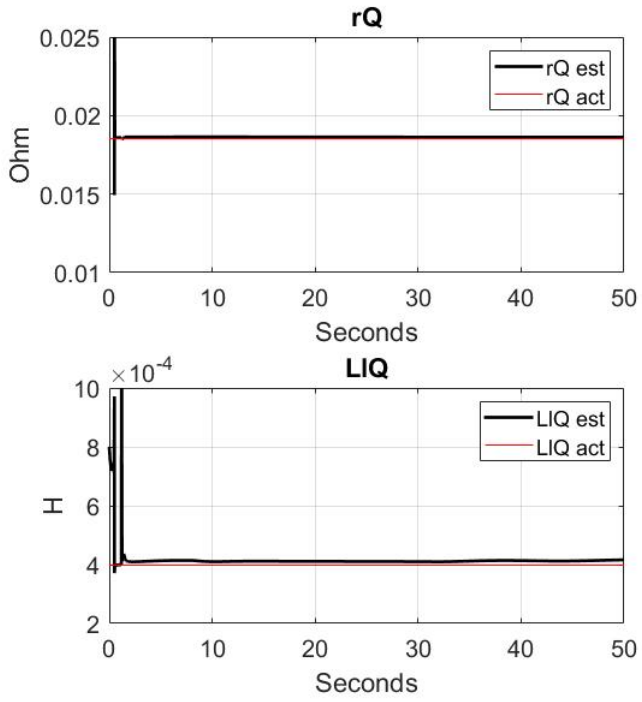

Figure C.4: Estimation of L_{lQ} and r_Q - zoomed out version

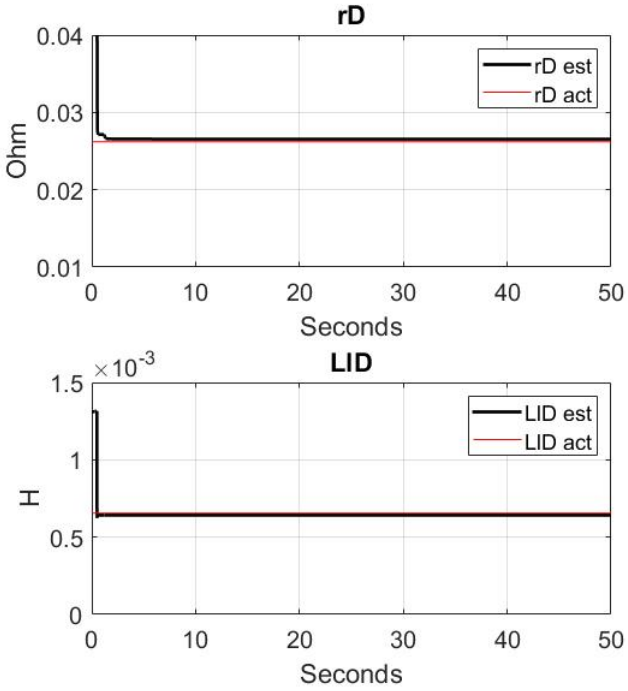

Figure C.5: Estimation of L_{lD} and r_D - zoomed out version

D. Voltage Transformer Testing Result

Table D.1: Voltage transformer - turn ratio

PT1			PT 2			PT 3		
Vp	Vs	Ratio	Vp	Vs	Ratio	Vp	Vs	Ratio
1.42	0.04	39.56	1.41	0.04	39.72	1.41	0.04	39.53
2.13	0.05	39.4	2.13	0.05	39.46	2.13	0.05	39.38
2.84	0.07	39.3	2.83	0.07	39.36	2.83	0.07	39.26
3.54	0.09	39.22	3.54	0.09	39.26	3.54	0.09	39.19
4.26	0.11	39.15	4.26	0.11	39.23	4.26	0.11	39.16
4.97	0.13	39.13	4.97	0.13	39.2	4.96	0.13	39.06
5.68	0.15	39.17	5.68	0.15	39.17	5.68	0.15	39.16
6.39	0.16	39.07	6.39	0.16	39.13	6.39	0.16	39.08
7.1	0.18	39.03	7.1	0.18	39.11	7.1	0.18	39.05
80	2.07	38.68	80	2.07	38.7	80	2.07	38.68
90	2.33	38.68	90	2.33	38.69	90	2.33	38.68
100	2.59	38.67	100	2.59	38.68	100	2.59	38.68
110	2.85	38.65	110	2.84	38.68	110	2.84	38.68
120	3.11	38.65	120	3.1	38.68	120	3.1	38.67
127	3.29	38.65	127	3.28	38.67	127	3.28	38.67
130	3.36	38.66	130	3.36	3.68	130	3.36	38.67
135	3.49	38.65	135	3.49	3.68	135	3.49	38.67
140	3.63	38.6	140	3.62	3.67	140	3.63	38.57
145	3.76	38.56	145	3.75	3.67	145	3.75	38.67

E. Measurement Correlation for Torque Transducer

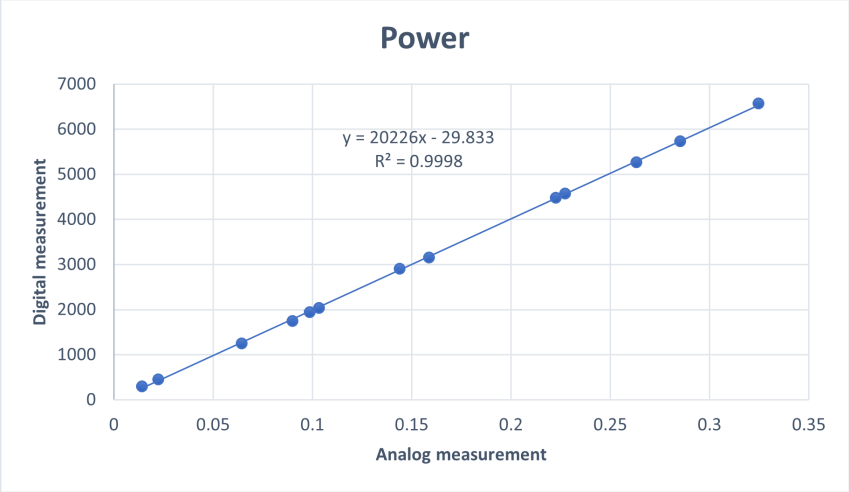

Figure E.1: Mechanical power - analog and digital measurment

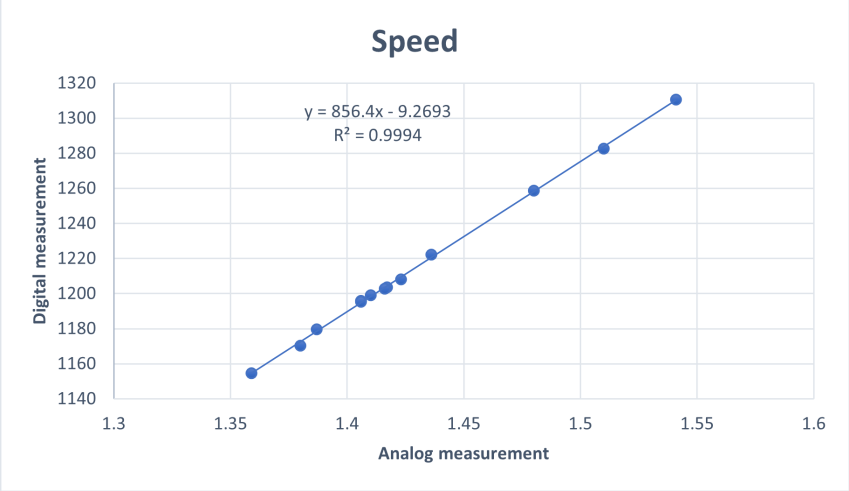

Figure E.2: Mechanical speed - analog and digital measurment

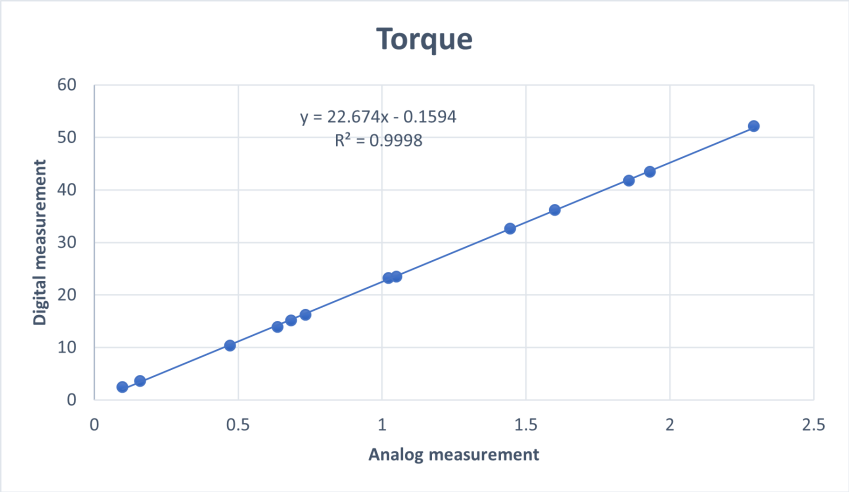

Figure E.3: Mechanical torque - analog and digital measurment

F. Source Code for the Zero-Crossings Method

F.0.1 Main Code

```
a=1

clear all

clc

 Fs = 80000;

 T_end= 2;

 t = 0:1/Fs:T_end;

 f_in_start = 60;

 f_in_end = 60;

 f_in1 = linspace(60, 60, Fs/4);

 f_in2 = linspace(60, 55,  Fs/4);

 f_in3 = linspace(55, 55,  Fs/4);

 f_in4 = linspace(60, 60,  (Fs/4)*2);

 f_in5 = linspace(60, 62, (Fs/4)*3+1);


f_in = [ f_in1 f_in2 f_in3 f_in4  f_in5];


phase_in = cumsum(f_in/Fs);

 Va= zeros(1,length(f_in));

 Vb= zeros(1,length(f_in));

 Vc= zeros(1,length(f_in));


 A = 100;

 Va= A*cos(2*pi*phase_in)+...
```

```
 A*0.2*cos(11*2*pi*phase_in)+...
 1*A*0.2*cos(3*2*pi*phase_in)+ 1*A*0.1*cos(7*2*pi*phase_in);
 Vb= A*cos(2*pi*phase_in-2*pi/3)+...
 A*0.2*cos(11*2*pi*phase_in-2*pi/3)...
 + 1*A*0.2*cos(3*2*pi*phase_in-2*pi/3)...
 +1*A*0.1*cos(7*2*pi*phase_in-2*pi/3);
 Vc= A*cos(2*pi*phase_in+2*pi/3)+...
 A*0.2*cos(11*2*pi*phase_in+2*pi/3)...
 + 1*A*0.2*cos(3*2*pi*phase_in+2*pi/3)+...
 1*A*0.1*cos(7*2*pi*phase_in+2*pi/3);

 Vact= A*cos(2*pi*phase_in);

figure
subplot(2,1,1)
plot(t,Va,'k')
grid on
axis([0 2 -200 200])
ylabel('Amplitude')
xlabel('Time (s)')
title('Simulated signal')
set(gca,'fontsize',15)
subplot(2,1,2)
plot(t,f_in,'k')
grid on
ylabel('Frequency (Hz)')
xlabel('Time (s)')
```

```
axis([0 2 54 62])
title('Frequency of the input signal')
set(gca,'fontsize',15)
%%
k=1;
cf = 90; % cutt of freq

Vaf_iir = Filter(Va,t,k,cf);

Vbf_iir = Filter(Vb,t,k,cf);
Vcf_iir = Filter(Vc,t,k,cf);
%%
kk=24;
xx = 0:t(2)/kk:t(end);
Vaf_iirx= spline(t,Vaf_iir,xx);
f_act_fir = interp1(t,f_in,xx);
Vbf_iirx= spline(t,Vbf_iir,xx);
Vcf_iirx= spline(t,Vcf_iir,xx);
f_inx =interp1(t,f_in,xx);

Vax= spline(t,Va,xx);
[ f_time, f, real_freq_av,f_ZC] = FindFreq(Vaf_iirx,xx,5);
%%
figure
plot(xx,f_inx,'k','LineWidth',1)
hold on
plot(xx,f_ZC,'r','LineWidth',1)
```

```
grid on
ylabel('Frequency (Hz)')
xlabel('Time (s)')
axis([0.22 0.32 58.5 60.5])
% yticks([54 55 56 57 58 59  60 61 62])
title('20Hz/s ramp')
legend('True', 'Measured')
set(gca,'fontsize',15)
%%
error = zeros(1,length(xx));
for i=1:length(xx)
   error(i) = 100*(f_inx(i)-f_ZC(i))/f_inx(i) ;
end
%%
figure
plot(xx,error)
grid on
ylabel('Error (%)')
axis([0 2 -10 10])
title('Error of zero-crossing method')
set(gca,'fontsize',15)

%%
% we want to track the fundamental
%freq so we will use Va filtered to track the
% zero crossing. This will track wt
%for the raw measurement
```

```
Pos_negVa = diff(sign(Vaf_iirx)); % look for change -1 0 or +1 0
Pos_VaZ = find(Pos_negVa>0); % the indices for postive ZC
Neg_VaZ = find(Pos_negVa<0);
% the time of positive Zero crossing of Va
t_wt1 = xx(Pos_VaZ);
% repeat each element in the time vector of
t_wt2 = repelem(t_wt1,2);
%zero crossing twice
 %  the  points of wt
Z_wt1 =zeros(1,length(t_wt2));
 % we add some delay so we can interpolate later.
T_delay = 5E-16;
% without this delay we will
%have error when we try to interpolate
t_wt= zeros(1,length(t_wt2));
for i=1:length(t_wt2)
        Z_wt1(i) = 2*pi;
        t_wt(i) = t_wt2(i);

        if rem(i,2)== 0
            Z_wt1(i) = 0;
            t_wt(i) = t_wt2(i)+T_delay*1;
        end
end

 t_wt_neg = xx(Neg_VaZ);
 wt_neg= ones(1,length(t_wt_neg))*pi;
```

```
c = 2;
n = numel(t_wt_neg(2:end));
k = c*n;
B = [reshape(t_wt(1:k),c,[]);t_wt_neg(2:end)];
% subdivide B vector into two
% rows and add the third row to be the A vector
t_wt_pos_neg = [t_wt_neg(1),B(:).',t_wt(k+1:end)];
c = 2;
n = numel(wt_neg(2:end));
k = c*n;
B0 = [reshape(Z_wt1(1:k),c,[]);wt_neg(2:end)];

Z_wt1x= zeros(1,length(t_wt2));

wt_pos_neg = [wt_neg(1),B0(:).',Z_wt1(k+1:end)];
Z_wt1x= zeros(1,length(t_wt2));

Z_wt1x= interp1(t_wt_pos_neg,wt_pos_neg,xx,'linear');
%wt aligned with other measurements
Z_wt1x(isnan(Z_wt1x))=0;
% eliminate NaN which is caused due to interpolation
wt_zd = 0;
% wt_zd = downsample(Z_wt1x,kk);
Z_wt1x_final3 = Z_wt1x;
%%
wt_Pos_neg = diff(sign(Vaf_iirx));
```

```
PeakVa_ind = find(wt_Pos_neg);


% re-decalre all the variable so we can
%re-ligend all the variables such as
% t=0 , Va(0)= Vapk


Z_wtx = Z_wt1x;
Vaxx=Vaf_iirx;
Vbxx=Vbf_iirx;
Vcxx=Vcf_iirx;
xx2 = xx;
j=2;
offset= 0;
xx2(length(xx)-(PeakVa_ind(j)+offset)+1:length(xx))=[];
Vaxx(1:PeakVa_ind(j)+offset)=[];
Vbxx(1:PeakVa_ind(j)+offset)=[];
Vcxx(1:PeakVa_ind(j)+offset)=[];
Z_wtx(1:PeakVa_ind(j)+offset)=[];
Time1= xx(PeakVa_ind(j))
%%
figure
plot(xx2,Vaxx*0.05)
hold on
plot(xx2,Z_wtx)
axis([0 0.1  -10 10])
%%
% Calculating the Idq0 and Vdq0
```

```
theta =zeros(1,length(xx2));
for i=1:length(xx2)

theta(i) =  Z_wtx(i)-1*pi/2+0.5;

end
Vd=zeros(1,length(xx2));
Vq=zeros(1,length(xx2));

V0=zeros(1,length(xx2));

for i=1:length(xx2)
%
Vq(i) = (2/3)*(Vaxx(i).*cos(theta(i)) +...
Vbxx(i).*cos(theta(i)-2*pi/3) + ...
Vcxx(i).*cos(theta(i)+2*pi/3));
Vd(i) = (2/3)*(Vaxx(i).*sin(theta(i))...
+Vbxx(i).*sin(theta(i)-2*pi/3)...
+Vcxx(i).*sin(theta(i)+2*pi/3));
V0(i) = (2/3)*(Vaxx(i)./2+ Vbxx(i)./2+ Vcxx(i)./2);
end
%%
figure
grid on
subplot(3,1,1)
```

```
plot(xx2, Vq,'r')
title('Vdq0 ')
ax = gca;
ax.TitleFontSizeMultiplier = 2;
grid on
legend ('Vq')
ylabel('Voltage (V)')
axis ([0 2 99.5 100.5 ])
subplot(3,1,2)
plot(xx2,Vd,'k')
grid on
ylabel('Voltage (V)')
legend ('Vd')
axis ([0 2 -0.5 0.5 ])
subplot(3,1,3)
plot(xx2,V0,'b')
axis ([0 2 -0.5 0.5])
grid on
legend ('V0')
ylabel('Voltage (V)')
xlabel('Time (s)')

%%
Vad = downsample(Vax,kk);
xx2d = downsample(xx,kk);

figure
```

```
plot(t,Va*0.05,'*r','LineWidth',3)
hold on
plot(xx2d,Vad*0.05,'ok','LineWidth',4)
plot(xx,Vax*0.05,'og','LineWidth',1)
axis([ 0.49999999 0.50000001 -3 -2])
% axis([ 0 0.05 -10 10])

grid on
legend ('Va act','Va DS','Va interp')
title('Upsampling & Downsampling')

for i=1:length(Vad)
zz(i) = Vad(i)-Va(i);

end
figure
plot(t,zz)
title('Va diifference between act and interp')
grid on
%%End
```

F.0.2 Filter Function

```
function Filtered = Filter(Signal,xx,k,cf)
Fs =1/xx(2);
s = Signal;
if k == 1
```

```
%cf = 90
    d = designfilt('lowpassiir', 'FilterOrder', 7,...
    'PassbandFrequency',cf, 'PassbandRipple'...
    ,0.001, 'StopbandAttenuation',cf+30, 'SampleRate',Fs);
    Filtered= filtfilt(d,s);

% fvtool(d)
else
    d = designfilt('lowpassfir', ...    % Response type
       'FilterOrder',12000, ...   % Filter order
       'PassbandFrequency',cf, ...   % Frequency constraints
       'StopbandFrequency',cf+40, ...
       'DesignMethod','ls', ... % Design method
       'PassbandWeight',1, ...  % Design method options
       'StopbandWeight',2, ...
       'SampleRate',Fs);    % Sample rate
%    Filtered= filtfilt(d,s);
     Filtered = filter(d,s);
%      fvtool(d)
% d = designfilt('lowpassiir', 'FilterOrder', 6,...
%     'PassbandFrequency', 0.002, 'PassbandRipple',....
%     0.5, 'DesignMethod', 'cheby1');

end
```

F.0.3 Frequency Tracking Function

```
function [ f_time, f, real_freq_av,f_vs_time] = FindFreq(Signal,xx,n)
% f_time is the time of freq before interpolate
% f is the freq value before interpolate
% real_freq_av is the average of the
%frequency which depend on value of n
% f_vs_time freq after interpolation
% Fs = (1/xx(2))*xx(end)*3;
% xxx = linspace(0,xx(end),Fs+1);
% Signalx= spline(xx,Signal,xxx);
Signalx=Signal;
xxx=xx;

Pos_negVa = diff(sign(Signalx));

Pos_VaZ = find(Pos_negVa>0);
Neg_VaZ = find(Pos_negVa<0);

Pos_VaZ_time = xxx(find(Pos_negVa>0));
Neg_VaZ_time = xxx(find(Pos_negVa<0));

% if b ==1
%  Pos_VaZ(113)=[]; % get rid of the switching ZC
%     Neg_VaZ(114)=[];
%
% end
Z_cro_total= 0;
% we need to know which one is
```

```
%starting first the pos ZC or neg ZC
if xxx(Neg_VaZ(1)) < xxx(Pos_VaZ(1))
Neg_VaZ2 = repelem(Neg_VaZ,2);
% repeat each element in the time vector of
g=1;
    for i=1:length(Neg_VaZ2)-1

        Z_cro_total(i)= Neg_VaZ2(i);
        if rem(i,2)== 0
            Z_cro_total(i)= Pos_VaZ(g);
            g=g+1;
        end

    end
else
Pos_VaZ2 = repelem(Pos_VaZ,2);
% repeat each element in the time vector of
g=1;
    for i=1:length(Pos_VaZ2)-1

    Z_cro_total(i)= Pos_VaZ2(i);
        if rem(i,2)== 0
        Z_cro_total(i)= Neg_VaZ(g);
        g=g+1;
        end

    end
```

```
end


Zero_cr= xxx(Z_cro_total);


f= 0;
f_time = 0;
N = length(Zero_cr);
for i=2:N
    diffT = Zero_cr(i)- Zero_cr(i-1);


    f(i)= (0.5/(diffT));
    f_time(i) = (Zero_cr(i));
end
% f_vs_time= spline(f_time,f,xx);
f_vs_time= interp1(f_time,f,xx);


% averging every three cycles
S  = numel(f);
x1 = reshape(f(1:S - mod(S, n)), n, []);
F_ave1= sum(x1, 1).' / n;
F_ave=0;
j=1;
for i=1:length(F_ave1)
F_ave(1,j:j+n-1) = repelem(F_ave1(i),n)  ;
   j=n+j;
end
```

```
real_freq_av = zeros(1,length(xx));
H=0;
for i=1:length(Z_cro_total)-n
    L = Z_cro_total(i);

   for j=1+H:L
      real_freq_av(j)= F_ave(i) ;

   end
   H=j;
end

end
```

G. MATLAB Code for the UKF

G.0.1 Main Code

```
%%
% load xEst.mat
% load PPred.mat
clearvars -except xEst PPred X Y EMTP_RV_LR_R Pm...
Nois11 Noz2 nosZ bi_noise Lap_noise Noise_g
% clear all
clc
% load EMTP_RV_LR_R.mat
% load Pm.mat
%%
t = X{1,1};
Ia = Y{1,1};
Ib = Y{1,2};
Ic = Y{1,3};
v0 = Y{1,4};
i0 = Y{1,5};
vd = Y{1,6};
id = Y{1,7};
psid = Y{1,8};
ifd = Y{1,9};
id1 = Y{1,10};
id2 = Y{1,11};
vfd = Y{1,12};
```

```
efd = Y{1,13};

vq = Y{1,14};

iq = Y{1,15};

psiq = Y{1,16};

iq1 = Y{1,17};

iq2 = Y{1,18};

iq3 = Y{1,19};

Teg = Y{1,20};

Texc = Y{1,21};

Pe = Y{1,22}*1E6;

MMF = Y{1,23};

Angle = Y{1,24};

oemga = Y{1,25}*60;

t1 =  Y{1,26};

%%

SB = 175E6;

VB = 14.7E3*sqrt(1/3);

IB = SB/(3*VB);

ZB = VB/IB;

LB = ZB/(2*pi*60);

%

RR= 2;

tfd = downsample(t(1:200000),RR);

VdFd =  downsample(-vd(1:200000)*sqrt(2/3),RR);

VqFd =  downsample(vq(1:200000)*sqrt(2/3),RR);

V0Fd =  downsample(v0(1:200000)*sqrt(2/3),RR);

IdFd =  downsample(-id(1:200000)*sqrt(2/3),RR);
```

```
IqFd =  downsample(iq(1:200000)*sqrt(2/3),RR);

I0Fd = downsample( i0(1:200000)*sqrt(2/3),RR);

psidd = downsample(psid(1:200000)*sqrt(2/3),RR);

psiqd = -downsample(psiq(1:200000)*sqrt(2/3),RR);


Ifd_Fd =  downsample(ifd(1:200000),RR);

Vfd_Fd = downsample(vfd(1:200000),RR);


delta_Fd = downsample(Angle(1:200000),RR);

freq_Vad =  downsample(oemga(1:200000),RR);

Pme=downsample(Pm(1:200000)*1E6,RR);

%%

Xd_s = 1.13;

Xq_s=  0.66;

Xls = 0.1;

NsNF = 0.0706433;

Xlf =  0.24819;

rf = 5.769*10^-4;

Ra = 1.5*10^-3;

Lls =Xls*LB*1;

Ll_kq1 =0.02;

Ll_kD = 0.18542*LB;

r_kq1 = 2.0081E-02;

r_kD= 0.02135*ZB;

Ll_FD =  Xlf*LB*1;

Lmq= (Xq_s*LB-Lls);

Lmd = (Xd_s*LB-Lls);
```

```
r_FD = rf*ZB;

rs =Ra*ZB;

rn = 1E6;

vf =    Vfd_Fd*NsNF;

iQ1=0; %In steady state, no current in the damper windings

iQ2=0;

ikD=0;

Ln =1E-9;

Poles = 16;  % poles

moment_ineti =4.25;

J=4.25E6;

%% setting the time start and end of the simulation

 i=1;

 startT = 1;

 EndT =round(12501/RR);

time = 0; % time start

endtime = tfd(EndT); % [sec]

global dt;

dt = (tfd(56)-tfd(55));

% [sec] This is global. we can find it in f(x,u)

nSteps = EndT;

%% calculating the intials

vd= VdFd(startT);

vq=  VqFd((startT));

iq=  IqFd((startT));

id=  IdFd((startT));

iFD = (2/3)*Ifd_Fd((startT))/(NsNF);
```

```
omega = 60*2*pi*freq_Vad;

omega_s=2*pi*freq_Vad((startT)); %

omega_r = 2*pi*freq_Vad(startT)/8;

Deltarad= delta_Fd(startT);

L_mq_a=(Lmq)*(1+0.5);

Lls_a = Lls*(1+0.000*randn(1,1));

Ll_FD_a = Ll_FD*(1+0);

L_md_a=(Lmd)*(1+0.5);

Ll_kq1 = 1.0365E-03;

Ll_kD = 4.9076E-04;

r_kq1 = 2.0081E-02;

r_kD= 1.1900E-02*0;

i0= 0;

psi_q = (-(Lls_a+L_mq_a)*iq);

psi_d = (-(Lls_a+L_md_a)*id+(L_md_a)*iFD);

psi_0 = (-(Lls_a+3*Ln)*i0);

psi_q1 =(-(L_mq_a)*iq);

psi_FD = (-(L_md_a)*id+(L_md_a+Ll_FD)*iFD);

Laq = 1/((1/L_mq_a)+(1/Lls_a));

Lad = 1/((1/L_md_a)+(1/Lls_a)+(1/Ll_FD));

SB = 15000;

H= 0.7;

J = 4.25;

psi_mq =(Laq*((psi_q/Lls_a)));

psi_md = (Lad*((psi_d/Lls_a)+(psi_FD/Ll_FD)));

Te =(8)*(3/2)*((psi_d*iq)-(psi_q*id));

psi_D = psi_md;
```

```
Tm = Pme(i)/omega_r;
VD= 0;
Omega_state = omega_s;
%checking the state before starting the estimation
Linkage_flux_d = (vd+(omega_s).*psi_q-...
(rs.*1./Lls).*(psi_d-psi_md));
Linkage_flux_q = (vq-(omega_s).*psi_d-...
(rs.*1./Lls).*(psi_q-psi_mq));
Linkage_flux_fd= (vf(i)+...
(r_FD./Ll_FD).*(psi_md-psi_FD));
Linkage_flux_kd = (VD+...
(r_kD./Ll_kD).*(psi_md-psi_D));     %psi_d
dot_meg = (1/J)*(Tm(i)-Te);     %omega dot

%%
Parameters = [Ll_kq1 Ll_kD r_kq1 r_kD Ll_FD J J ...
omega_s rs rn Ln r_FD Lls Lmd Lmq];
% intial

x0 = [psi_d; psi_q;psi_0;psi_FD;L_md_a;L_mq_a];
%initial state vector
% x0=xEst;

disp('Unscented Kalman Filter (UKF) start')
xEst=x0;
% som=9;
```

```
% Q=diag([1E-1 1E-1 1E-1 1E-1 1E-1 1E-1]).^som;
% R=diag([1E-1 1E-1 1E-1 1E-1]).^(som);
PEst=diag([1E-8 1E-8 1E-8 1E-7 1E-8 1E-8]).^1;
% PEst=PPred;
% Covariance Matrix for predict or the system

% Q depends on uncertaintt of inputs,
% sampling frequency and accuracy of the model
Q=diag([1E-3 1E-3 1E-9 1E-5 1E-10 1E-10]).^1;
%uncertainty of the measrements
R=diag([1E-3 1E-3 1E-3 1E-3]);

% UKF Parameter
alpha=0.1;
beta =2;
kappa=0;

n=length(xEst);%size of state vector
lamda=alpha^2*(n+kappa)-n;

%calculate weights as vector
% this the weight of vector 0
wm=[lamda/(lamda+n)];
wc=[(lamda/(lamda+n))+(1-alpha^2+beta)];
% then calculate the rest of 2n. to tal 2n+1
for i=1:2*n
    wm=[wm 1/(2*(n+lamda))];
```

```
    wc=[wc 1/(2*(n+lamda))];
end
gamma=sqrt(n+lamda);

tic;

for i=startT : nSteps*10
    time = time + dt
vd= VdFd(6251);
vq=  VqFd((6251));
iq=  IqFd((6251));
id=  IdFd((6251));
i0=  I0Fd((6251));
v0=  V0Fd((6251));
vfd = vf((6251));

iFD = (2/3)*Ifd_Fd((6251))/(NsNF);
omega = 2*pi*freq_Vad((6251));
omega_s=2*pi*freq_Vad((6251));
omega_r = 2*pi*freq_Vad(6251)/3;
% Tm =  PDC/omega_r;
% Tm =  PDC/3;
Delta8_rad = delta_Fd((6251));
% u1 = [vd;vq;vf(6251);v0;id;iq;omega;Pme(6251)];
u = [vd;vq;vf(6251);v0];

z1=[id;iq;i0;iFD];
```

```
z= (z1)';
    % ------ Unscented Kalman Filter --------
    sigma=(GenerateSigmaPoints(xEst,PEst,gamma));

% the below function has the prediction
%function which pass the sigma point to it
    sigma=(PredictSystem(sigma,u,Parameters,Q));
    xPred=((wm*sigma')'); % this is the mean
    PPred=(CalcSimgaPointsCovariance(xPred,sigma,wc,Q));
    % generate sigma points for the update function
    sigma=(GenerateSigmaPoints(xPred,PPred,gamma));
    % pass the sigma points to h function
    zSigma=(PredictMeasurement(sigma,Parameters));
    zb=(wm*(zSigma)')';
    St=(CalcSimgaPointsCovariance(zb,zSigma,wc,R));
    Pxz=(CalcPxz(sigma,xPred,zSigma,zb,wc));
    K=Pxz/(St);
    xEst = xPred + K*(z'-zb);
    PEst=PPred-K*St*K';
%%
id_act(i-startT+1) = z(1);
iq_act(i-startT+1) = z(2);
i0_act(i-startT+1) = z(3);
ifd_act(i-startT+1) = z(4);

Id_z(i-startT+1) = zb(1);
Iq_z(i-startT+1) = zb(2);
```

```
I0_z(i-startT+1) = zb(3);
Ifd_z(i-startT+1) = zb(4);
% delta_z(i-startT+1) = zb(6);

flux_d(i-startT+1)= xEst(1);
flux_q(i-startT+1)= xEst(2);
flux_0(i-startT+1)= xEst(3);
% flux_q1(i-startT+1)= xEst(4);
flux_fd(i-startT+1)= xEst(4);
% flux_kd(i-startT+1)= xEst(5);

% est_r_kq1(i-startT+1) = xEst(11);
% est_Ll_kq1(i-startT+1) = xEst(12);
Lmd_est(i-startT+1)= xEst(5);
Lmq_est(i-startT+1) = xEst(6);

end
%%

Lmd_act= Lmd*ones(1,length(Lmd_est));
Lmq_act= Lmq*ones(1,length(Lmd_est));
t8=tfd;
offset = 0;
   figure
   subplot(2,1,1)
   plot(t8(startT:i-offset),flux_d(1:end),'k')
   hold on
```

```
%  plot(t8(startT:i-offset),psid(startT:i-offset),'r')
%     legend('flux d est','flux d act')
   title('Flux d')
   grid on
   hold on
%   axis([t8(startT) t8(i+startT) 0 40])
  axis([t8(startT) 0.1 20 50])
   set(gca,'fontsize',15)

   ylabel('V.s')
   xlabel('Time (s)')
   subplot(2,1,2)
   plot(t8(startT:i-offset),flux_q(1:end),'k')
   hold on
%    plot(t8(startT:i-offset),psiq(startT:i-offset),'r')
   title('Flux q')
   grid on
%    axis([t8(startT) t8(i+startT) -40 40])
%    axis([t8(startT) 0.1 -40 -10])
   set(gca,'fontsize',15)

%    legend('flux q est','flux d act')
   ylabel('V.s')
   xlabel('Time (s)')
    figure
   subplot(2,1,1)
   plot(t8(startT:i-offset),flux_0(1:end),'k')
```

```
   title('Flux 0')
   grid on
   set(gca,'fontsize',15)
   axis([t8(startT) t8(i+startT) -30 30])
%    axis([t8(startT) 0.1 -10 10])
   ylabel('V.s')
   xlabel('Time (s)')
   subplot(2,1,2)
   plot(t8(startT:i-offset),flux_fd(1:end),'k')
   title('Flux fd')
   grid on
   set(gca,'fontsize',15)

   axis([t8(startT) t8(i+startT) 0 50])
%    axis([t8(startT) 0.1 30 60])
   ylabel('V.s')
   xlabel('Time (s)')
% %    subplot(3,2,5)
% %    plot(t8(startT:i-offset),flux_kd(1:end))
% %    title('Flux kd')
% %    grid on
% %    axis([t8(startT) t8(i+startT) -30 30])
% %    subplot(3,2,6)
% %    plot(t8(startT:i-offset),omega_state(1:end),'k')
% %    hold on
% % %    plot(t8(startT:i-offset),omega_act(1:end),'r')
% %   legend('omega est','omega act')
```

```
% %   title('omega')
% %    grid on
% %   axis([t8(startT) t8(i+startT) 375 380])
   figure
   subplot(2,1,1)
   plot(t8(startT:i-offset),Lmd_est(1:end),'k','LineWidth',2)
    hold on
   plot(t8(startT:i-offset),Lmd_act(1:end),'r')
  legend('Lmd est','Lmd act')
   title('Lmd')
   axis([0 2 0 0.01])
% xlim([0.2 0.33])

%    axis([t8(startT) 0.1 0 0.005])
     set(gca,'fontsize',15)

    grid on
    hold off
   ylabel('H')
   xlabel('Time (s)')
   subplot(2,1,2)
   plot(t8(startT:i-offset),Lmq_est(1:end),'k','LineWidth',2)
    hold on
       plot(t8(startT:i-offset),Lmq_act(1:end),'r')
grid on
      title('Lmq')
        legend('Lmq est','Lmq act')
```

```
   axis([0 2 0 0.005])
%    axis([t8(startT) 0.1 0 0.005])
% xlim([0.2 0.33])

   ylabel('H')
   xlabel('Time (s)')
     set(gca,'fontsize',15)

   figure
   subplot(2,1,1)
   plot(t8(startT:i-offset),Id_z(1:end),'k','LineWidth',2)
    grid on
    hold on
   plot(t8(startT:i-offset),id_act(1:end),'r')
    title('Id')
%     axis([[0.2 0.33] 4000 4400])
%     axis([t8(startT) 0.1 4200 4500])
% xlim([0.2 0.33])

   legend('Id est','Id act')
    hold off
   ylabel('Current (A)')
   xlabel('Time (s)')
   set(gca,'fontsize',15)

   subplot(2,1,2)
   plot(t8(startT:i-offset),Iq_z(1:end),'k','LineWidth',2)
```

```
   hold on
   grid on
   plot(t8(startT:i-offset),iq_act(1:end),'r')
   legend('Iq est','Iq act')
   title('Iq')
   hold off
   ylabel('Current (A)')
   xlabel('Time (s)')
   set(gca,'fontsize',15)



%       axis([[0.2 0.33] 7200 7600])
%    axis([t8(startT) 0.1 7300 7450])
% xlim([0.2 0.33])

   figure
   subplot(2,1,1)
   plot(t8(startT:i-offset),I0_z(1:end),'k','LineWidth',2)
   hold on
   grid on
%    axis([[0.2 0.33] -5 5])
%    axis([t8(startT) 0.1 -5 5])
% xlim([0.2 0.33])

    ylabel('Current (A)')
   xlabel('Time (s)')
   set(gca,'fontsize',15)
```

```
   plot(t8(startT:i-offset),i0_act(1:end),'r')
    title('I0')
%     axis([[0.2 0.33] -1 1])
%     axis([t8(startT) 0.1 -1 1])
% xlim([0.2 0.33])

    ylabel('Current (A)')
   xlabel('Time (s)')
   set(gca,'fontsize',15)
   legend('I0 est','I0 act')
    hold off
    subplot(2,1,2)
   plot(t8(startT:i-offset),Ifd_z(1:end),'k','LineWidth',2)
    hold on
    grid on
   plot(t8(startT:i-offset),ifd_act(1:end),'r')
    title('Ifd')
%     axis([[0.2 0.33] 12500 13500])
%     axis([t8(startT) 0.1 12800 13100])
   set(gca,'fontsize',15)

%     axis([t8(startT) t8(i+startT) 8200 9200])

   legend('Ifd est','Ifd act')
    hold off
    ylabel('Current (A)')
```

```
xlabel('Time (s)')
```

G.0.2 System Function

```
function x = f(x, u,Parameters)


global dt;
Vd = u(1);
Vq = u(2);
vf = u(3);
V0= u(4);
psi_d = x(1,:);
psi_q = x(2,:);
psi_0 = x(3,:);
% psi_q1 = x(4,:);
psi_FD = x(4,:);
L_md = x(5,:);
L_mq= x(6,:);


% Known parameters
% Ll_kq1   = Parameters(1,1);
%     Ll_kD    = Parameters(1,2);
%     r_kq1    = Parameters(1,3);
%     r_kD     = Parameters(1,4);
    Ll_FD    = Parameters(1,5);
    J        = Parameters(1,6);
    Poles    = Parameters(1,7);
    omega_s  = Parameters(1,8);
```

```
    rs       = Parameters(1,9);
    rn       = Parameters(1,10);
    Ln       = Parameters(1,11);
    r_FD     = Parameters(1,12);
    Lls      = Parameters(1,13);
    omega_a =  Parameters(1,8);
%     L_md      = Parameters(1,14);
%     L_mq      = Parameters(1,15);

Laq = 1./((1./L_mq)+(1./Lls));

Lad = 1./((1./L_md)+(1./Lls)+(1./Ll_FD));
psi_mq =Laq.*((psi_q/Lls));
psi_md = Lad.*((psi_d/Lls)+(psi_FD./Ll_FD));

xdot(1,:) = (Vd+(omega_a).*psi_q+...
(rs.*1./Lls).*(psi_md-psi_d))  ;
xdot(2,:) = (Vq-(omega_a).*psi_d+...
(rs.*1./Lls).*(psi_mq-psi_q))   ;
xdot(3,:) = (V0-((rs)./(Lls)).*psi_0);

xdot(4,:) = (vf+(r_FD./Ll_FD)...
.*(psi_md-psi_FD));
omega_r = omega_a/8;
xdot(5,:)= 0; %r_kD
xdot(6,:) = 0; %Ll_kD
```

```
check =  xdot;

xa = x+ xdot*dt;

x= xa;
```

G.0.3 Measurement Function

```
function z = h(x,Parameters)

%Observation Model


% Known parameters

Ll_FD  = Parameters(1,5);

J  = Parameters(1,6);

Poles = Parameters(1,7);

omega_s  = Parameters(1,8);

rs  = Parameters(1,9);

rn  = Parameters(1,10);

Ln  = Parameters(1,11);

Lls = Parameters(1,13);


psi_d = x(1,:);

psi_q = x(2,:);

psi_0 = x(3,:);

psi_FD = x(4,:);


L_md = x(5,:);

L_mq= x(6,:);
```

```
Laq = 1./((1./L_mq)+(1./Lls));
Lad = 1./((1./L_md)+(1./Lls)+(1./Ll_FD));
psi_mq =Laq.*((psi_q/Lls));
psi_md = Lad.*((psi_d/Lls)+(psi_FD./Ll_FD));

y(1,:) = (1./Lls).*(psi_md-psi_d);
y(2,:) = (1./Lls).*(psi_mq-psi_q);
y(3,:) = -(1./(Lls)).*psi_0;
y(4,:) = (1./(Ll_FD)).*(psi_FD-psi_md) ;

z= y;
```

G.0.4 Predicted Measurement

```
function Zsigma=PredictMeasurement(sigma,Parameters)

% Sigma Points predition with measurement model
Zsigma = zeros(4,length(sigma(1,:)));

for i=1:length(sigma(1,:))
    Zsigma(:,i)=h(sigma(:,i),Parameters);
end
```

G.0.5 Predicted System

```
function sigma=PredictSystem(sigma,u,Parameters,Q)

for i=1:length(sigma(1,:))
```

```
    sigma(:,i)=f(sigma(:,i),u,Parameters);
end
```

G.0.6 Generate Sigma Points

```
function sigma=GenerateSigmaPoints(xEst,PEst,gamma)
sigma=xEst;
PEst1 = nearestSPD(PEst);
Psqrt=chol(PEst1,'Lower');
n=length(xEst);
%Positive direction
for ip=1:n
    sigma=[sigma xEst+gamma*Psqrt(:,ip)];
end
%Negative direction
for in=1:n
    sigma=[sigma xEst-gamma*Psqrt(:,in)];
end
```

G.0.7 System Covariance

```
function P=CalcSimgaPointsCovariance(xPred,Sigma,wc,Q)
nSigma=length(Sigma(1,:));
d=Sigma-repmat(xPred,1,nSigma);
P=Q;
for i=1:nSigma
    P=P+wc(i)*d(:,i)*d(:,i)';
```

```
end
```

G.0.8 Cross Covariance

```
function P=CalcPxz(sigma,xPred,zSigma,zb,wc)
nSigma=length(sigma(1,:));
dx=sigma-repmat(xPred,1,nSigma);
dz=zSigma-repmat(zb,1,nSigma);
P=zeros(length(dx(:,1)),length(dz(:,1)));
for i=1:nSigma
    P=P+wc(i)*dx(:,i)*dz(:,i)';
end
```

G.0.9 Symmetric Positive Definite matrix

```
function Ahat = nearestSPD(A)
% arguments: (input)
%  A - square matrix, which will
%be converted to the nearest Symmetric
%    Positive Definite Matrix.
%
% Arguments: (output)
%  Ahat - The matrix chosen as the nearest SPD matrix to A.

if nargin ~= 1
  error('Exactly one argument must be provided.')
end
```

```
% test for a square matrix A
[r,c] = size(A);
if r ~= c
  error('A must be a square matrix.')
elseif (r == 1) && (A <= 0)
  % A was scalar and non-positive, so just return eps
  Ahat = eps;
  return
end

% symmetrize A into B
B = (A + A')/2;

% Compute the symmetric polar factor of B. Call it H.
% Clearly H is itself SPD.
[U,Sigma,V] = svd(B);
H = V*Sigma*V';

% get Ahat in the above formula
Ahat = (B+H)/2;

% ensure symmetry
Ahat = (Ahat + Ahat')/2;

% test that Ahat is in fact PD.
%if it is not so, then tweak it just a bit.
p = 1;
```

```
k = 0;
while p ~= 0
  [R,p] = chol(Ahat);
  k = k + 1;
  if p ~= 0
    % Ahat failed the chol test.
    %It must have been just a hair off,
    % due to floating point trash,
    %so it is simplest now just to
    % tweak by adding a tiny multiple
    %of an identity matrix.
    mineig = min(eig(Ahat));
    Ahat = Ahat + (-mineig*k.^2 + eps(mineig))*eye(size(A));
  end
end
```